Methanol Drive

A methanol-fuelled Solid oxide fuel cell - internal combustion engine combined cycle for maritime applications

Graduation Thesis

Luca Sopar

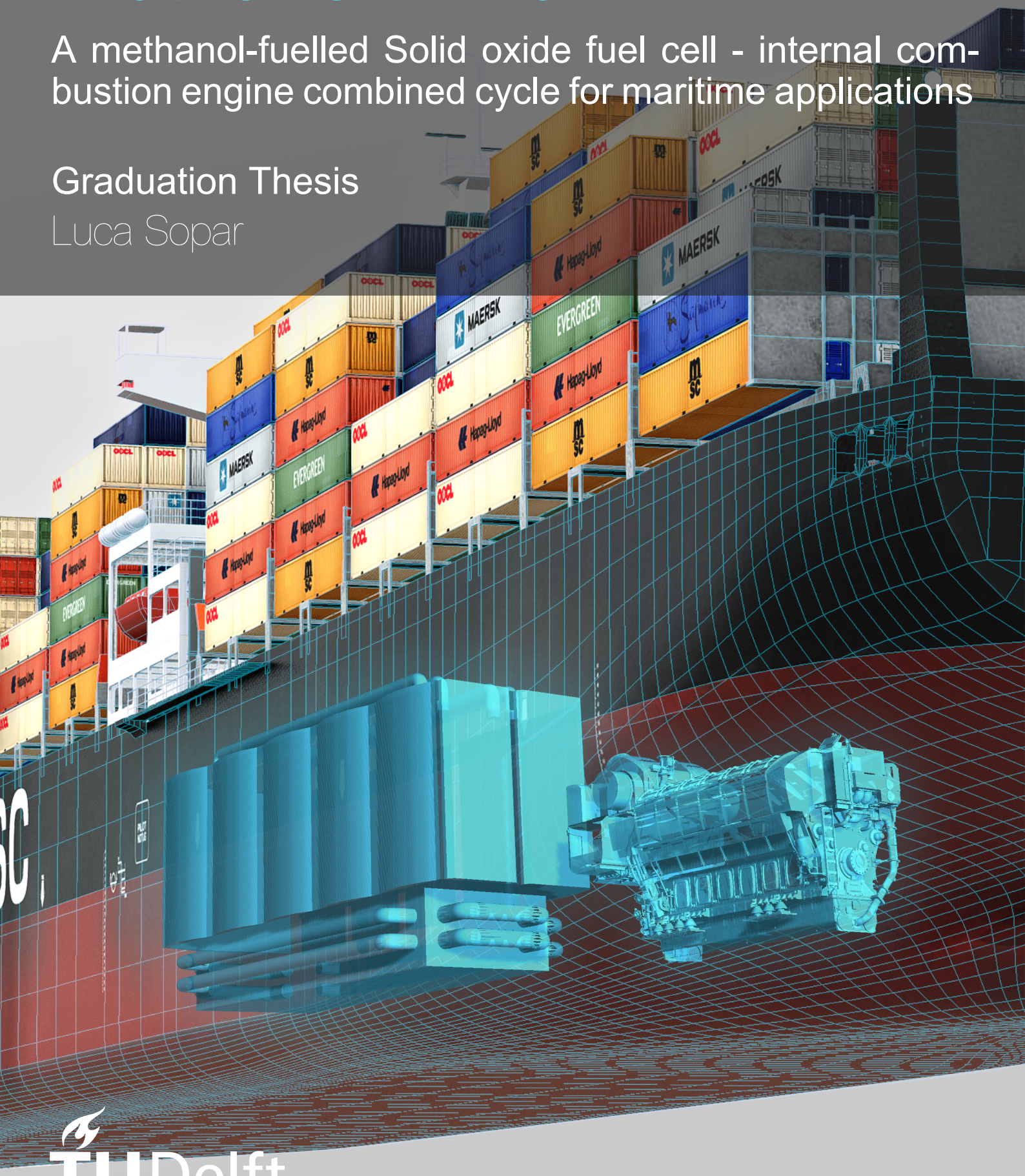

TU Delft

Methanol Drive

A methanol-fuelled Solid oxide fuel cell - internal combustion engine combined cycle for maritime applications

by

Luca Sopar

Student Name	Student Number
Luca Sopar	4487117

Instructor: Peter de Vos
Project Duration: February, 2022 - March, 2023
Faculty: Faculty of 3ME, Delft

TU Delft

Abstract

With the increasing concerns of the emission of greenhouse gases and other pollutants and the push towards sustainable and greener means of transportation, there is a need for new drive systems running on alternative fuels. One fuel that holds significant potential as a marine fuel for the future is methanol. When produced utilising carbon capture methods and green energy, it has the potential to be a net zero fuel. Among other high-potential future fuels, methanol has the added benefit of being liquid at room temperature. Additionally, methanol has the potential to be utilised in novel drive systems, such as the combination of a solid oxide fuel cell (SOFC) and a reciprocating internal combustion engine (ICE). This concept utilises the high efficiency and negligible NOx formation of the SOFC, while the ICE provides dynamic load capabilities. This study concentrates on the electrical efficiency of this type of plant for maritime applications.

This work presents an in MATLAB & Simulink constructed first principles based model of a methanol fuelled SOFC-ICE combined cycle. The zero-dimensional SOFC model consists of a temperature controlled methanator which maintains an external reforming ratio of 0.5; a cell mass balance; a cell energy balance, and an electrochemical model. The ICE model core consists of a turbocharged five-state Seiliger cycle. It simulates Wärtsilä 12V31DF fuelled with methanol and dehydrated hydrogen-rich anode of gas (AOG). The SOFC efficiency and its separate losses are evaluated for different temperatures, current densities, fuel utilisation factors UF and steam-to-fuel ratio's in combined cycle operations. Additionally, the standalone SOFC performance, without the use of waste heat from the ICE and disuse of residual fuel in the AOG, is evaluated, but only for the nominal condition. The ICE efficiency and losses are evaluated for a power range between 1% and 100%. By varying the ammount of cells, the following power splits P_{SOFC}/P_{ICE} have been evaluated: 0/100 25/75; 50/50; 75/25 and 100/0. The combined cycle performance is evaluated for different temperatures and current densities.

This study found that while varying the steam-to-fuel ratio and fuel utilisation factor (UF) have minimal impact on the electrical efficiency of the SOFC in combined cycle operations, temperature and current density have a significant effect on the efficiency of the SOFC. For a steam-to-fuel ratio of 1:1, a UF of 0.8, a current density of 5000 $A \cdot m^{-2}$ and a mean cell temperature of 1073K an efficiency of 58.6% was obtained. The standalone SOFC, or 100/0 power split, obtained an efficiency of 48.4%. The stand-alone ICE genset, or 0/100 power split, operates at a nominal efficiency of 42.3%. When the ICE is used in a direct drive configuration, it corresponds to an efficiency of 43.6%. The combined cycle obtained efficiencies of 45.4%, 49.1% and 53.4% for 25/75, 50/50 and 75/25 power splits, respectively. These results are compared to the results of a similar study investigating an ammonia-fuelled SOFC-ICE combined cycle for maritime applications, which reported efficiencies of 47%, 50% and 52% for 25/75, 50/50 and 75/25 power splits, respectively, under similar operating conditions.

The efficiency gain of the methanol-fuelled 75/25 configuration compared to the direct drive is limited. This raises the questions about whether the added complexity of introducing an SOFC is justified for the limited efficiency gain. The highest efficiency was obtained with the methanol-fuelled 75/25 power split, but due to the large proportion of SOFC power, it is less tolerant to dynamics in the load, making it questionable whether it can fully meet the dynamic power demand of a ship. Therefore, the 50/50 power split configuration is expected to be the most viable option in terms of both technological feasibility and efficiency gain. A change in the power split to 100/0 results in a decrease in system efficiency due to the lack of waste heat from the ICE and the inability to utilise residual fuel in the exhaust. When considering efficiency, the values for the ammonia fuelled and methanol fuelled plant are similar.

The 50/50 powersplit configuration is 5.6 percentpoints more efficient than the methanol fuelled direct drive ICE and 1.2 percentpoints more efficient than the methanol-fuelled standalone SOFC. This clearly shows the synergistic benefits of combining a methanol-fuelled SOFC with an ICE. However, when compared to the ammonia fuelled combined cycle with 50/50 power split, it is 0.9 percentpoints less efficient. Nevertheless, it is important to exercise caution when drawing further conclusions from

this last figure as the model has been constructed at a system level and no thorough uncertainty analysis has been conducted. Furthermore, the requirements regarding the power and energy density are strongly dependent on the type of ship and its operational profile. Therefore, future research should include the implementation of dynamic load capabilities in the model to evaluate its technological feasibility and overall net efficiency gain in various operational profiles of ships. Also, further research is required on the methanol-fuelled ICE cylinder process and the heat integration of the combined cycle.

Contents

Abstract i

Nomenclature v

1 Introduction 1

2 Literature 3
2.1 Solid Oxide Fuel Cells . . . 3
2.1.1 Solid-oxide fuel cell system fundamentals . . . 3
2.1.2 Methanol-fuelled SOFC . . . 8
2.2 Internal Combustion Engines . . . 10
2.2.1 Methanol as fuel . . . 10
2.2.2 Methanol-AOG mixture as fuel . . . 11
2.2.3 Safety risks . . . 12
2.2.4 Emissions . . . 12
2.2.5 ICE modelling . . . 13
2.3 SOFC-ICE combined cycles . . . 14
2.3.1 Combined cycle research . . . 14
2.4 Problem statement . . . 16

3 Methodology 18
3.1 Solid oxide fuel cell model . . . 18
3.1.1 Method in existing model . . . 18
3.1.2 SOFC adaptions . . . 21
3.2 Internal combustion engine model . . . 25
3.2.1 Method in existing model . . . 25
3.2.2 ICE adaptions . . . 26
3.3 Combined cycle model . . . 27
3.3.1 System specifications . . . 28

4 Results 30
4.1 SOFC . . . 30
4.1.1 SOFC performance . . . 30
4.1.2 Comparing SOFC performance . . . 33
4.2 ICE standalone performance . . . 34
4.3 Combined SOFC-ICE . . . 36
4.3.1 Combined cycle performance . . . 36
4.3.2 Comparing combined cycle performance . . . 37
4.4 Research and modelling approach reflection . . . 38

5 Conclusion and recommendations 40
5.1 Conclusion . . . 40
5.2 Recommendations . . . 42

References 43

A Appendix: Diesel model description 48

B Appendix: MATLAB code for pressure ratio calculation 56

C Appendix: MATLAB code for AOG flammability 59

D Appendix: Tables with data from result section 60

E Concept paper: A methanol-fuelled SOFC-ICE combined cycle for maritime applications 63
E.1 Introduction . . . 64
E.1.1 Hybrid cycle research . . . 64
E.1.2 Maritime scope . . . 65
E.2 Modelling approach . . . 65
E.2.1 SOFC model . . . 65
E.2.2 ICE model . . . 68
E.3 Results . . . 68
E.3.1 SOFC performance . . . 68
E.3.2 ICE results performance . . . 69
E.3.3 Combined SOFC-ICE performance . . . 70
E.3.4 Research and modelling approach reflection . . . 71
E.4 Conclusion . . . 72
E.5 Appendix: modelling parameters . . . 73

Nomenclature

Nomenclature incomplete. method chapter not included yet

Abbreviations

Abbreviation	Definition
AFR	Air-to-fuel ratio
AOG	Anode of gas
APU	Auxiliary power unit
ADR	Ammonia decomposition reaction
amb	Ambient condition
atm	Atmospheric condition
BoP	Balance of plant
CFD	Computational fluid dynamics
CI	Compression ignition
CIG	cathode-in-gas
DI	Direct injected
DIR	Direct internal reforming
ECR	External cracking ratio
EMF	Electromotive force
FC	Fuel cell
GHG	Greenhouse gas
GT	Gas turbine
HCCI	Homogeneous charge compression ignition
HEX	Heat exchanger
HFO	Heavy fuel oil
HOR	Hydrogen oxidation rate
HT-HEX	High temperature heat exchanger
ICE	Internal combustion engine
IIR	Indirect internal reforming
IMO	International maritime organisation
LH_2	Liquid hydrogen
LHV	Lower heating value
LNG	Liquefied natural gas
LT-HEX	Low temperature heat exchanger
MCFC	Molten carbonate fuel cell
MDO	Marine diesel oil
MDR	Methane decomposition rate
MeOH	Methanol
MeOHDR	Methanol decomposition reaction
MGO	Marine gas oil
MSR	Methane steam reforming
NG	Natural gas
PEMFC	Proton exchange membrane fuel cell
PEN	Positive-electrolyte-negative
PFI	Port fuel injection
PM	Particulate matter
Powersplit	P_{SOFC}/P_{ICE}
SI	Spark ignition

Abbreviation	Definition
SOFC	Solid oxide fuel cell
TDC	Top dead centre
TPB	Three-phase boundary
UF	Utilisation factor
WGS	Water gas shift
YSZ	Yttria-stabilized zirconia

Symbols

Symbol	Definition	Unit
$c_{p,I}$	Specifif heat capacity of interconnect	$J \cdot kg^{-1} \cdot K^{-1}$
$c_{p,PEN}$	Specifi heat capacity of PEN structure	$J \cdot kg^{-1} \cdot K^{-1}$
c_p	Specific heat capacity at constant pressure	$J \cdot K^{-1} \cdot kg^{-1}$
c_{tc}	Turbocharger constant	$s \cdot kg^{-1}$
$D_{eff,an}$	Effective diffusion coefficient of anode	$m^2 \cdot s^{-1}$
$D_{eff,ca}$	Effectice fdiffusion coefficient of cathode	$m^2 \cdot s^{-1}$
e	Charge of an electron	V
E	EMF	V
E_0	EMF at standard pressure	V
E_{an}	Activation energy of i_0 at anode	$J \cdot mol^{-1}$
E_{ca}	Activation energy of i_0 at cathode	$J \cdot mol^{-1}$
err	External reforming ratio	$-$
F	Faraday constant	$C \cdot mole^{-1}$
Δg	Change in gibbs free energy	$J \cdot mole^{-1}$
Δg^0	Change in standard gibbs free energy	$J \cdot mole^{-1}$
h	Specific enthalpy	$J \cdot mole^{-1}$
h	Channel height	m
Δh	Enthalpy of formation	$J \cdot mole^{-1}$
$heatloss$	Heatloss of the SOFC to the environment	$-$
i	Current density	$A \cdot m^{-2}$
i	Amount of cylinders	$-$
i_0	Exchange current density	$A \cdot m^{-2}$
K	equilibrium constant	$-$
k_{an}	Pre-exponential facytor of i_0 at canode	$A \cdot m^{-2}$
k_{ca}	Pre-exponential factor of i_0 at cathode	$A \cdot m^{-2}$
L	Cell length	m
m	Mass	kg
M	Molar mass	$kg \cdot mole^{-1}$
n	Amount of electrons per molecule fuel	$-$
N	Avogrado number	$-$
n	Engine speed	rps
$N\dot{N}$	Molar flow	$mole \cdot s^{-1}$
P	Absolute pressure	pa
p	pressure	pa
$p^{\#}_{\#}$	Partial pressure	pa
p_i	Partial pressure of substance i	pa
p_{meth}	operating pressure of the methanator	pa
p_{opp}	Operating pressure of the SOFC	pa
Q	Heat	J
q	Specific heat input	$J \cdot kg^{-1}$
R	Gas constant	$J \cdot K^{-1} \cdot mole^{-1}$
$r_{s,f}$	Steam to fuel ratio	$-$

Symbol	Definition	Unit
$r_{s/f}$	Steam to fuel ratio	$-$
$s\Delta s$	Change in entropy	$J \cdot K^{-1} \cdot mole^{-1}$
T	Temperature	K
T_C	Temperature of cold reservoir	K
T_H	Temperature of hot reservoir	K
T_{meth}	Operating temperature of the methanator	K
T_{opp}	Operating temperature of the SOFC	K
v	Stoichiometric coefficient	$-$
V_c	Cell voltage	V
W	Cell width	m
x	Mole fraction	$-$
η_{DCAC}	DC-AC converter efficiency	$-$
η_{Carnot}	Efficiency of Carnot cycle	$-$
η_{is}	Isentropic efficiency	$-$
η_{mech}	Mechanical efficiency of the fuel and air blowers	$-$
κ	Heat capacity ratio	$-$
ρ_I	Mass density of interconnect	$kg \cdot m^{-3}$
ρ_{PEN}	Mass density of PEN structure	$kg \cdot m^{-3}$
σ	conductivity	
σ_{an}	Eelectric conductivity of anode	$\Omega^{-1}m^{-1}$
σ_{ca}	Electric conductivity of cathode	$\Omega^{-1}m^{-1}$
σ_{el}	Ioninc conductivity of electrolyte	$\Omega^{-1}m^{-1}$
τ	thickness	m
τ_{an}	Thickness of anode	m
τ_{ca}	Thickness of cathode	m
τ_{el}	Thickness of electrolyte	m
τ_I	Thickness of interconnect	m

1 Introduction

The IPCC published their latest report in August 2022. The alarming prospects on climate change show the magnitude of the challenge that humanity is now facing to meet the Paris Agreements of 2015 [39]. Rapid integration of current technologies and the development of new technologies is essential to overcome these challenges [90].

Current state of maritime engineering

In June 2021, only 6.7% of the global fleet used a modern eco-engine. Modern eco-engines refer to engines with electronic injection and contracted in 2012 or later [54]. This indicates that a large portion of the current world fleet still uses underdeveloped drive systems. These systems often use highly polluting fuels. By 2018, Heavy Fuel Oil (HFO) was the dominant type of fuel: 79% of the maritime energy consumption consists of HFO. Other important fuels are Marine Diesel Oil (MDO) and liquified Natural Gas (LNG) [36]. In the period between 2012 and 2018, the amount of greenhouse gas (GHG) emissions resulting from the shipping industry has increased from 977 to 1076 million tonnes of CO_2e. Here, CO_2e is the equivalent unit of CO_2. In addition, the share of global GHG emissions, attributed to shipping, has increased from 2.76% to 2.89% [36].

However, the International Maritime Organisation (IMO) does see development trends in the shipping industry. The IMO estimates that, even though total GHG emissions have increased in relative and absolute value, the relative and absolute use of HFO have decreased by 3% and 7% respectively [36]. Besides the transition in fuel type usage, also advanced drive systems are under development. These vary from modern fuel injection and ignition methods to entirely new drive concepts. Research indicates that efficiencies can be improved by a few percentage points when using these modern injection and ignition methods. Currently, these developments are still unstable and not deployment-ready [74].

One such advanced drive system that is under development is the combination of a fuel cell and an internal combustion engine (ICE) in a combined cycle. This system combines the high efficiency and low emissions of a fuel cell with the reliability and flexibility of an ICE. The hybrid system can use a variety of fuels, such as diesel, natural gas, hydrogen, ammonia or methanol, to generate electricity and power the ship's propulsion system. Research has shown that these hybrid systems have the potential to significantly improve the efficiency and reduce the emissions of ships [6] [74] [21] [67] [44]. However, the development of these systems is still in the early stages and further research and development is needed to optimise their performance and make them ready for deployment in the maritime industry.

Research objective

The motivation of this thesis is to develop and implement a novel type of power plant, fuelled with an alternative clean fuel in maritime applications. This research focusses on a solid oxide fuel cell (SOFC) combined with a reciprocating internal combustion engine (ICE) fuelled with green methanol. This research aims to answer the following research question:

How does a methanol-fuelled SOFC-ICE combined cycle perform as power plant for ships compared to alternative, comparable power plants?

In order to answer this question, the following subquestions are formulated:

- **What are the performance characteristics of a methanol-fuelled SOFC-ICE combined cycle in maritime applications?**
- **How will the system's performance be modelled and verified?**
- **How does the implementation of the combined cycle influence the efficiency performance of the ship at nominal output compared to a stand-alone methanol-fuelled ICE or an ammonia-fuelled combined cycle?**

Report Structure

The second chapter is dedicated to the literature study, aimed at establishing a knowledge base for this research. From the literature research, a knowledge gap is identified. This resulted in the formulation of the research question with subquestions for the graduation thesis. The second chapter delves into the methodology employed for modelling the power plant under investigation. In the following chapter, the obtained results will be evaluated and compared to to those from literature. This chapter will be concluded with a review of the approach. This report will be concluded with a conclusion and recommendations for future work.

The report has been composed by the author under the guidance of his graduate mentor, Peter de Vos, and with the contribution of Lindert van Biert's expertise. The utilisation of Writefull and ChatGPT was employed for the purpose of ensuring accurate formulation and performing an advanced spell-check.

2 Literature

2.1. Solid Oxide Fuel Cells

In this chapter, the fundamental workings of the solid oxide fuel cell (SOFC) will be explained first. This is supplemented by research literature. After that, the impact of using methanol in an SOFC is discussed.

2.1.1. Solid-oxide fuel cell system fundamentals

In the maritime energy transition, one proposed drive system is the fuel cell (FC) [1]. An FC is an electrochemical cell that uses hydrogen in a redox reaction to create an electric potential between the electrodes, see Figure 2.1. By connecting individual cells, a stack is formed. Cells can be connected in series to obtain higher voltages or in parallel to obtain higher currents. FCs can use other types of fuel than hydrogen without reforming, but, due to poor reaction kinetics, this results in lower power densities [5].

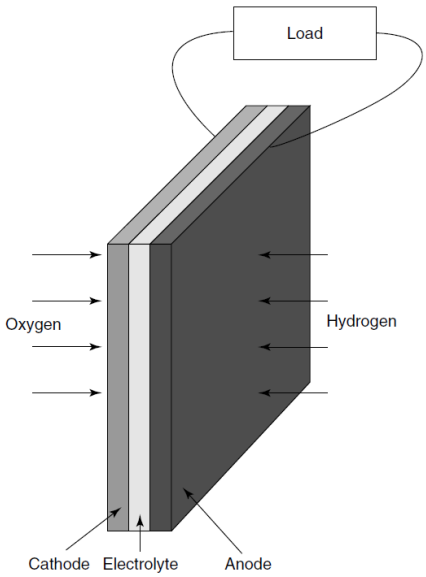

Figure 2.1: Schematic view of a single Cell [48].

Several types of FCs exist. The distinction comes from the electrolyte. It is often stated that the solid oxide fuel cell (SOFC) is the most promising type of FC for maritime applications [5]. Therefore, the SOFC is the type of FC of interest for this research.

[1] In this section on Fuel Cells, all information that does not have a citation comes from [48].

The electrolyte of SOFCs conducts negative ions from the cathode to the anode. The oxygen from the air flows along the cathode and there it will gain two electrons per oxygen atom. The electrolyte conducts these oxide ions. At the anode, the oxide ions react with hydrogen or carbon monoxide, which releases electrons. These flow via an external circuit to power a load and return to the cathode side. This is schematically visualised in Figure 2.2. The electrolyte is often made of zirconia stabilised with yttria (YSZ). The oxide conducting property comes from the presence of $Y3^{+}$ ions in the $Zr4^{+}$ crystalline structure. This leads to $O^{=}$ vacancies in the structure. To obtain low internal resistance, the electrolyte layer is extremely thin, in the order of tens of micrometres. The oxide conductivity of YSZ increases with temperature. Therefore, SOFCs are operated at elevated temperatures (500-1000 °C).

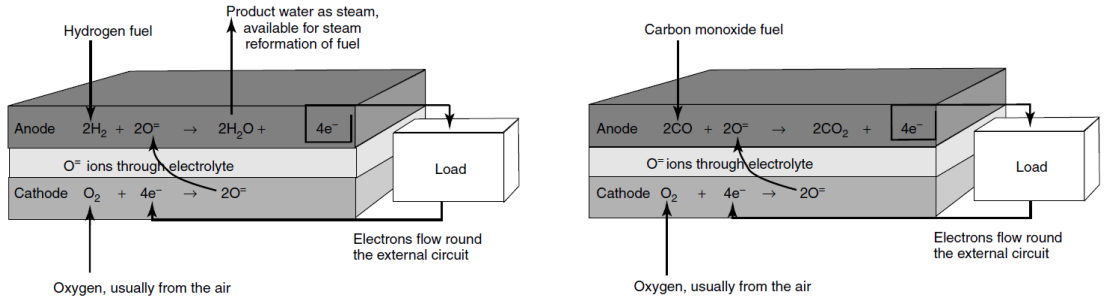

Figure 2.2: Schematic view of the reactions in an SOFC fuelled with hydrogen (first figure) or carbon monoxide (second figure) [48].

Fuel cell efficiency

FCs have an advantage over heat engines in terms of efficiency. Whereas heat engines convert chemical energy first into thermal energy and then into mechanical energy (and then possibly into electrical energy), FCs convert chemical energy directly into electrical energy. Therefore, the efficiency of an FC is not limited by the Carnot efficiency:

$$\eta_{carnot} = \frac{T_H - T_c}{T_H} \tag{2.1}$$

Here T_H is the temperature of the hot reservoir in K and T_c the temperature of the cold reservoir in K. The cold temperature is bound to the surrounding temperature. The hot temperature is limited by the mechanical properties of the materials and the formation of harmful emissions. For FCs, theoretical the efficiency is defined as:

$$= \frac{g}{h} \tag{2.2}$$

Here g is the change in Gibbs free energy and h the change in enthalpy of formation between reaction products. In this case, this reaction is the oxidation of the fuel. This enthalpy can therefore be exchanged for its calorific value. Gibbs free energy is defined as:

$$g = h - Ts \tag{2.3}$$

As can be seen from Equation 2.3, in case of a reversible process, the Gibbs free energy would simplify to the enthalpy of formation. This means that if it were a reversible process, an efficiency of 100% could be achieved. It can also be seen that the ideal efficiency of an FC is negatively influenced by temperature. In fact, for higher temperatures, this upper limit can be lower than the Carnot limit; see Figure 2.3. Note that the dependence of the Gibbs free energy on temperature varies for different types of fuel.

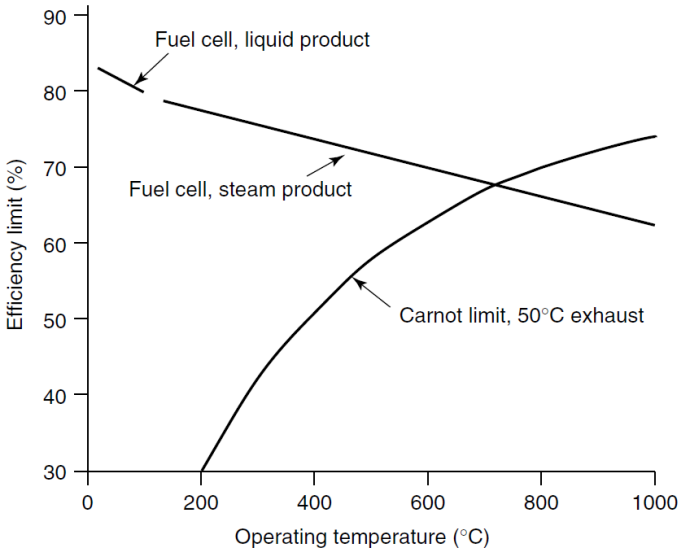

Figure 2.3: maximum efficiency of a hydrogen FC and heat engine [48].

Nernst equation

The efficiency of an FC can be calculated in a more practical manner using the ratio between operational and theoretical maximum voltage. The theoretical maximum voltage of an FC can be calculated using Equation 2.4:

$$E = -\frac{h}{n \cdot N \cdot e} \tag{2.4}$$

where E is the electromotive force (EMF); n the amount of electrons passing through the electrodes per molecule of fuel; N the Avogrado number and e the charge of an electron. For hydrogen FCs, this EMF is 1.25V when using the lower heating value (LHV) for h. The efficiency of a purely hydrogen fuelled FC, relative to the LHV, can therefore be described as in Equation 2.5.

$$= \frac{V_c}{1.25} \tag{2.5}$$

The operating cell voltage can be calculated using the Nernst equation; see Equation 2.6.

$$V_c = E_0 - \frac{RT}{nF} ln(\frac{p_J^j \cdot p_K^k}{p_M^m}) \tag{2.6}$$

With:

$$jJ + kKmM \tag{2.7}$$

as standard reaction; E_0 the EMF at standard pressure and $p_\#^\#$ the partial pressure. Here, the dependence of the efficiency on temperature is clearly visible.

Losses

Losses in FCs occur mainly as a result of four major irreversibilities: Activation losses, ohmic losses, fuel crossover losses and concentration losses. Activation losses occur due to the fact that energy is required to drive the reaction. Ohmic losses result from the internal resistance of the electrodes, the electrolyte and the interconnects. Fuel crossover losses occur when fuel leaks from the anode to the cathode. This can happen through leakage in the sealing or through the electrolyte. Electron transfer through the electrolyte also contributes to this type of loss, although to a smaller extent. The concentrations or partial pressures of fuel products affect the cell potential. This can be seen from Equation 2.6. The operating pressure can be isolated from Equation 2.6. From this isolation, the dependence of the EMF on operating pressure can be seen, where P is the absolute pressure:

$$V = \frac{RT}{nF} ln(P^{j+k-m}) \tag{2.8}$$

The ideal efficiency of an FC decreases with temperature and therefore, one would expect that the real efficiency decreases with temperature as well. This is, in fact, not the case. Due to the higher temperatures, the activation losses are reduced. A typical value of the activation loss for a low-temperature FC operating at 70 degrees Celsius is 25%. For an SOFC operating at 800 degrees Celsius, this is about 2 to 3%.

Balance of Plant
FC stacks cannot operate on their own. They may require heaters, coolers, ventilators/pumps, compressors transformers and fuel processors. These auxiliary components are called the balance of plant (BoP) and often require power, causing parasitic losses and thus possibly reducing the overall efficiency of the plant. These components can make up a significant part of the total system, reducing the power and energy density of the system. The required BoP depends on the type of FC and the type of fuel.

Fuel treatment
Practically all FC types are prone to sulphur poisoning. This is because sulphur compounds have a strong tendency to be adsorbed to the metal surface of the catalyst. This blocks the surface and therefore deactivates the catalyst. As sulphur is a component of fossil fuels, desulphurisation is required. Biofuels may also contain sulphur [2]. Only systems that run on very pure fuels do not require desulphurisation. This research focusses on green methanol. Due to to the production process of green methanol, it can be considered as 100% methanol and thus contains no sulphur [91]. Hence, desulphurisation is not further discussed.

As stated before, fuel cells often run on hydrogen. Therefore, fuels often have to be reformed. This will be further discussed in Section 2.1.2.

Power densities
Power density can be divided into the gravimetric power density, expressed in W/kg and the volumetric power density, expressed in W/L. In maritime operations, the volumetric power density is often rather the limiting factor than the gravimetric power density. For slow-speed diesel engines, this power density ranges from 20 to 80 W/L; for medium-speed engines between 40 and 250 W/L and for high-speed engines between 125 and 350 W/L [79]. However, these values do not contain auxiliary systems like cooling water- and lubrication oil circuits, exhaust treatment, fuel pumps, fuel treatment, etc. In addition to that, if the vessel has electric propulsion, the generator can comprise a large part of the plant. For the medium speed Wärtsilä 31 diesel engine, when considering the outer dimensions, the power density is about 120 W/L. For the W31 generator set, this is reduced to 65 W/L [96]. SOFC systems barely reach these power density values. Different studies report power densities between 8 W/L and 60 W/L [26], [23], [22], [5]. The low values include BoP components. The higher values only consider the dimensions of the FC. All these values are estimates by the corresponding authors. Installations that are now on the market have power densities of around 10W/L [13]. In this value, BoP components are included.

When considering energy density, another trend is visible. Although SOFC systems are bulkier than internal combustion engine (ICE) systems, their efficiencies often exceed those of an ICE. When fuel storage is also considered, the relative energy density of an SOFC system with respect to an ICE increases with running time. In Figure 2.4 power densities and energy densities for different operational durations are plotted on a Ragone chart.

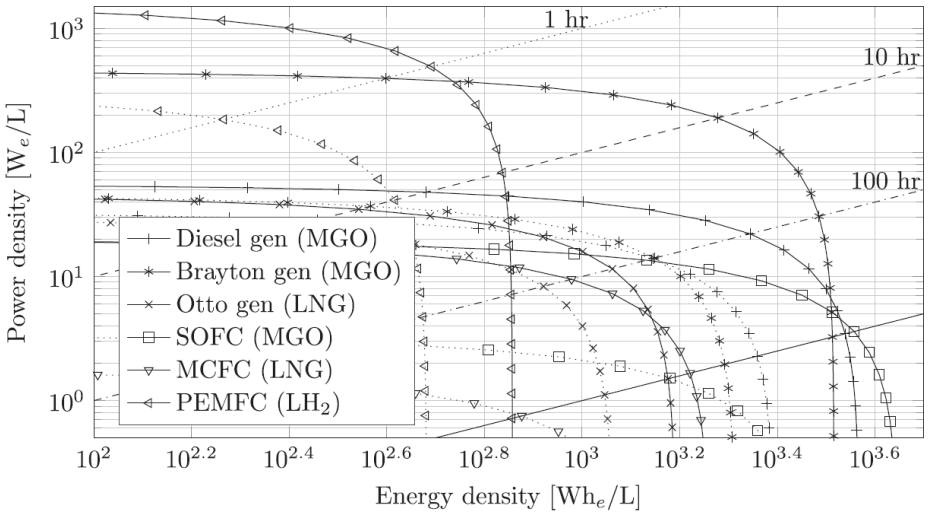

Figure 2.4: Power densities and energy densities for different drive systems and fuels. The dashed lines corresponds to the conservative estimates and the solid lines correspond to the upper estimates. [5]

Dynamic behaviour

One of the main obstacles to implementing SOFC systems in commercial power generation is the load-following capabilities of the system [103].

The resistance of the electrolyte increases exponentially with a decrease in temperature. Therefore, SOFCs are designed to operate at their temperature limit. In addition to that, reaction kinetics increase with higher temperatures. This means that the power density decreases drastically with a decrease in operating temperature.

If more power is drawn from the system, the reaction rate increases, resulting in higher heat production. This heat is partially consumed by the increase in fuel reforming, if internally reformed. To remove the remaining heat, additional cooling is required. This must be provided by the cathode air. As air is a poor cooling agent, large flow rates are required. An additional problem is the control system. When an increase in temperature is detected in the anode off-gas (AOG), correction can already be too late. The increase in AOG temperature also has a strengthening effect. The heat from the AOG is used in heat exchangers to preheat the fuel stream. This means that the fuel stream is additionally preheated due to the increase in temperature of the AOG. Together, this means that a rapid increase in power results in increased stack temperatures, which result in sintering of the porous layers and therefore a decrease in surface area for reactions to occur [9].

A possibility to avoid this obstacle is the use of low-temperature SOFCs. Gao et al. [29] investigated such system at a temperature between 500 to 600° C. By using electrolytes with a carbonate content (wt%) of 30%, a power density of 577 mW cm^{-2} was obtained. However, no values on efficiency were stated. Also, at such low temperatures, carbon deposition can occur.

Due to the thermal coupling between different components of the SOFC plant, the heat management of such a plant is complex. Hence, it is expected that the heat management is expected to be a major part of the design process.

Bottoming and combined cycles

As explained in Section 2.1.1, the EMF depends on the partial pressures of the fuel. This means that close to the exhaust, where the partial pressure of the fuel is lower due to fuel utilisation, the EMF drops. Resulting in either a drop in efficiency or power density. Therefore, not all fuel is used and the AOG still contains fuel. As the SOFC operates at elevated temperatures, thermal energy is left in the AOG as well. This heat can be used in heat exchangers or in bottoming cycles. Bottoming cycles burn the fuel that is in the AOG to drive a heat engine. This can be a gas turbine, a steam turbine or a combination of these two. Using both heat and fuel, very high efficiencies of over 70% can be obtained [5]. In such a system, the bottoming cycle only assists the SOFC in reaching a high efficiency, i.e. the majority of the power is delivered by the SOFC. This means that the problems with dynamic behaviour discussed in Section 2.1.1 are not solved.

By increasing the power split ratio of bottoming cycle / SOFC, a so-called combined cycle is obtained. The heat engine is no longer completely dependent on the AOG, but also has its own additional fuel flow. This means that now a reciprocating engine is also a realistic option, which generally has a higher efficiency than the steam or gas turbine. Because the power split is increased, favouring the ICE, the total efficiency is reduced, relative to that of the SOFC with the bottoming cycle. However, literature mentions examples of combined cycle that can achieve higher efficiencies than the stand-alone SOFC or ICE [5], [74], [6]. In exchange for efficiency, dynamic performance is obtained. In addition, when the ICE is also provided with an additional fuel line, the coupling between the ICE and the SOFC is significantly reduced in complexity [74]. The SOFC can provide a base load and the ICE can cope with the changes in load. This system has the advantage of the high efficiency of the SOFC; AOG energy usage of the bottoming cycle; and the dynamic capabilities of the ICE.

Modeling SOFC systems

SOFC models can be classified into three groups: the white-, gray- and black-box approach. The white box models include physical models and equivalent circuit models based on Electrochemical Impedance Spectroscopy. Black-box models are based on experimental data and use methamatical models or artificial intelligence to make predictions. Grey box models are physical models in which some components or phenomena are empirically modelled [94]. The models can range from zero-dimensional to three-dimensional, where higher-dimensional models are best suited for cell design and lower-dimensional models are more applicable to system designs [94], control engineering or voyage simulations. As this research involves the performance of a combined SOFC-ICE system, it is expected that the SOFC model will be a low-dimensional grey model.

2.1.2. Methanol-fuelled SOFC

As discussed earlier, FCs often run on hydrogen. This means that either the pure hydrogen is stored onboard or it is contained in a hydrogen carrier. For hydrogen carriers, fuel reforming is required. For SOCFs, this can be done externally and, under certain conditions, internally. This research focusses on a methanol-fuelled SOFC.

Reforming

When fuel gasses, such as methanol and CO, are heated in anaerobe conditions, they decompose into C and H_2 and C and CO_2 respectively. These carbon formations can form an isolating layer on the electrodes, obstructing its performance. This deactivation of the electrodes is a permanent consequence and shortens the lifespan of the stack. Therefore steam is added to the fuel gas stream to provide for the steam reforming reaction. For methanol, the reactions that occur are:

$$CH_3OH \longrightarrow 2H_2 + CO \quad [\Delta h = +90.7\ kJ\ mol^{-1}] \tag{2.9}$$

$$CO + H_2O \longrightarrow H_2 + CO_2 \quad [\Delta h = -41.2\ kJ\ mol^{-1}] \tag{2.10}$$

The reactions from Equations 2.9 and 2.10 together form the reforming reaction, resulting in the following.

$$CH_3OH + H_2O \longrightarrow 3H_2 + CO_2 \quad [\Delta h = +49.7\ kJ\ mol^{-1}] \tag{2.11}$$

This reaction is endothermic. When the reforming process happens in an external reformer, it consumes additional heat and or power and thus possibly lowers the overall efficiency. Due to the high temperatures at the anode, the reforming may be possible internally. As the process consumes heat, internal reforming provides additional cooling to the system. Therefore, cooling systems consume less power, resulting in higher efficiencies. Also, the BoP can be less bulky. These reforming processes can have a large impact on the heat management of the system.

In addition to the steam reforming reaction, the methanation reactions can occur [40]:

$$CO + 3H_2 \longrightarrow CH_4 + H_2O \quad [\Delta h = -205.9\, kJ\, mol^{-1}] \tag{2.12}$$

$$CO_2 + 4H_2 \longrightarrow CH_4 + 2H_2O \quad [\Delta h = -164\, kJ\, mol^{-1}] \tag{2.13}$$

These reactions consume hydrogen and it was therefore expected that they were unwanted unwanted. It is also an exothermic reaction, producing additional heat. the expectation was that this required additional cooling, but it can also provide heat for the reforming of methanol.

It was expected that these reactions, which consume hydrogen, would be detrimental to the process. Additionally, it was believed that the exothermic nature of the reactions would necessitate additional cooling. However, the heat produced by these reactions can also be utilised for the reforming of methanol, providing a potential benefit to the process. The fact that there still exists methane in the AOG is not necessarily a problem. If fuel is still present in the AOG, it can be consumed in a bottoming or combined cycle. The significance of the methanation reactions will be further discussed in Section 3.1.2.

Although water is added, carbon deposition can still occur. The amount of carbon deposition can be influenced with the methanol/steam ratio, temperature and reforming method. For a smaller ratio and higher temperatures, the carbon formation goes down. Furthermore, for both conditions, the hydrogen yield increases [47].

Direct and indirect internal reforming

The internal reforming process can be direct (DIR) and indirect (IIR). DIR occurs in the cell at the anode. Here, the hydrogen that is produced is directly consumed again by the anode. This again lowers the partial pressure of hydrogen and thus, due to Le Chatelier's principle, favours the right-going reaction from Equation 2.11. It makes the reforming process more efficient, resulting in a high hydrogen yield. During the consumption of hydrogen at the anode, steam is also produced. This means that less steam has to be added to the fuel stream.

DIR might induce thermal stresses. Because the concentration of methanol is highest at the cell entrance, most of the reforming takes place at this entrance. As the concentration of the methanol drops towards the end of the cell, the concentration of hydrogen rises. This increases the reactivity of hydrogen at the anode. As this anode reaction is endothermic, a temperature gradient can occur, leading to thermal stresses [11].

With IIR, the product stream flows along the cell, where it reforms, before entering the cell. The advantage of this is that there is significantly less carbon deposition on the anodes. There is also less methane production [47]. This offers the possibility of using temperatures lower than those of DIR [47]. A disadvantage relative to DIR is that the system requires a more complex layout of the fuel supply channels; reforming channels adjacent to the cells receive most of the heat from the anode reactions. Also, because the hydrogen is not directly consumed, the right-going reaction from equation 2.11 is less favoured than with DIR, resulting in a lower hydrogen yield. Similarly to methane in AOG, the lower hydrogen yield is not necessarily a problem, as it can be consumed in a bottoming cycle.

To promote the reforming process, catalysts are used. In DIR, catalytic anodes are used. Often, Ni/YSZ is used as anode material because it meets the SOFC requirements and because of its costs [47]. In IIR, Ni/Ce–ZrO_2 can be used in the reforming channels to prevent carbon deposition on the Ni/YSZ anodes [47]. However, Ni-based alloys can also work as a catalyst in the methanation reaction from Equation 2.12 [101]. To bypass this effect, Peppley [68] investigated a copper-based alloy. He reported that methane formation was completely avoided with this type of alloy.

AOG composition

As discussed in Section 2.1.1, the AOG not only contains reaction products from the anode but also contains other products. The reforming reactions are in equilibrium, resulting in methanol left in the the AOG. Also, there is the methanation process from Equations 2.12 and2.13. However, the use of copper-based catalysts can prevent this. Other reaction products from the reforming process are carbon monoxide and carbon dioxide [47]. The resulting blend can consist of methanol, methane, hydrogen, carbon monoxide, carbon dioxide and steam. The partial pressures depend on the operation conditions of the SOFC and its BoP, type of reforming and type of catalyst.

Methanol-fuelled SOFCs for Maritime applications
In 2010, Wärtsilä installed their WFC20 SOFC system on the car carier Undine to provide auxilairy power. This SOFC runs on methanol and provides 20 kW of power. An emission reduction was demostrated, consisting of no carbon monoxide no SO_2, reduced NO_x and a reduction of 40% CO_2 [83]. Unfortunately, no figures on efficiency were reported. As far as the author is aware, there are no other documented cases of methanol-fuelled SOFCs onboard ships. However, there are publications on methanol-fuelled SOFCs for maritime applications. Rechberger et al. [70] developed a demonstration system for a methanol SOFC Auxiliary power unit (APU) for ships. The 4.5 kW installation achieved efficiencies of 40 to 50% for a fuel utilisation factor of 0.6. the remaining fuel in the AOG is mixed with the COG and then burned in a catalytic burner to provide heat for the reforming process.

2.2. Internal Combustion Engines

The mature and well-understood technology of the internal combustion engine (ICE) is superior to the SOFC in power density, load following capabilities, CAPEX, and life span. However, questions may be raised when talking about the actual power density numbers. The power density of an SOFC consists of the stacks and the entire BoP. This must also be considered with the ICE as briefly discussed in Section 2.1.1. In addition, the total power density of the entire drive system should also include fuel storage. As, generally speaking, an SOFC has a higher efficiency, it requires less fuel for the same voyage. The results of this can be seen in Figure 2.4. As discussed in Section 2.1.1, the efficiency of an ICE is generally lower than that of an SOFC due to the irreversibilities in the combustion process, frictional losses, etc. In this section, when ICE's are discussed, reciprocating engines are meant.

In the first section, the properties of methanol as an ICE fuel are discussed. Then the behaviour of an AOG-methanol mixture is evaluated. The resulting emissions are then discussed. This chapter is concluded with a brief discussion on ICE modelling.

2.2.1. Methanol as fuel

Methanol is closely related to ethanol, considering their combustion behaviour. This is due to their similar octane number, heat of evaporation and their stoichiometric ratio [92]. As there is a lot of existing data on ethanol combustion, this similarity makes it easier to predict the behaviour of methanol. However, methanol does has its advantages over ethanol. First, there are the production methods that are possible. Ethanol is produced in a biological process. Methanol can be produced in a chemical process, which is faster than a biological process [92]. Secondly, methanol does not contain carbon-to-carbon bonds. This reduces the risk of pollutant emissions. The emissions of methanol are further discussed in section 2.2.3. A disadvantage of methanol, compared to ethanol, is its toxicity. However, Gable [28] reported in its research that a fatal dose of ethanol, per kg of body mass, is only twice as much as methanol. The toxicity will be further discussed as well in section 2.2.3.

Methanol has a high autoignition temperature (738 K). Together with its high heat of evaporation and low air-to-fuel ratio (AFR), this corresponds to its high octane number [20], which results in good knock resistance. For a spark ignition (SI) engine, this means higher compression ratios can be obtained. This in term results in a higher efficiency. When methanol is used in a compression ignition (CI) engine, a high minimal compression ratio is expected.

The cetane number of methanol is very low. This number represents the time it takes to ignite the fuel. Therefore, methanol has a long ignition delay [92]. This can be problematic for CI. Due to the longer ignition delay, it can be challenging to time the fuel injection in order to obtain peak pressure shortly after top dead centre (TDC) [92]. This is desirable for a higher thermodynamic efficiency. Also, the engine speed is limited due to the same effect. To deal with this problem, a pilot fuel would be required for a CI engine. However, an SI engine would not require pilot fuel. As the spark initiates the ignition, SI is not affected by the cetane number. Besides that, the burning velocity of methanol is relatively high [92]. This ensures a rapid combustion, and therefore peak pressure shortly after TDC.

Due to the hydroxyl group in a methanol molecule, hydrogen bonds are formed within the liquid [92]. These bonds contribute to the high heat of evaporation of methanol. This has some beneficial effects, besides its contribution to the octane rating [20]. To get as much oxygen into the cylinder as possible, intercoolers are used between the turbocharger and the engine intake. In a port injection engine, the heat of evaporation causes the intake air to be cooled. As methanol has such a high heat evaporation, less intercooling is required. This also results in lower cylinder temperatures [92]. As a result, there are

less heat losses. Also, as the peak temperature is reduced, a significant reduction in NO_x formation is obtained [92]. As the hydroxyl group contains already an oxygen atom, the stoichiometric air-to-fuel ratio is relatively low. This means that more fuel will be injected for the same cylinder volume. This in term means additional evaporation cooling.

Compared to diesel and methane, methanol has a significantly reduced LHV. This reduced LHV means that more fuel has to be injected for the same power. This, in combination with the low stoichiometric ratio, results in additional cooling, as described in the previous paragraph. However, the low stoichimetric and LHV also have balancing effect on air consumption. Both values are roughly half of that of diesel. This means that the air consumption is in the same order of magnitude. It is therefore expected that less changes are required to air feed system, including the turbocharger. The larger amount of fuel required results also in longer injection durations. This can be disadvantageous for CI. These properties, along with the properties discussed in previous paragraphs, are shown for these three fuels in Table 2.1. Here, F76 is representing diesel fuels.

Table 2.1: Fuel properties of methanol, F76 and methane.

parameter	methanol [92]	F76	methane [92]	unit
Lower heating value	20.09	42.58 [88]	50	[MJ kg^{-1}]
Cetane number	3	45.1 [88]	-10	[-]
Octane number (motor - research)	92-109	N/A	120 - 120	[-]
Density (STP)	790	840 [87]	0.65	[kg m^{-3}]
Heat of evaporation	1100	270 [75]	510	[kJ kg^{-1}]
Autoignition temperature	738	527 [75]	813	[K]
Stoichiometric AFR	6.5	14.8 [87]	17.65	[kg kg^{-1}]
C content	37.48	86.6 [88]	74.87	[wt.%]
H content	12.58	13.1 [88]	25.13	[wt.%]
S content	0	0.05 [88]	0	[wt.%]

Methanol in maritime applications

Svanberg et al. [86] indicated the barriers to the implementation of biomass methanol in the maritime sector. Svanberg found the following potentials to improve the implementation of methanol in the maritime sector: optimisation of the feedstock supply chains; larger scales for testing of renewable methanol production; research to the required purity of the methanol; and policy drivers for reducing emissions in the shipping industry. MAN is developing a four-stroke methanol engine for maritime applications. The market introduction of the first methanol ready solution is expected in mid-2022. It will be a port fuel injection spark ignition engine [58]. Wärtsilä is already offering a methanol version of its W32 engine line. In fact it is a multi-fuel engine, as it can also run on HFO, MDO and liquid biofuels [97]. Since 2015, they have tested the system on the Stena Germanica ferry. The system is now implemented in a new vessel from Van Oord [97].

2.2.2. Methanol-AOG mixture as fuel

In this research, we will focus on a combined SOFC-ICE cycle. This means that the ICE will not be fuelled solely with methanol. The AOG is a mixture of methanol, methane, steam, hydrogen, carbon dioxide and carbon monoxide. By cooling this mixture, the steam is removed from the AOG. The combustible products in the remainder AOG stream are methanol, methane, hydrogen and carbon monoxide.

The combustion properties of these substances can vary. The composition of this product stream depends on the operational conditions of the SOFC plant. This, together with the additional injected methanol, results in a non-consistent fuel composition. Therefore, the autoignition temperature of the mixture is not constant. This may impose problems for a CI engine. The fact that the fuel is not consistent could also cause problems for an SI engine. Because the mixture is non-consistent, its octane rating and therefore its knock behaviour may vary. However, for this fuel blend, this is not a problem. The octane ratings for methane, hydrogen and carbon monoxide all exceed that of methanol [92], [69], [82].

As the AOG is a gas, high pressure injection is not practical, as it requires significant compression work [74]. This presents an additional challenge for CI. High pressure direct injection results in a short fuel injection timing, resulting in a pressure peak closely after TDC, which is desirable for obtaining maximum brake torque [64]. Also, it ensures that the fuel brakes up in minuscule droplets that easily evaporate, but for a gas, this is of course not necessary.

The low cetane number of methanol, the inconsistent mixture of fuel and the gaseous phase of the AOG, led to the decision that this research will focus on a port injected SI engine. However, during the modelling phase, it was observed that there were issues with insufficient heat. This is further discussed in Section 3.2.2.

2.2.3. Safety risks

The toxicity of methanol causes resistance to the implementation of it as a fuel. Methanol itself is not toxic, but due to the metabolism of the human body, it gets converted to formaldehyde and then to formic acid before it gets converted to carbon dioxide and water [92]. The former two substance are toxic and may damage the nervous system. Methanol can enter the body via ingesting, inhalation, eye contact and skin contact. Doses between 1 to 2 mg per kg of body mass are lethal [92]. It is therefore important to handle the fuel with care.

According to Machiele [56], the flammability index of methanol is comparable to that of diesel. However, its flashpoint is significantly lower (12°C [92] against minimum of 55°C [31]) than that of diesel fuels. Therefore, methanol requires extra safety measurements [85]. However, there is a major advantage of methanol regarding fire safety. As methanol is miscible with water, methanol fires can be extinguished with water. A drawback of methanol fires over diesel fires is that pure methanol flames are barely visible in sunlight [92]. This can make detection harder.

An additional problem with methanol is its corrosive nature. Due to its polarity it can attack both metals, especially aluminium, as well as softer materials used for seals, fuel lines, etc. Methanol is corrosive to the aluminium oxide layer that covers and protects the aluminium against further oxidation. When this layer is destroyed by methanol, the underlay aluminium oxidises due to contact with the air and the cycle starts over [63]. Also, because methanol is an electronically conductive material, it can lead to galvanic corrosion [92]. Metals that are often used in situations where methanol is present are austenitic stainless steel and zinc- or nickel- alloy coated metals. Additional substances in the fuel can increase the level of corrosion, but in this research, pure methanol is assumed.

2.2.4. Emissions

In this research, green methanol is considered. This means that no fossil fuel is used for the production of methanol; neither as feedstock nor as an energy source. Moreover, the methanol will either be produced with biomass from agricultural residue's, to prevent the conflict between food production and energy supply [42]. The other option would be to use carbon capture in combination with green hydrogen to produce methanol. This makes it a net-zero fuel. Therefore, carbon dioxide emissions are compensated during the production process. However, the CO_2 emissions can still be compared, for instance, to diesel or methane. When it is assumed that different fuel types have no effect on system efficiency, it can be calculated that methanol has about a 25% increase in CO_2 emissions compared to methane and close to 10% less CO_2 emissions as diesel. [2]

NO_x emissions form due to the oxidation of nitrogen and oxygen from the air. The formation depends largely on the duration of the combustion process, the peak temperature in the cylinder and the partial pressure of oxygen [80]. Due to the long ignition delay of methanol and that it will not be a CI engine, the air-fuel mixture will be better mixed. This results in a more homogeneous mixture and therefore less pockets of richer air-fuel mixtures. This reduces the risk of high local peak temperatures. This, together with the high heat of evaporation of methanol, lower adiabatic flame temperature and high burned gas heat capacity, result in a lower overall and local peak temperatures [92]. This makes methanol a promising fuel when considering NO_x reduction.

As the methanol is produced as a green fuel using carbon capture, it can be assumed that the fuel has no sulphur content, and therefore eliminating emissions related to sulphur. These contents of methanol, F76 and methane can be compared in Table 2.1.

[2] This can be checked by looking at the mass fraction of carbon in fuel, divided by its lower heating value. For methanol this is roughly $\frac{12}{32} \cdot \frac{1}{20} = 0.01875$, For methane this is $\frac{12}{16} \cdot \frac{1}{50} = 0.015$, for diesel, using Table2.1, this is $\frac{0.866}{42.58} = 0.0203$.

As a result of incomplete combustion, unburned hydrocarbons can be emitted. This type of emission can be influenced by the equivalence ratio of the mixture and can be minimised by a homogeneous air-fuel mixture [92]. An additional source of unburned hydrocarbons can be the partial burning of lube oil [80]. Additionally, methanol does not consist of long-chained hydrocarbons. Therefore, the change to form particulate matter (PM) in the cylinders due to incomplete combustion is significantly reduced. Also, there are no sulphur compounds present that would otherwise condensate on PM [80].

Despite the numerous benefits of methanol as a fuel source, it does possess one notable drawback in the form of formaldehyde (HCHO) emissions. It is an intermediate species in the oxidation process of methanol. Its formation peaks at moderate temperatures (1000K). with PFI engines, methanol can enter slits during the compression stroke but then escapes these slits during the expansion stroke. They are therefore more susceptible to HCHO emissions than DI engines. As such, the development and implementation of effective aftertreatment methods for formaldehyde reduction is crucial for the reduction of harmful emissions [92].

2.2.5. ICE modelling

As with the SOFC, an ICE can be modelled from zero up to 3 dimensions. The use of higher order of dimensions results in additional complexity and computational time, but gives more detailed insights. Lower dimensional models are more suited for system analysis. The cylinder can also be discretised into multiple zones going from a single zone to the level of CFD calculations. These models give more insight in the local combustion behaviour. This can be useful for predicting emissions [73].

In a 0-dimensional model, the combustion process is often modelled using a single or double Wiebe function [72]. The Wiebe function represents the heat release using the mass-burn rate as a function of the crank angle [73]. The model requires empirically determined coefficients to match experimental data. This approach has proven to be an efficient method for modelling engine processes [72].

Another approach for modelling the combustion of a 0-dimensional model is the use of the Seiliger process [72]. The combustion of the Seiliger process consist of isochoric, isobaric and isothermal combustion. The model does not give insight of the combustion progress as a function of crank angle, but discretises the cyclic cylinder process in six stages. Still, the Seiliger process can provide sufficient information on the in-cylinder process for low computational effort [72], depending on the research objective. There is also the possibility to use the five-stage Seiliger cycle, which is more widely used nowadays [24]. Here, the combustion is modelled only as an isochoric and an isobaric phase.

In the work of Sapra [73], the author compared the Wiebe with the Seiliger approach against experimental data for a lean-burn SI hydrogen-NG (natural gas) engine. Although the Wiebe approach gave accurate estimates of the pressures and temperatures, it was overall less accurate than the Seiliger approach regarding the work output and combustion heat estimates. Using a turbocharged SI NG marine engine in a test setup, test data was acquired. The maximum deviation from the measured data of the Wiebe approach was found to be 5.2 % where as the Seiliger approach only deviated 2%.

2.3. SOFC-ICE combined cycles

In this chapter, research on combined cycles will be discussed. From this the knowledge gap will be exposed. In the problem statement section, the research question will be formulated. This chapter will be concluded with a prospect of the research.

2.3.1. Combined cycle research

The promising technique of the fuel cell, and in particular the SOFC, can provide fuel savings and reduced emissions over traditional maritime power plants. As discussed in Section 2.1.1, combining an SOFC with an ICE can improve efficiency and improve dynamic behaviour. Park et al. [67] compared the performance of a stand-alone SOFC, an SOFC-GT and an SOFC-HCCI cycle on NG. For this he modelled the stack as lumbed body (0D) for the thermal analysis and used SOFC specifications that were in line with the technology state during the time of writing. The gas turbine (GT) was modelled as an isentropic model with corresponding efficiencies. The HCCI ICE was modelled as an Otto cycle. with an SOFC fuel utilisation factor of 0.75, the combined SOFC-ICE cycle reached a net efficiency of 59.5%, the SOFC-GT 58.6% and the standalone SOFC an efficiency of 51.7%. However, in this research, the ICE replaced the catalytic combustor, i.e. it was a bottoming cycle and not a combined cycle. This is reflected in the ICE/SOFC power split of 13/87.

Sapra et al. [74] evaluated an NG hybrid plant as well. He modelled an SOFC by extrapolating a single-cell model. The 0-dimensional model is based on the work of Aguiar et al. [1]. The lean-burning SI engine model was based on the Seiliger-cycle and experimental data. The engine operated on AOG and additional introduced NG, making it a combined cycle. The optimal performance from an efficiency perspective was obtained with a power split of 67/33 and a fuel utilisation factor of 0.85 resulting in a total efficiency close to 45%. This is low compared to the work of Park et al.[67]. This can be explained by the fact that Sapra et al.[74] modelled an ICE with limited efficiency. Besides that, he modelled a combined cycle and Park et al. [67] a bottoming cycle.

Koekkoek [44] conducted a similar research for his graduation thesis. However, he did not use NG but ammonia as fuel. Ammonia itself is not a suitable fuel for an ICE. A pilot fuel is required. This pilot fuel is provided from an excess of reformed ammonia from either internal reforming in the SOFC or from an external reformer. In order to provide enough hydrogen in all evaluated power splits in the work of Koekkoek [44], an external reformer was added to the plant. The SOFC was operating on elevated pressures and was 0-dimensionally modeled. Using heat exchangers, heat from the SOFC is reused. In the condenser, the water is removed from the AOG. The resulting hydrogen/nitrogen mixture is lead to the turbocharged ICE, where additional ammonia is introduced, making it a combined cycle. As with the research of Sapra et al.[74], the ICE was modeled with a Seiliger-cycle. The resulting engine exhaust gases are treated before being emitted into the atmosphere. The model can be seen in Figure 2.5. With a $P_{SOFC}P_{ICE}$ 75/25 power split, an efficiency of 58% was obtained. This is remarkably higher than the combined cycle of Sapra et al.[74]. This can partly be explained by the fact that Sapra et al. [74] modelled the ICE with an efficiency of approximately 34% and Koekkoek [44] at 43%.

One research was found that modelled an SOFC combined cycle on methanol and compared a plant with internal and external reforming to an internally reforming NG combined cycle. However, in this research by Cocco and Tola [21], the SOFC was combined with a GT. This makes it a different plant than with a reciprocating ICE, but still valuable for comparison purposes. The fuel utilisation factor of 0.85 was constant for all cases. For the internal reforming methanol plant, a power split of 72/28 was obtained, resulting in a total efficiency of 63.6%. The external reforming methanol plant operated at a power split of 73/27 and a total efficiency of 68.5%.

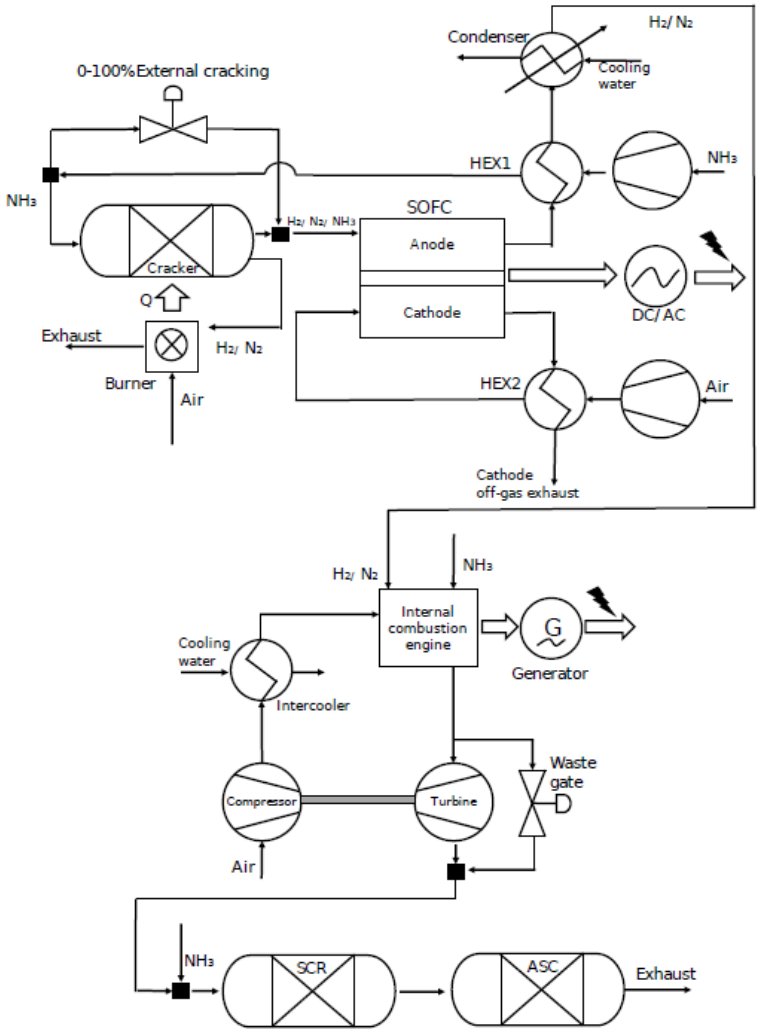

Figure 2.5: SOFC-ICE model from the research of Koekkoek [44].

2.4. Problem statement

The development of new technologies and fuel usage is essential for reducing the environmental impact for all sectors [90]. The IMO indicated methanol as a promising alternative fuel for the maritime industry [37]. Together with the promising results from the studies on combined SOFC-ICE cycles discussed in Section 2.3.1, this led to the proposal of the development of a novel drive system.

In this research a methanol fuelled SOFC-ICE combined cycle will be analysed. This analysis will be used to evaluate the performance of such a plant in maritime applications. This led to the following research question:

How does a methanol-fuelled SOFC-ICE combined cycle perform as power plant for ships compared to alternative, comparable power plants?

In order to answer this question, the following subquestions are formulated:

- **What are the performance characteristics of a methanol-fuelled SOFC-ICE combined cycle in maritime applications?**
- **How will the system's performance be modelled and verified?**
- **How does the implementation of the combined cycle influence the efficiency performance of the ship at nominal output compared to a stand-alone methanol-fuelled ICE or an ammonia-fuelled combined cycle?**

Research prospect

Using model simulations, the performance of a methanol fuelled SOFC-ICE plant will be evaluated. This model will be constructed with MATLAB & Simulink. As the model will evaluate a combined system, the choice is made to make it zero-dimensional. It will consist of an SOFC model, an ICE model and the sub-models for all additional components such as reformers, heat exchangers, compressors etc.

The existing model of Koekkoek [44] will function as the basis for the SOFC model. The reforming process is expected to be the point of interest with the most significant adaptations.

The Diesel Engine A model from the department or Maritime and Transport Technology of the TU Delft will be used as the basis for the ICE model. There is also the aim to improve the models accuracy during the isentropic compression and expansion, without intensifying the computational effort of the model.

With results from literature that modelled in a similar way, the model will be validated. The performance of the plant will then be evaluated for different power splits and, if time allows, part load conditions. By using similar models and assumptions as [44] the performance characteristics between an ammonia and methanol-fuelled plant can be compared. This is of particular interest as both fuels are promising alternatives for fossil fuels.

Suitability characteristics of maritime power plant have to be defined, in order to evaluate the implementation of a methanol fuelled SOFC-ICE into a ship to provide the main power generation for propulsion and auxiliary power. Van Biert [11] indicated the following characteristics in his PhD thesis:

- Electrical efficiency;
- Power and energy density;
- Environmental impact;
- Load transients;
- System start-up;
- Safety and reliability;
- Economics.

The aim of this research is to address the first four characteristics. The most important factor for a power plant design is the operational profile of the vessel. Thus, a plant will be designed after the operational profile of the vessel has become known. If time allows, a case study will be conducted. As the focus of this research is to investigate the possibilities of an alternative power plant, a reverse approach is used. When the performance profile of the power plant is known, the operational profile of a vessel has to be matched. Then the performance of the vessel will be evaluated with three different power plants:

- The proposed combined methanol-fuelled SOFC-ICE plant;
- The combined methanol-fuelled SOFC-ICE plant proposed by Koekkoek [44];
- A stand-alone methanol-fuelled ICE plant

From this a conclusion can be drawn about the possibilities of a methanol fuelled SOFC-ICE combined drive system in maritime applications.

3

Methodology

In this chapter, the methodology of this research will be presented. Two different models in MATLAB & Simulink will be adopted and combined. First the initial models will be discussed and their key characteristics will be outlined. Then the adaptations to fit the specific research needs are explained. Finally, we will discuss how the models were combined to form a unified whole.

3.1. Solid oxide fuel cell model

In this study, a zero-dimensional model of an SOFC will be developed. By using a zero-dimensional approach, we aim to provide a simplified representation of the SOFC that can capture its essential characteristics and behavior.

3.1.1. Method in existing model

The SOFC model proposed by Koekkoek [44] forms the basis of the SOFC model. In his work he extrapolated a single cell zero-dimensional model. The BoP components that where included are an external cracker with heater, heat exchangers and fuel/air pumps.

The model consists of several submodels:

- Cell mass balance.
  Using defined reaction rates, a mass balance per substance is made. This balance is made for the cathode- and anode channel separately.
- Cell energy balance.
  With the results of the cell mass balance in combination with the temperature-dependent enthalpies of the substances, the energy balance is set up.
- Cell electrochemical model.
  As with the cell energy balance, the mass balance is used here as input. Together with the operating temperature and partial pressures, the open circuit voltage is calculated. From this, the ohmic, activation and concentration losses are withdrawn.
- External cracker.
  The external cracker consists of a mass balance and an energy balance that includes a heat exchanger. From this the additional heat from a methanol burner is calculated.
- Air and fuel blower.
  Due to a pressure drop over the cell, energy is required. The increase in pressure due to the blowers result in a temperature increase, which corresponds to the power required by the blowers.
- Heat integration.
  This submodel evaluates the possibility to preheat the anode and cathode inlet flows with the corresponding outletflows. Here, also the condenser for the AOG is modelled.
- output.
  The output block acts like a dashboard of the model. It provides values for operating parameters such as efficiencies, powers, voltage, molar flows, etc.

These submodels are visualised in Figures 3.1 and 3.2.

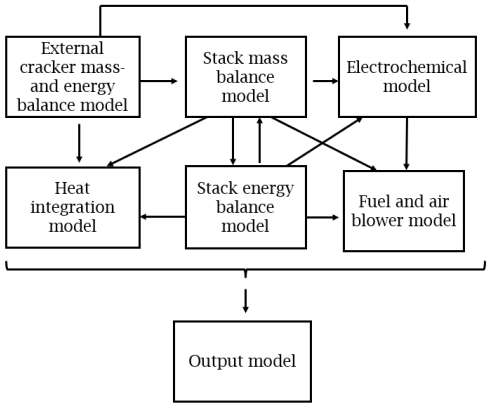

Figure 3.1: Block overview of the SOFC model proposed by Koekkoek [44].

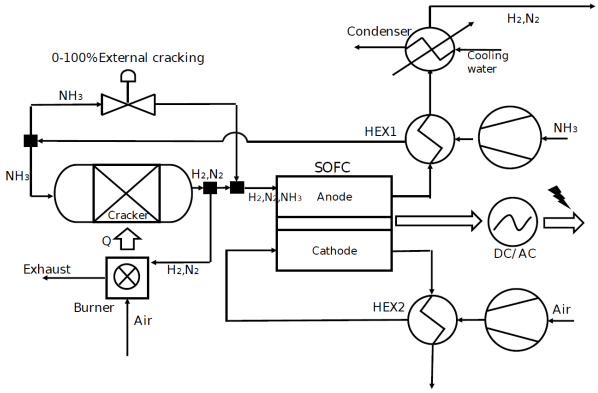

Figure 3.2: Layout of the SOFC model proposed by Koekkoek [44].

Mass balance of the cell

For solving the mass balance, the same method as Kang et al.[41] is used. This method is based on the assumption that only a hydrogen oxidation reaction (HOR) and a fuel decomposition reaction (ammonia decomposition reaction, ADR) occur at the anode of the SOFC:

$$H_2(g) + \frac{1}{2}O_2(g) \longrightarrow H_2O(g) \tag{3.1}$$

$$NH_3(g) \longrightarrow 1\frac{1}{2}H_2(g) + \frac{1}{2}N_2(g) \tag{3.2}$$

The rates at which these reactions occur are the input to the mass balance. The HOR rate per surface area is determined by the current density:

$$r_{HOR} = \frac{i}{n_e F} \tag{3.3}$$

Here i is the current density $[A/m^2]$. It is assumed that all ammonia is decomposed. This means that the ADR rate is determined by the molar flow of ammonia. The mass balance for a substance is then defined as

$$\frac{PV}{RT}\frac{\mathrm{d}x^{out}}{\mathrm{d}t} = \dot{N}^{in} - \dot{N}^{out} + WL \cdot (v_{HOR}r_{HOR} + v_{ADR}r_{ADR}) \tag{3.4}$$

Here $\dot{N}$ is the molar flow in the channel; W the width of the channel; L the length of the channel; v the stoichiometric coefficient of the substance in the corresponding reaction; and $\frac{dx}{dt}$ denotes the

dynamic component of the total molar change of the substance. This can be done for both the anode and the cathode.

Heat management is controlled using the air excess ratio. Therefore, a PID controller is implemented in the mass balance.

Cell energy balance

The energy balance per cell is given by 3.5. The proposed model neglects the heat capacity of gaseous substances, instead focussing exclusively on the solid components of the cell, specifically the PEN structure and interconnects, in the calculation of the $m \cdot c_p$ component. $\dot{N}$ is the molar flow vector containing all substances. Using the corresponding enthalpy vector $\bar{h}$, the inflow and outflow enthalpies are determined. The enthalpy vector is determined using Shomate polynomials[66]. The heat loss $\dot{Q}_{loss}$ is assumed to be 5% of sensible heat gain of the cell structure.

$$m \cdot c_p \frac{\mathrm{d}T^{out}}{\mathrm{d}t} = \dot{N}^{in}\bar{h}^{in} - \dot{N}^{out}\bar{h}^{out} - iV_{cell}WL - \dot{Q}_{loss} \tag{3.5}$$

The PID controller mentioned above maintains a temperature gradient of 100 K between the cell in- and outlet.

Cell electrochemical model

The assumption is made that all ammonia immediately decomposes upon entering the cell, leading to the operation of the cell as a pure hydrogen fuel cell. Since the SOFC is modelled with zero dimensions, an average temperature and partial pressure is estimated for the purposes of the model.

The open circuit voltage is determined using the Nernst equation:

$$E = -\frac{\Delta g^0}{n_e F} + \frac{\bar{R}T}{2F} ln \left(\frac{\frac{P_{H_2}}{p^0} \cdot \left(\frac{p_{O_2}}{p^0}\right)^{\frac{1}{2}}}{\frac{p_{H_2O}}{p^0}} \right) \tag{3.6}$$

With Δg^0 as the standard Gibbs free energy for the HOR. The obtained voltage is corrected with the activation loss, ohmic loss and concentration loss, which are defined respectively:

$$\Delta V_{act} = \frac{2\bar{R}T^{stack}}{n_e F} \left(sinh^{-1}\left(\frac{i}{2 \cdot i_{0,cat}}\right) + sinh^{-1}\left(\frac{i}{2 \cdot i_{0,an}}\right) \right) \tag{3.7}$$

Where i_0 is the temperature dependent exchange current density.

$$\Delta V_{con} = \frac{\bar{R}T^{stack}}{2F} ln\left(\frac{p_{H_2O,TPB} \cdot p_{H_2}}{p_{H_2O} \cdot p_{H_2,TPB}}\right) + \frac{\bar{R}T^{stack}}{4F} ln\left(\frac{p_{O_2}}{p_{O_2,TPB}}\right) \tag{3.8}$$

With $p_{,TPB}$ as the partial pressure at the three-phase boundary.

$$\Delta V_{ohm} = i\left(\frac{\tau_{an}}{\sigma_{an}} + \frac{\tau_{el}}{\sigma_{el}} + \frac{\tau_{ca}}{\sigma_{ca}}\right) \tag{3.9}$$

With thickness τ and conductivity σ. Where the electrode condictivities are assumed constant and the electrolyte conductivity is temperature dependant as follows:

$$\sigma_{el} = 33.4 \cdot 10^3 \cdot e^{\frac{-10300}{T}} \tag{3.10}$$

This results in the following:

$$V_{cell} = E - \Delta V_{act} - \Delta V_{con} - \Delta V_{ohm} \tag{3.11}$$

As can be seen, the current density and operating temperature are expected to be of great influence on the efficiency of the system. According to Aguiar et al. [1], a current density of 5000 $A \cdot m^{-2}$ is a decent choice regarding power density and efficiency. The temperature choice is strongly dependent on the materials used. intermediate temperature (873-1073 K) SOFCs have the advantage to be able to use metal-ceramic materials where HT (1073-1273 K) SOFCs need to use ceramic materials. This can bring the cost down.

External cracker
The external cracker is used to partially crack ammonia into hydrogen and nitrogen. Otherwise, the system could run into instabilities [44]. This reaction is endothermic [55] and, therefore, a burner is installed to provide this heat.

$$2NH_3 \rightleftarrows 3H_2 + N_2 \quad [\Delta H^0 = +92\ kJ\ mol^{-1}] \tag{3.12}$$

In this block, the fuel consumption is defined using:

$$\dot{N}^{in} = \frac{iWL}{2F(1.5x^{in}_{NH_3} + x^{in}_{H_2})UF} \tag{3.13}$$

With UF as the fuel utilisation factor. In this definition, the fuel required for the burner is not included. The cracking process occurs at elevated temperatures (800 K) such that over 99% of the ammonia decomposes, assuming its 100%. The amount of ammonia that is cracked in the external cracker is controlled with a bypass that is managed with the ECR parameter (external cracking ratio).

The amount of heat required for the cracker is determined by solving for Q:

$$0 = \dot{N}^{in}\bar{h}^{in} - \dot{N}^{out}\bar{h}^{out} + Q \tag{3.14}$$

In which the temperature-dependent entalphies h are again determined with the Shomate polynomials [66].

Heat integration
Using heat exchangers, the fuel stream is heated before entering the cracker using the heat from the AOG. The same is true for the cathode stream. The fact that the SOFC produces heat instead of consuming, causes both AOG and COG streams to contain sufficient heat to heat their corresponding incoming stream. Even though due to migration of oxygen ions through the PEN structure, the COG has lower mass flow than the CIG (cathode-in-gas), it still has sufficient heat. As the AOG is used in the ICE, steam is removed. In the heat integration block, the amount of cooling water, required for condensing the steam from the AOG, is calculated. The power required by the cooling pump system is neglected as it is expected to have a limited impact on overall performance.

Air and fuel blowers
Blowers are modelled that compensate for the pressure loss over the stack. This volume flow-dependent pressure loss is determined using data from the literature [19]. It is assumed that the compression due to the blower is non-isentropic, resulting in a temperature rise. This rise in temperature, in combination with a mechanical efficiency, corresponds to a required power.

Output
In the output block, the important operating parameters are determined and displayed. It calculates different efficiencies and the net power.

3.1.2. SOFC adaptions
The model from Koekkoek [44] forms the basis of the SOFC model for this research. The adaptations have to do with the difference in fuel type. The changes with the most impact are made in the heat integration, mass balance and the cracker. From which the latter is no longer a cracker, but a fuel reformer.

Reformer model
The proposed SOFC model runs on hydrogen. Therefore, the fuel has to be reformed to hydrogen. Internal steam reforming is an efficient way of cooling the system, but it can also cause instabilities. However, methanol has some implications. Methanol is relatively unstable compared to methane [10]. This instability causes methanol to rapidly decompose within the SOFC. This decomposition is an endothermic process and, therefore, induces a strong cooling effect on the cell entrance. The consumption of hydrogen, however, is a less spontaneous process. Due to this misalignment in heat consumption and heat production, large thermal gradients can occur, which in term cause stresses, possibly damaging the PEN structure. Therefore, methanol is often cracked and partially reformed to methane.

An additional advantage of methane over methanol is the lower risk of carbon formation at the anode [47]. According to Laosiripojana and Assabumrungrat [47], when sufficient steam is added, methane has no carbon deposition at temperatures as low as 750 °C. This is 50°C lower than the operating temperatures of the SOFC.

This means that in the reformer multiple processes take place. In this research, it is assumed that the following reactions are dominant such that others can be neglected:

$$CH_3OH \longrightarrow 2H_2 + CO \tag{3.15}$$

$$CH_4 + H_2O \rightleftarrows 3H_2 + CO \tag{3.16}$$

$$CO + H_2O \rightleftarrows CO2 + H_2. \tag{3.17}$$

As a result of the instability of methanol, the methanol decomposition reaction (MeOHDR) is assumed to be, and therefore modelled as, a one-way going reaction. The methane steam reforming (MSR) and water gas shift (WGS) however, are equilibrium reactions. Because MeOHDR is modelled to occur spontaneously, the process can be split into two processes.

Process 1 is the MeOHDR. It is assumed that all methanol is consumed in the MeOHDR. This means that after the MeOHDR there is only steam, hydrogen and carbon monoxide. Note that this steam is added to consume carbon monoxide and prevent carbon deposits. These three components are the feedstock for the methanator.

The following three stages are defined: stage 1, before entering the methanator; stage 2, after the MeOHDR; stage 3, after the methanisation and thus after the methanator:

$$\dot{N}^0 = \dot{N}^0_{H_2O} + \dot{N}^0_{CH_3OH} \tag{3.18}$$

$$\dot{N}^1 = \dot{N}^1_{H_2O} + \dot{N}^1_{H_2} + \dot{N}^1_{CO} \tag{3.19}$$

$$\dot{N}^2 = \dot{N}^2_{H_2O} + \dot{N}^2_{H_2} + \dot{N}^2_{CO} + \dot{N}^2_{CH_4} + \dot{N}^2_{CO_2} \tag{3.20}$$

With $\dot{N}^{\#}_i$ the molar flow rate at stage $\#$ of substance i. For process two, the five unknowns from Equation 3.20 have to be determined. First, two equations, using equilibrium constants, are set up. These equations are based on partial pressures. For the WGS reaction, this is no problem, as all stoichiometric coefficients are equal to 1. Therefore, partial pressures can be switched for molar flowrates as these relate to each other the same way. For the MSR, this is different.

$$K_{WGS} = \frac{p^2_{CO_2} \cdot p^2_{H_2}}{p^2_{CO} \cdot p^2_{H_2O}} = \frac{\dot{N}^2_{CO_2} \cdot \dot{N}^2_{H_2}}{\dot{N}^2_{CO} \cdot \dot{N}^2_{H_2O}} \tag{3.21}$$

$$K_{MSR} = \frac{p^2_{CO} \cdot (p^2_{H_2})^3}{p^2_{CH_4} \cdot p^2_{H_2O}} = \frac{\dot{N}^2_{CO} \cdot (\dot{N}^2_{H_2})^3}{\dot{N}^2_{CH_4} \cdot \dot{N}^2_{H_2O}} \cdot \left(\frac{p_{eq}}{p_{ref}}\right)^2 \frac{1}{(\dot{N}^2_{H_2O} + \dot{N}^2_{CH_4} + \dot{N}^2_{H_2} + \dot{N}^2_{CO} + \dot{N}^2_{CO_2})^2} \tag{3.22}$$

With K representing the reaction constants; p_i partial pressures of substance i; p_{eq} the reaction pressure at equilibrium; and p_{ref} a reference pressure set to p_{atm}. Note that even though, CO_2 is an inert gas to the MSR, it does have an influence on the partial pressures and therefore influences the equilibrium constant K. These constants are determined per reaction using:

$$K = e^{\frac{-\Delta G}{RT}} \tag{3.23}$$

$$\Delta G = \Delta H - T\Delta S \tag{3.24}$$

The temperature-dependent H and S are determined using the Shomate polynomials using data from NIST [66]. From reactions 3.17 and 3.16 the following stochiometric balances can be computed:

$$\dot{N}^2_{H_2} = \dot{N}^1_{H_2} + \dot{N}^2_{CO_2} - 3 \cdot \dot{N}^2_{CH_4} \tag{3.25}$$

$$\dot{N}^2_{CO} = \dot{N}^1_{CO} - \dot{N}^2_{CO_2} - \dot{N}^2_{CH_4} \tag{3.26}$$

$$\dot{N}^2_{H_2O} = \dot{N}^1_{H_2O} - \dot{N}^2_{CO_2} + \dot{N}^2_{CH_4} \tag{3.27}$$

Equations 3.21, 3.22, 3.25, 3.26 and 3.27 can be solved for a given temperature, pressure and $\dot{N}^0$.

According to Van Biert [10], a common figure for the external cracking ratio is 0.5. This provides stable operation of the SOFC as well as the advantage of cooling due to internal cracking. Rechberger et al. [70] conducted experiments on a setup for a methanol-fuelled SOFC with methanator. A 45/55 ratio (steam/methanol) was preheated to 375°C. After the methanator, the temperature has risen to 520°C. This resulted in the following mole fractions:

$$[x_{H_2} \quad x_{CH_4} \quad x_{CO_2} \quad x_{H_2O} \quad x_{CO}] = [0.33 \quad 0.14 \quad 0.14 \quad 0.36 \quad 0.03] \tag{3.28}$$

Using Cantera, the same process was simulated. This process was simulated to equilibrium, resulting in:

$$[x_{H_2} \quad x_{CH_4} \quad x_{CO_2} \quad x_{H_2O} \quad x_{CO}] = [0.33 \quad 0.17 \quad 0.15 \quad 0.31 \quad 0.03]. \tag{3.29}$$

However, the values from Rechberger [70] do not provide a complete depiction of the process inside the reactor. That is because the atom ratio of the constituents before and after the reactor are not the same. Several factors can contribute to this phenomenon, including measurement errors in the inflow or outflow rates or potential system leakage. Nevertheless, the fact that these values are comparable in magnitude to the experimental results lends support to the hypothesis that the process kinetics are sufficiently rapid to assume equilibrium. Note that the sum of equation 3.29 is 0.99. That is because the simulation in Cantera is not limited to the WGS and MSR reactions and thus results in 48 other substances which together account for the additional mole fraction of 0.01. This also confirms the assumption of the one-way going MeOHDR. The combined endothermic mEOHDR and exothermic methanisation process result in small fuel consumption of the heater.

Mass balance model

The approach to mass balances remains unchanged. The various mass balances are coupled with an HOR and the decomposition rate of hydrogen-carrying fuel methane (MDR) is defined. However, the substances present in the cell are altered to include hydrogen, methane, carbon dioxide, steam, methanol, and carbon monoxide, each with its own mass balance. Since it is assumed that all of the methanol is consumed in the MeOHDR , the methanol balance is included for completeness but does not contribute to the overall processes. Additionally, the small amount of carbon monoxide present is expected to be immediately consumed by the WGS reaction on entering the cell. Thus, the carbon monoxide mass balance is also included for the sake of completeness. The resulting reactions occur in the cell:

$$CH_4 + H_2O \longrightarrow 3H_2 + CO \tag{3.30}$$

$$CO + H_2O \longrightarrow CO2 + H_2 \tag{3.31}$$

$$H_2 + O^{2-} \longrightarrow H_2O + 2e^- \tag{3.32}$$

Again, it is assumed that all fuel is reformed in the cell. This assumption is supported by the use of the methanator model. When the temperature is set to the operating temperature of the SOFC, almost all the CH_4 is consumed. In the methanator model, hydrogen is not consumed by the HOR. However, in the cell, the hydrogen is consumed, resulting in an even more right-going process in reaction 3.30 due to the resulting lower partial pressure of hydrogen.

From the WGS reaction it follows that per mole CO present, a mole of hydrogen is formed. This causes the $\dot{N}^{in}$ from Equation 3.4 to change for the hydrogen mass balance. This also has an additional influence on the stoichiometric coefficient v. From the MSR reaction, it can be concluded that this coefficient would increase from 1.5 to 3. However, the MSR reaction results in additional CO and therefore hydrogen, which causes it to increase to 4.

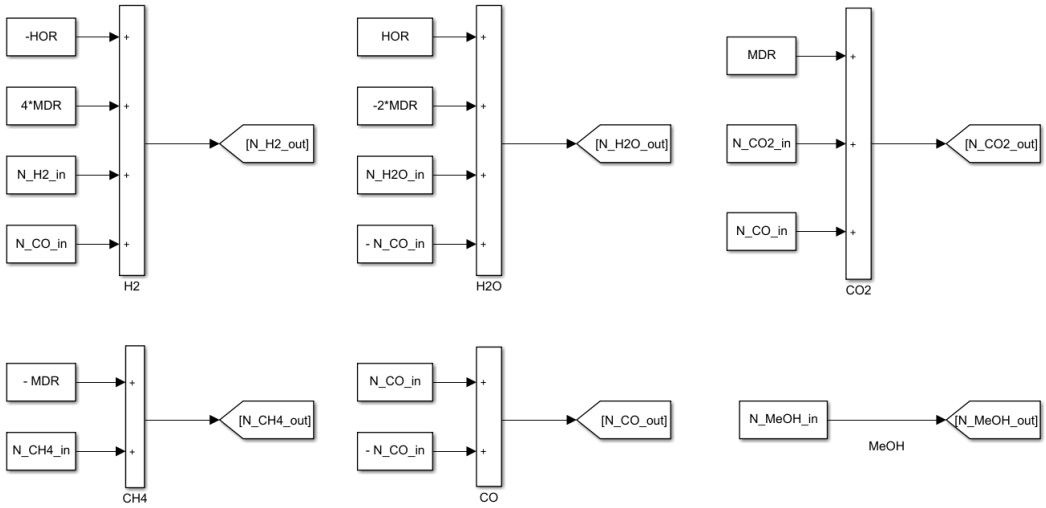

Figure 3.3: Schematic view of the mass balances per substance.

The methane mass balance is, as with the ammonia in the original model, determined by the decomposition rate. The CO_2 mass balance is determined by Reaction 3.31, which in term is determined by the initial amount of CO present and the decomposition rate due to its CO production. The H_2O mass balance is determined by both the decomposition rate and the hydrogen oxidation rate. By combining these reactions (3.30 and 3.31) the dependence on the decomposition rate is visible:

$$CH_4 + 2H_2O \longrightarrow 4H_2 + CO_2 \tag{3.33}$$

In HOR, it can be seen that one mole of water is formed per mole of hydrogen.

The amount of methanol remains zero. The amount of CO goes to zero, as it is consumed by the WGS reaction. An overview of the balances can be found in Figure 3.3.

Heat integration model

A layout of the implemented heat integration can be seen in Figure 3.4. A minor modification was implemented in the cathode channel with regards to heat integration. In contrast, a more substantial alteration was made to the heat integration of the anode channel. That is because of the different fuel stream properties and modelling methods for the pre-reformer. Water and methanol, as liquids at ambient temperature, necessitate evaporation in order to be transported by a blower. The economiser uses the heat from the AOG to preheat the liquids to evaporation temperatures. In the evaporator the liquids are evaporated by oxidising the AOG/COG mixture, thereby allowing for transportation of the gaseous mixture via the blowers.

Further modifications have been made to the heat integration regarding the pre-reformer. As the pre-reformer operates at a defined temperature, a secondary heat exchanger has been incorporated. The low-temperature heat exchanger (LT-HEX) superheats the incoming fuel stream from saturated temperatures to the operating temperature of the reformer. The high temperature heat exchanger (HT-HEX) superheats the fuel stream from reforming temperature to the SOFC entrance temperature.

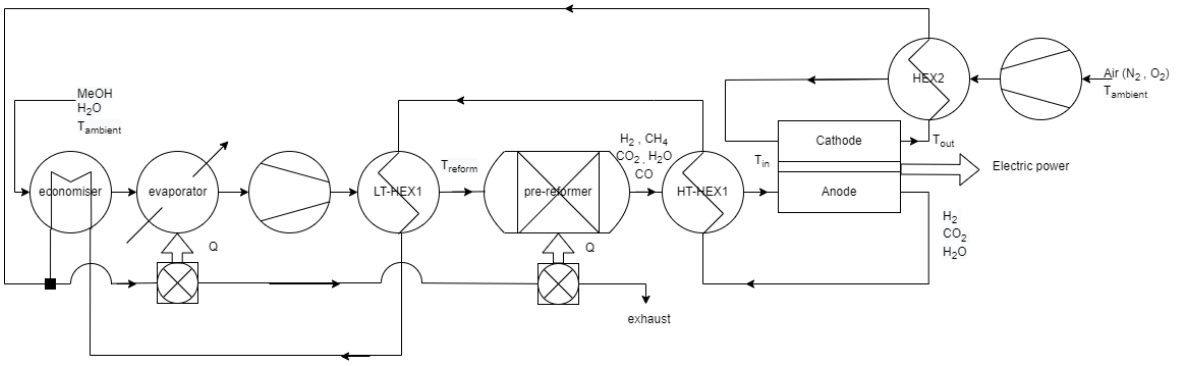

Figure 3.4: Layout of the SOFC plant including the heat integration.

3.2. Internal combustion engine model

An existing zero-dimensional model will be utilised and modified to suit the fuel requirements of methanol in the ICE, similar to the SOFC model.

3.2.1. Method in existing model

The existing model consists of a zero-dimensional turbocharged cylinder process. The generated mechanical power drives either a propeller load depending on an open water diagram or a generator load. The fuel supply is managed by the fuel governor using a PID controller.

For the cylinder process, the five-stage Seiliger cycle is used. This cycle consists of the following processes:

- 1-2 Polytropic compression
- 2-3 Isochoric combustion
- 3-4 Isobaric combustion
- 4-5 Polytropic expansion
- 5-1 Isochoric heat dissipation

In this model, it is assumed that there is no additional fuel mass added to the air mass already inside the cylinder. Only the heat from the combustion is added during the two combustion phases. The distribution of heat over these combustion phases is determined by the specified peak pressure and the fraction of the nominal engine speed. The turbocharger is assumed to be a function of air mass and engine speed. This information is incorporated in the total heat rejection. However, this imposes a dimensional mismatch in Equation 3.34. To non-dimensionalise the fraction, the turbocharger constant c_{tc} in [s/kg] is introduced.

$$p_1 = p_{amb}\left(\frac{c_{tc}\cdot \dot{Q_{5-1}}}{c_p \cdot T_{amb}} + 1\right)^{\frac{\kappa}{\kappa-1}} \tag{3.34}$$

For the model to run, it requires input parameters. The key engine parameters regarding the thermodynamic model are:

- Charge pressure & temperature after intercooler; determine the initial condition before compression;
- Compression ratio; determines stage two;
- Max cylinder pressure; provides pressure ratio and thus temperature ratio for stage three. Also determines the division of heat input over the combustion phases and therefore condition four;
- Brake specific fuel consumption (bsfc);
- Rated power output;

A more detailed description of the model can be found in Appendix A.

3.2.2. ICE adaptions

First the fuel properties of the model are adapted, since the original model was for a diesel engine. The most influential properties of the fuel are the calorific value and the stoichiometric air to fuel ratio σ. For comparison purposes with the work of Koekkoek [44], the Wärtsilä 12V31DF [96] has been selected for this research. The relevant specifications are implemented in the model, as well as the provided bsfc, corrected for the change in calorific value.

An additional change to the model is the introduction of a generator efficiency. This was previously not present in the model. This efficiency was made variable between 95% and 97% as for the W31 itself [99].

Injection and ignition

The switch from diesel to methanol necessitates significant alterations to the injection and ignition method. With a cetane number of only 3, methanol has poor compression ignition properties [92]. This means that for CI, pilot fuel would be required. However, the addition of diesel would mean that the fuel would no longer be a net zero fuel.

As AOG will be port-fuel-injection (PFI), it was attempted to use PFI for the methanol as well. Therefore, it was evaluated whether there is sufficient heat in the intake air after the turbocharger to evaporate the methanol. In this evaluation, it is assumed that the heat for the evaporation of methanol is provided by the intake air only.

The lower flammability limit of methanol, regarding the air-excess ratio, is 1.81 [92]. This sets the maximum air-excess ratio. At first, it is assumed that the compressor works isentropic. During this evaluation, data from CoolProp is used [4]. For a given pressure ratio, the corresponding air and evaporation temperature of methanol are known. Also, the evaporation heat is known. This determines the total heat available and required according to:

$$Q_{av} = m_a \cdot c_{p,a} \cdot (T_a - T_{evap}) \tag{3.35}$$

$$Q_{req} = m_{meoh}(c_{p,meoh} \cdot (T_{evap} - T_{meoh}) + \Delta h_{evap}) \tag{3.36}$$

With Q_{av} as the available heat and T_{meoh} the injection temperature of the methanol. The minimum pressure ratio can be found by iteratively varying the pressure ratio. When $Q_{av} = Qreq$, the minimal pressure ratio is found. Using a for loop, a minimal pressure ratio of 5.3 is obtained. This is unrealistically high for a turbocharger. However, in this evaluation, isentropic operation of the compressor was assumed. Which is incorrect. When it is assumed that the compressor has an efficiency of 80% and a first estimate of the pressure ratio of 3.6, the isentropic efficiency can be determined by solving:

$$1 + \frac{1}{\eta_c}\left(r_p^{\frac{\kappa-1}{kappa}} - 1\right) = r_p^{\frac{\kappa-1}{\kappa \cdot \eta_{is}}} \tag{3.37}$$

Using η_{is} the actual enthalpy after the compressor can be determined using:

$$\eta_{is} = \frac{h_{2s} - h_1}{h_2 - h_1} \tag{3.38}$$

The provided enthalpy and pressure ratio are used as state variables for the previously described iterative process. The elevated temperature, compared to the isentropic situation, provides a larger available heat. Now a minimal pressure ratio of 4.0 is required. This is significantly lower than the 5.3. However, it is still too high. In addition to that, we are evaluating the situation with the absolute maximum air-excess ratio. For higher power output, the air-excess ratio lowers to 1.5 and the pressure ratio settles at 4.6. This shows the problems with PFI for methanol as a result of its high evaporation heat. The MATLAB code can be found in Appendix B.

Therefore, direct injection is more probable. By using low-pressure direct injection, a well-mixed mixture can be obtained. However, there is a limit to the compression ratio due to the auto-ignition temperature. In this calculation, it is assumed that there is only air present in the cylinder. The procedure to estimate the maximum ratio will now be described using the enthalpy:

$$\Delta H_{max} = c_{p,a}(m_a + m_{meoh})(T_{auto} - T_1) \tag{3.39}$$

The change in enthalpy must remain lower than this value. The change in enthaly is due to added work in the form of compression. This results in an increase in temperature. However, the evaporation of methanol has a cooling effect. In reality, this evaporation also corresponds to a rise in enthalpy. However, under the assumption that there is only air in the cylinder, the evaporation results in a negative contribution enthalpy.

$$\Delta H_{max} \geqslant \Delta H_c - \Delta H_{evap} \tag{3.40}$$

These terms are defined with:

$$\Delta H_c = T_1 \left(r_c^{\kappa-1} - 1 \right) c_p m_a \tag{3.41}$$

$$\Delta H_{evap} = \Delta h_{evap} \cdot m_{meoh} \tag{3.42}$$

In which Equation 3.41 is based on:

$$T_2 = T_1 \cdot r_c^{\kappa-1} \tag{3.43}$$

$$\Delta H = \Delta T c_p m_a \tag{3.44}$$

Combining and rewriting Equations 3.39 to 3.42 results in:

$$r_c \leqslant \left(\frac{H_{max} - H_{evap}}{c_p m_a T_1} + 1 \right)^{\frac{1}{\kappa-1}} \tag{3.45}$$

When taking the same initial conditions ($T_1 = 325K$) as in the work of Koekkoek [44] and the maximum air-excess ratio of 1.81 a maximum compression ratio of 11.3 is obtained. However, in the work of Koekkoek [44], an effective compression ratio of 15.2 is used. To make a better comparison between the fuels, this value is maintained, meaning that low-pressure injection is not feasible.

The intake air is mixed with the dehydrated AOG of the SOFC, which contains hydrogen. Therefore, it was evaluated whether this AOG/air mixture experiences conditions for autoignition. According to the calculations in Appendix C, there is too much air in the cylinder to be combustible. It exceeds the lower flammability limit by over 1.75 times and, therefore, creates little risk of knock. This means that the hydrogen in the AOG does not create limitations on the pressure ratio.

This brings us to the founding that high-pressure direct injection is the most probable solution. Unfortunately, as discussed earlier, CI is not viable. According to Verhelst et al. [92] a glow plug could provide a solution. However, it should be noted that, even though hydrogen may not be present in combustible ratios, it can still react with the oxygen present around the glow plug during the compression phase, potentially leading to an undesired increase in pressure. While the exact contribution of this phenomenon to the overall process is uncertain, it falls outside the scope of the current research.

To overcome these ignition problems, it is suggested to use SI, possibly in combination with prechambers. Prechambers can result in rapid combustion and increased efficiency [57]. This effect could be amplified by the high buring velocity of methanol [92]. In a Seiliger cycle, this would translate in a partial shift of the isobaric combustion towards the isochoric combustion, getting closer towards the theoretically more efficient Otto cycle.

The evaluation above clearly indicates that the injection and ignition of methanol requires extra attention in future research on methanol fuel in maritime applications.

3.3. Combined cycle model

The SOFC and ICE models are related in two ways: via the AOG which is fed to the cylinder; and the the use of heat from the exhaust to provide for the evaporator. First the AOG coupling is discussed.

After the heat exchangers, the AOG is dehydrated. This results in a mixture of H_2 and CO_2. This hydrogen-rich gas is added to the ICE intake air. The amount of H_2 and CO_2 added per thermodynamic cycle is obtained via:

$$m_{H_2,cyc} = \frac{\dot{N}_{H_2} \cdot M_{H_2} \cdot k}{n_{eng} \cdot i} \tag{3.46}$$

$$m_{CO_2,cyc} = \frac{\dot{N}_{CO_2} \cdot M_{CO_2} \cdot k}{n_{eng} \cdot i} \tag{3.47}$$

In which M is the molar mass, k the indicator for two- or four-stroke (1 or 2), n the engine speed and i the amount of cylinders. As with the addition of methanol, hydrogen does not contribute to the cylinder mass. However, the additional mass of H_2 and CO_2 is accounted for in the specific heat input [J/kg] which is used in determining the efficiency:

$$q_{spec} = \frac{m_{H_2,cyc} \cdot LHV_{H_2} + m_{MeOH,cyc} \cdot LHV_{MeOH}}{m_{a,cyc} + m_{CO_2,cyc} + m_{H_2,cyc}} \tag{3.48}$$

The second coupling is via the exhaust gasses. As discussed in Section 3.1.2, heat is required for the evaporator. This heat can be generated by the oxidation of hydrogen in the AOG stream. However, There is sufficient heat in the ICE exhaust gasses (after the turbocharger) to evaporate both water and methanol in the fuel stream. This approach effectively utilises waste heat from the ICE, thereby mitigating the consumption of high-grade energy in the form of hydrogen. The outcome is a more efficient SOFC system without compromising the efficiency performance of the ICE. A visualisation of the total model can be found in Figure 3.5.

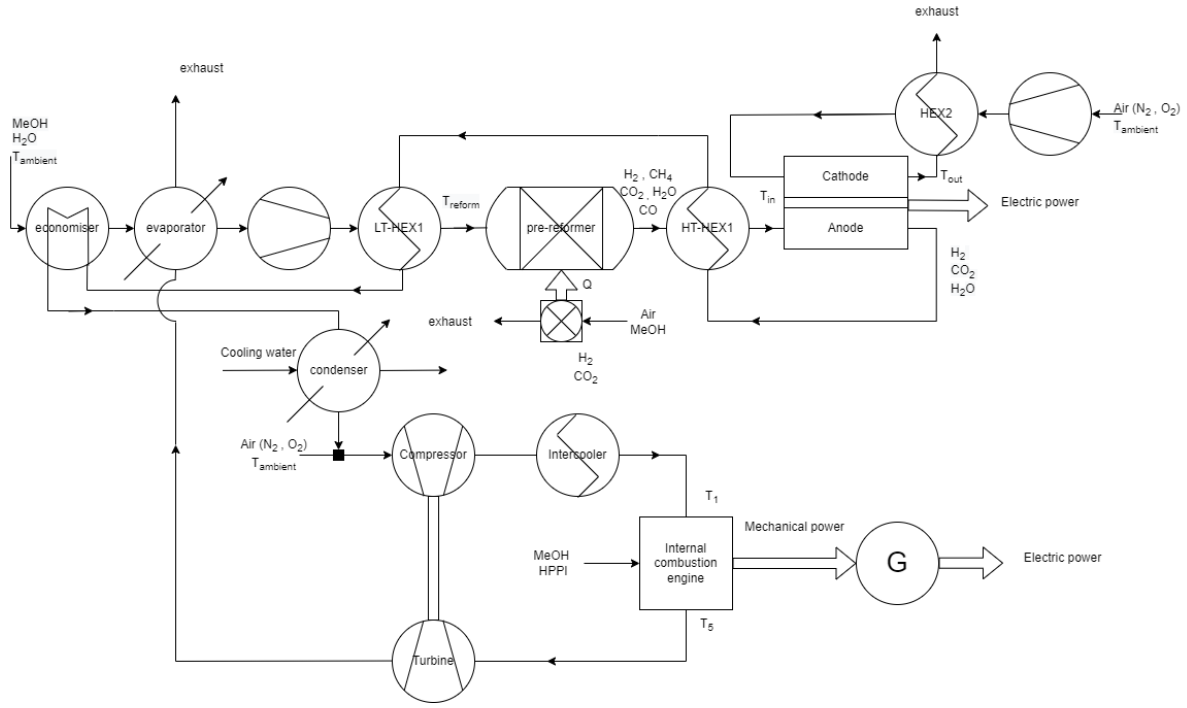

Figure 3.5: Schematic representation of the combined SOFC-ICE cycle.

3.3.1. System specifications

The model proposed by Koekkoek [44] is based on the work of Aguiar et al. [1]. The model, modified with the proposed adaptations, result in the properties from table 3.1. The properties of the ICE model are defined in Table 3.2

Table 3.1: Properties of the SOFC system

parameter	value	unit	description
W	0.1	m	Cell width
L	0.1	m	Cell length
h	$1 \cdot 10^{-3}$	m	Channel height
τ_{an}	$500 \cdot 10^{-6}$	m	Thickness of anode
τ_{ca}	$50 \cdot 10^{-6}$	m	Thickness of cathode
τ_{el}	$20 \cdot 10^{-6}$	m	Thickness of electrolyte
τ_I	$500 \cdot 10^{-6}$	m	Thickness of interconnect
σ_{an}	$80 \cdot 10^3$	$\Omega^{-1}m^{-1}$	Electric conductivity of anode
σ_{ca}	$8.4 \cdot 10^3$	$\Omega^{-1}m^{-1}$	Electric conductivity of cathode
σ_{el}	$33.4 \cdot 10^3 exp(\frac{-10300}{T})$	$\Omega^{-1}m^{-1}$	Ioninc conductivity of electrolyte
$D_{eff,an}$	$3.66 \cdot 10^{-5}$	$m^2 \cdot s^{-1}$	Effective diffusion coefficient of anode
$D_{eff,ca}$	$1.37 \cdot 10^{-5}$	$m^2 \cdot s^{-1}$	Effective diffusion coefficient of cathode
$c_{p,PEN}$	500	$J \cdot kg^{-1} \cdot K^{-1}$	Specifi heat capacity of PEN structure
$c_{p,I}$	500	$J \cdot kg^{-1} \cdot K^{-1}$	Specific heat capacity of interconnect
ρ_{PEN}	5000	$kg \cdot m^{-3}$	Mass density of PEN structure
ρ_I	8900	$kg \cdot m^{-3}$	Mass density of interconnect
k_{an}	$2.35 \cdot 10^3$	$A \cdot m^{-2}$	Pre-exponential factor of i_0 at anode
k_{ca}	$6.54 \cdot 10^3$	$A \cdot m^{-2}$	Pre-exponential factor of i_0 at cathode
E_{an}	$140 \cdot 10^3$	$J \cdot mol^{-1}$	Activation energy of i_0 at anode
E_{ca}	$137 \cdot 10^3$	$J \cdot mol^{-1}$	Activation energy of i_0 at cathode
η_{is}	0.6	$-$	Isentropic efficiency of the fuel and air blowers
η_{mech}	0.9	$-$	Mechanical efficiency of the fuel and air blowers
η_{DCAC}	0.95	$-$	DC-AC converter efficiency
$heatloss$	0.05	$-$	Heat loss of the SOFC to the environment
T_{op}	1073	K	Operating temperature of the SOFC
p_{op}	101325	pa	Operating pressure of the SOFC
T_{meth}	843	K	Operating temperature of the methanator
p_{meth}	101325	pa	operating pressure of the methanator
i	5000	$A \cdot m^{-2}$	Current density
$r_{s,f}$	$1:1$	$-$	Steam to fuel ratio

Table 3.2: Properties of the ICE

Parameter	Value	Unit	Description
P_{nom}	7200	kW	Nominal power output
n	750	rpm	Engine speed
ϵ	16	$-$	Geometric compression ratio
D	0.32	m	Bore
S	0.4	m	Stroke
i	12	$-$	Number of cylinders
k	2	$-$	revolutions per cycle
p_{charge}	$3.6 \cdot 10^5$	pa	Nominal charge pressure
T_1	328	K	Starting T of the closed cylinder process
p_{max}	$186 \cdot 10^5$	pa	Max cylinder pressure
η_{mech}	0.95	$-$	Mechanical efficiency at nominal speed
η_{gen}	$0.95 - 0.97$	$-$	Speed dependant generator efficiency
$bsfc$	380	g/kWh	Brake specific fuel consumption

4

Results

In this section, the results of the model will be presented and analysed. First the performance of the SOFC will be evaluated. Subsequently, the results obtained from the SOFC will be compared with those reported in the existing literature. After that, the ICE performance will be evaluated. This leads to the overall performance of the combined cycle. Its will be evaluated and compared with the results reported in the literature. This chapter will be concluded with a modelling approach reflection. The data that is used for the bar graphs in this chapter can be found in Appendix D.

4.1. SOFC

Initially, the performance of the methanator will be discussed. Then the performance of the SOFC system will be evaluated under different conditions. Since the SOFC will be incorporated in a combined cycle, its performance will be analysed in that specific configuration. This means that any residual fuel in the anode off-gas will not be considered as a loss, as it can be utilised in the ICE. Furthermore, there is an abundance of heat available in the ICE exhaust, which can be utilised to heat the evaporator, thus eliminating the need for consumption of fuel in the evaporator. The results will then be compared to the outcomes of other research with the same and different fuels.

4.1.1. SOFC performance

The operations of the methanator can be controlled with the pressure, temperature and the fuel-to-steam ratio entering the system ($r_{s/f}$). However, the ambient pressure operating parameter of the SOFC excludes pressure as a control parameter. As discussed earlier, an external reforming ratio (err) of aproximately 0.5 is maintained. Due to the heat management of the heat exchangers, the operating temperature of the methanator does not influence the operating conditions in the cell; however, $r_{s/f}$ does influence it. Therefore, the $r_{s/f}$ is varied. The temperature is used to maintain the err at 0.5. This results in Figure 4.1. The amount of control by only varying the temperature is shown in Figure 4.2. From Equation 3.33 can be seen that a hydrogen to methane ratio of 4 is needed for an err of 0.5. This is obtained around a temperature of 843 K, where the molar fraction of hydrogen is approximately 4 times higher than the molar fraction of methane.

The parameters that will be varied in this evaluation of the SOFC are $r_{s/f}$, the fuel utilisation factor (UF) of the FC, operating temperature and current density. The standard operating conditions are defined as in table 4.1. The different losses and efficiencies per parameter will be discussed.

Table 4.1: Standard operating of the SOFC

Parameter	Value	Unit
UF	0.8	-
$r_{s/f}$	1:1	-
T_{op}	1073	K
i	5000	$A \cdot m^{-2}$

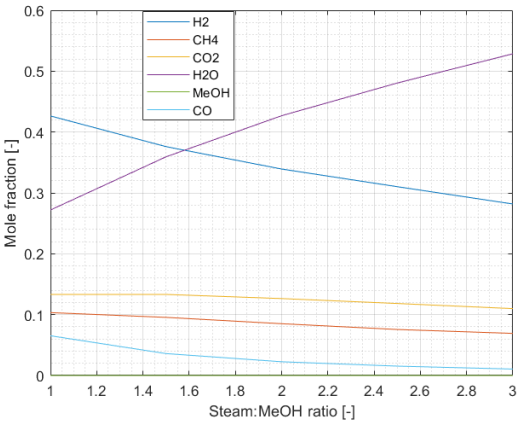

Figure 4.1: Varying $r_{s/f}$ while maintaining err ≈ 0.5.

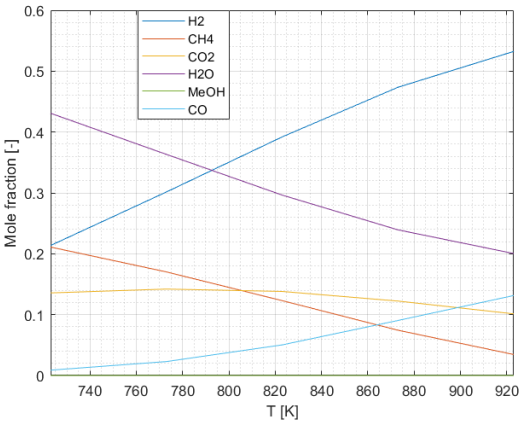

Figure 4.2: Varying T for $r_{s/f}$ = 1:1.

The influence of $r_{s/f}$, on the SOFC performance, can be seen in Figure 4.3. To change $r_{s/f}$ and maintain the power output (assuming constant efficiency), the amount of steam fed to the system should be increased. This results in a lower concentration of the fuel. From Equation 3.6 can be seen that the open circuit voltage (only reversible losses) will decrease with the decreasing partial pressure of hydrogen. As a result of increasing molar flow, the blowers consume more power. The increase in concentration losses is approximately 9.5 %. However, the concentration loss itself is very small. Therefore, this change is of negligible proportions. The largest increase is the consumption by the methanator burner. When the amount of steam is increased, a lower amount of additional heat is required. This can be explained by the fact that the operating temperature of the methanator has to change in order to maintain the err. This temperature change influences the enthalpy of formation of the different substances. These effects combined result in a small difference with the highest efficiency for $r_{s/f}$ = 1:1 and the lowest for 1:3, resulting in 58.6 % and 56.7 % respectively.

By varying UF the system efficiency barely changes, see Figure 4.4. To change the UF and maintain power output (assuming constant efficiency), the amount of fuel fed to the system should be increased. By increasing the fuel, a higher average concentration of hydrogen will be present in the cell. The same effect occurs as with the variation of $r_{s/f}$. This effect is counteracted by the increase of burner power as a result of a larger amount of methanol that should be cracked. This results in an efficiency of 58.6 % to 58.31 % for a UF of 0.7 to 0.9 respectively. No values of UF exceeding 0.9 are presented in this study as they are considered to be unrealistic.

When the operating temperature is varied, larger differences occur, see Figure 4.5. First, the open circuit voltage decreases with increasing T. This can be seen in Equation 3.6. However, the loss mechanisms are more affected by increasing T and, therefore, the system efficiency increases. In the model, the electric conductivities of the electrodes are assumed to be constant. This assumption can be justified by the fact that the ionic conductivity of the electrolyte is orders of magnitude smaller than the conductivities of the electrodes. Therefore, the ohmic loss is dominated by the electrolyte. Due to the exponential nature of Equation 3.10, the temperature has a large effect on this loss. Temperature also has an influence on the activation losses, although it is less obvious. The correlation can be seen from Equation 3.7. As the efficiency of the system increases, the ACDC converter losses increase as well, but this effect is linear. Finally, a decrease in blower loss can be seen. The power output remains the same. This means that the fuel supply must increase with decreasing efficiency. Also, to maintain a lower operating temperature and to compensate for the additional heat production due to a lower efficiency, more cooling air in the cathode channel is required. The resulting efficiencies are between 34.7% and 65.2% for temperatures between 973 and 1173 K respectively.

In Figure 4.6 the dependency on the current density can be observed. The current density does not have a significant influence on the open circuit voltage. However, a decrease in system efficiency can be observed. From Equations 3.7 and 3.9 this dependency is clearly visible. For the concentration losses in Equation 3.8, this link is less obvious. However, it is due to the partial pressures. At the triple phase boundary (TPB), where the electrode, electrolyte and fuel meet, the reaction occurs. When the current density increases, the fuel consumption increases. As more fuel is consumed, the partial

pressure at the TPB of the fuel is reduced and that of the reaction product increases. The efficiencies decrease from 65.6% to 43.8% for current densities from 2500 to 10.000 $A \cdot m^{-2}$.

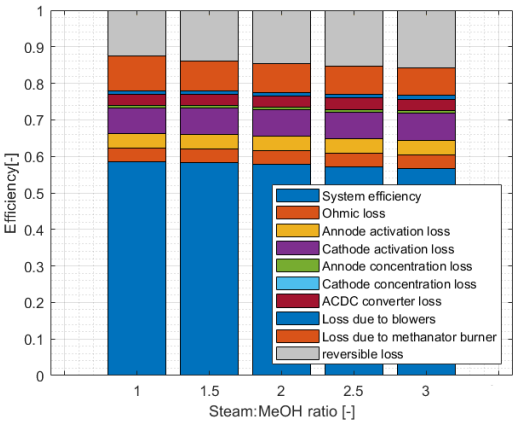

Figure 4.3: Different losses per steam:methanol ratio.

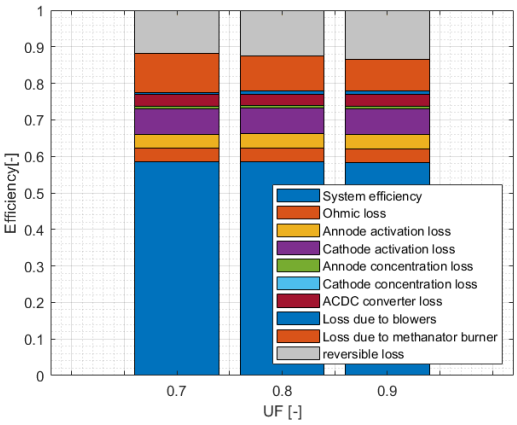

Figure 4.4: Different losses per UF.

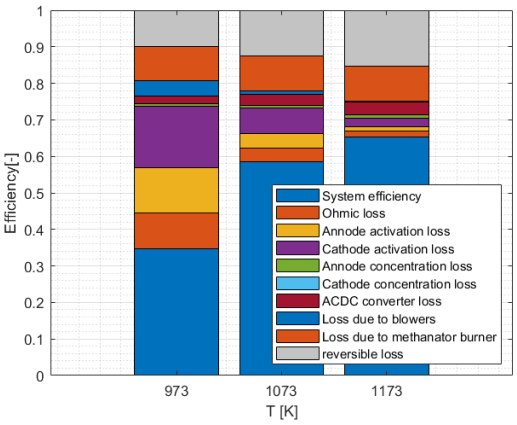

Figure 4.5: Different losses per T.

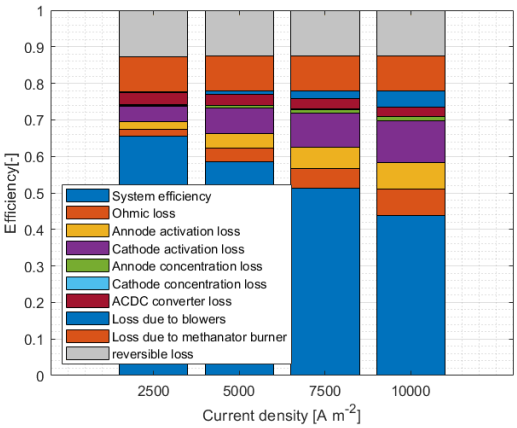

Figure 4.6: Different losses per current density.

By multiplying the operating voltage by the current density, the power density is obtained, see Figure 4.7. The decrease in operating voltage is not sufficient to create an optimum of the power density in the evaluated spectrum. However, the curve is flattening and eventually resulting in a decreasing power density, and thus creating an optimum.

As stated in the beginning of this section, the efficiency performance is evaluated for a combined configuration. However, a standalone configuration has a different performance. This can be seen in Figure 4.8. The residual fuel in the AOG will not be used in the ICE but, it can be used for evaporating the fuel and fuelling the methanator. As a result, the efficiency is reduced to 45.4% compared to 58.6% in the combined configuration. This clearly shows the synergistic benefits of combining a methanol-fuelled SOFC with an ICE.

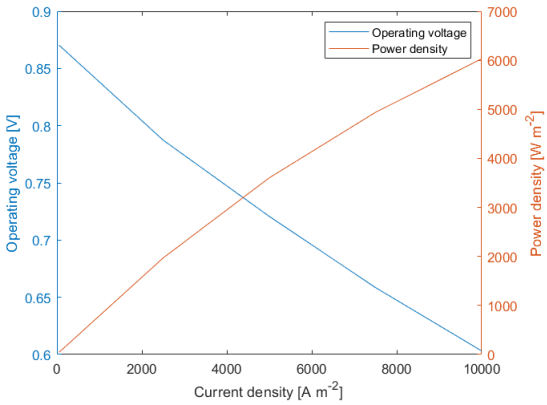

Figure 4.7: The operating voltage and power density of the cell against the current density.

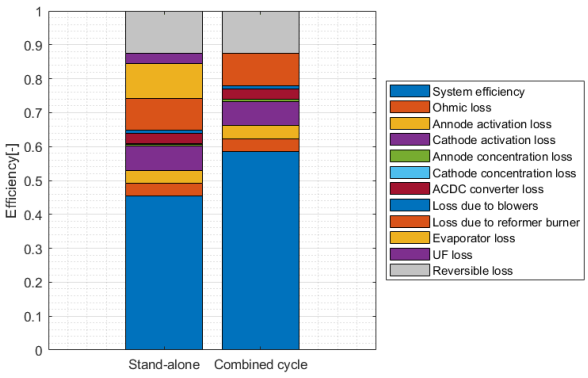

Figure 4.8: Methanol-fuelled SOFC efficiency performance in standalone and combined cycle condition.

4.1.2. Comparing SOFC performance

The model in this research is based on the model of Koekkoek [44]. It therefore makes a good comparison. It can be seen (Figures 4.9 and 4.10) that the open circuit voltage of the ammonia-fuelled SOFC exceeds that of the methanol-fuelled plant. This can be explained with the fact that for an ammonia-fuelled installation, there is no steam required to prevent carbon deposition and therefore, it has higher fuel partial pressures. This causes the operating voltage to be lower for the methanol installation. In addition, there are no significant differences between operating voltages and losses between the fuels. However, when looking at the entire system, the figures lay closer together, see Figure 4.11. This has to do with the burner and blower power consumption. The reforming process of the MeOH requires less energy than the cracking of ammonia. Therefore, the burner consumes more power. In addition, the process inside the cell produces more heat for the ammonia and therefore requires a higher air excess ratio, thus blowing power. This results in a system efficiency of 58.2% and 58.6% for ammonia and MeOH respectively.

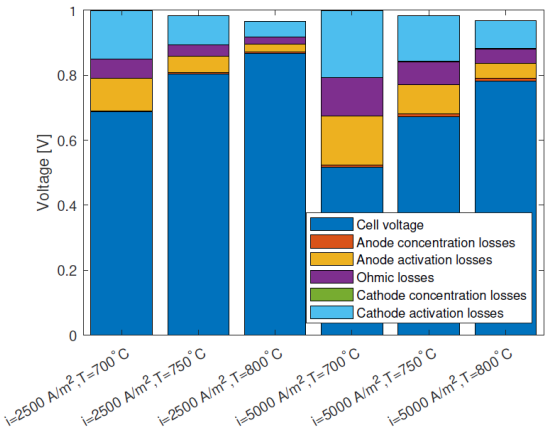

Figure 4.9: Cell voltages for different current densities and temperatures while running on ammonia by Koekkoek [44].

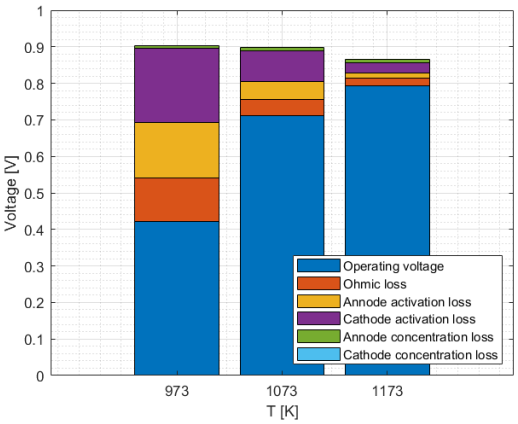

Figure 4.10: Cell voltages for different temperatures at a current density of 5000 $A \cdot m^{-2}$ while running on MeOH.

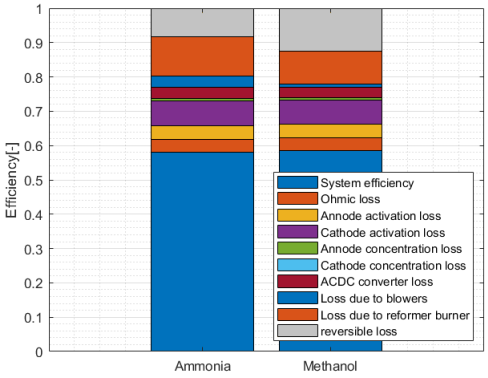

Figure 4.11: Different losses per fuel for standard conditions (Table 4.1).

Rechberger et al. [70] evaluated a MeOH-fuelled SOFC with methanator in an experimental test setup. The system is fed with a 45:55 steam:MeOH ratio. The methanator results in an err of approximately 1/3. The SOFC is preheated to a temperature of 1123 K. Efficiencies between 40% and 50% are obtained with an UF of 0.6. These values are used as input parameters for the proposed model. However, things as current density, parasitic losses and physical properties of the system are unknown and are therefore assumed to be the same for both systems.Furthermore, the definition of efficiency was not explicitly stated, and it was uncertain whether the residual fuel in the anode off-gas was considered as a loss. Based on these assumptions, the proposed model predicted an efficiency of 40.66% if the residual fuel was not considered a loss. However, when using a current density of $2500A \cdot m^{-2}$, the model predicted an efficiency of 44.4%. Despite the close match between the experimental results and the model predictions, it is important to note that not all parameters and definitions were known, making it challenging to make definitive statements.

4.2. ICE standalone performance

In this section, the performance of the ICE genset will be evaluated. As discussed in Section 3.2.1, the ICE model is based in the 5-stage Seiliger cycle. The cycle, as calculated by the model, can be observed in Figure 4.12. It is evident from the figure that the five stages of the cycle can be identified.

In Figures 4.13 4.14 the different losses and efficiencies of the ICE can be seen. As stated in Section 3.2.1, the bsfc at the nominal point is one of the input parameters, thus the effective efficiency at the nominal point is given. The mechanical efficiency is given as a percentage of the nominal power. Therefore, at low power, it makes up a larger portion of the total loss. The efficiency of the generator is dependent on the power output. However, it ranges from 95% to 97% so its dependency is limited.

The reversible loss is the result of the reversible thermodynamic cycle. The heat input loss is the part that captures the hard to determine factors, such as unburned fuel in the exhaust and heat loss to the cylinder wall. This factor is iteratively fitted to the nominal point and assumed constant through the simulation.

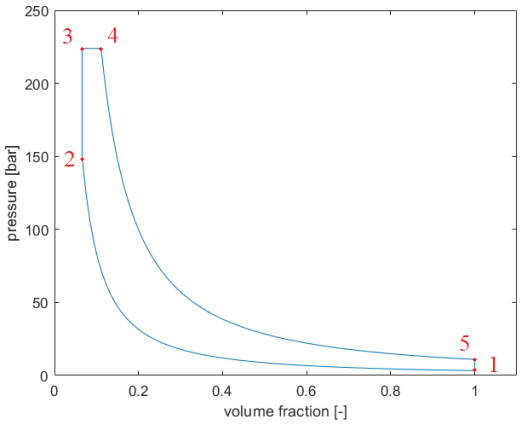

Figure 4.12: p-V diagram at nominal load with numbered Seiliger cycle stages.

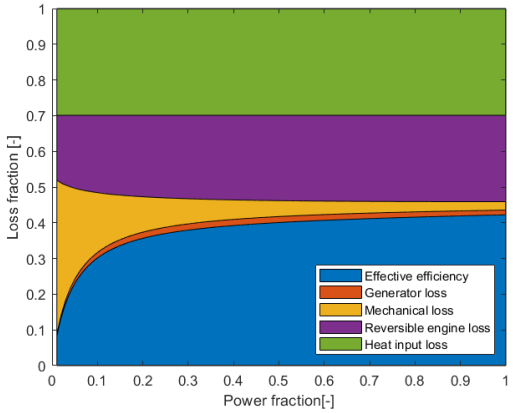

Figure 4.13: Different losses between 1% and 100% nominal power.

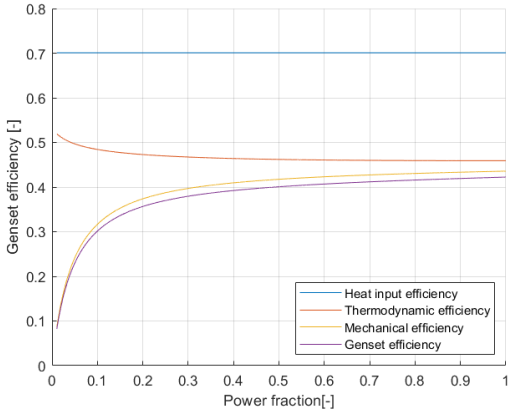

Figure 4.14: Different efficiencies between 1% and 100% nominal power.

The operational field of the genset is rather broad. As can be seen in Figure 4.15, it has full operation possibilities throughout the power range due to the fact that it is a genset for a single speed. In Figure 4.16 the air excess ratio can be seen. For a PFI engine, which has a more homogeneous mixture, this ratio is a limiting factor. However, for a DI engine, most of the combustion occurs at the front between the injected droplets and the air. Therefore, there will always be a combustible mixture somewhere in the cylinder.

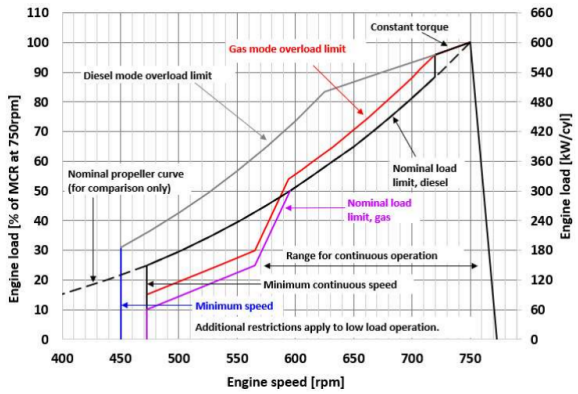

Figure 4.15: Engine envelope of the W31 [96].

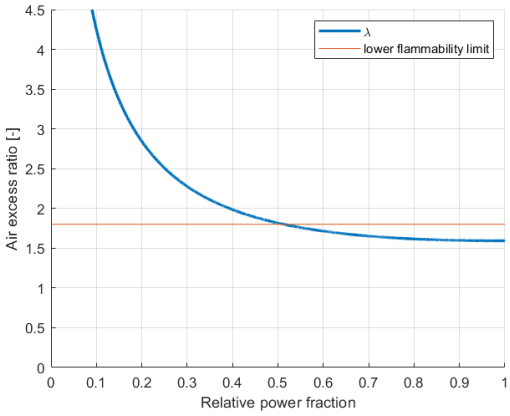

Figure 4.16: Air excess ratio and lower flammability limit [92].

4.3. Combined SOFC-ICE

In the combined configuration, several power splits (P_{SOFC}/P_{ICE}) will be evaluated: a 0/100 25/75, a 50/50, a 75/25 and a 100/0 split. This will be done by changing the number of cells in the SOFC or running the SOFC model in standalone condition. Also, the ICE direct drive efficiency will be shown. That is because a genset is not necessary if the cycle is not combined. Evaluation will be carried out for several conditions discussed in Section 4.1.1. As the influence of the UF and $r_{s/f}$ is limited, these are not evaluated. Also, an operational temperature of 973 K is not taken into consideration. This is because the efficiency of the SOFC would then be lower than that of the ICE and would therefore only add complexity without efficiency gain. The same reason holds for the choice not to evaluate the current density of 10.000 $A \cdot m^{-2}$ as it has practically the same efficiency as the ICE direct drive system (43.8% vs. 43.6%). After that, the system will be compared with relative work.

4.3.1. Combined cycle performance

In figure 4.17 the efficiency of the system can be seen for different operational temperatures. The impact of the lack of waste heat from the engine is evident in the 100/0 condition, which is presented here solely for the sake of completeness and is deemed less practical given its lack of load-following capabilities from the ICE. Please note that these simulations are conducted an nominal load. If the SOFC maintains its power output while the ICE operates in part-load, the heat management system may encounter challenges. In the 25/75 configuration, the ICE provides adequate heat across a significant portion of its power range. Conversely, the 75/25 configuration experiences heat management issues at relatively high part-loads. Further investigation is necessary to develop a sophisticated heat management design that incorporates an effective control strategy. This observation also holds true for configurations with varying current densities.

When looking at the current density dependency in Figure 4.18, we see that the difference between the power splits increases with the reduction of the current density. The efficiency gain with low current density is more significant. For example, when considering the case that has a current density of 7500 $A \cdot m^{-2}$. It is questionable whether the limited efficiency gain compared to the ICE direct drive can compensate for the added complexity of implementing an SOFC.

When comparing the 1173 K and 2500 $A \cdot m^{-2}$ case, there are only very small differences (0.06 to 0.5%). In maritime applications, where power density is a limiting factor, this would advocate for increasing the operational temperature compared to decreasing the current density. However, the increase in cost and durability due to the need for other materials is not evaluated in this research and should be further evaluated in new research.

All values can be found in Table 4.2. The choice for a certain power split depends on the availability of space onboard the ship and the fluctuations in power demand. These fluctuations strongly depend on the sea state [34]. In future research, a load profile should be taken into account and load mitigating measures such as batteries and capacitors should be taken into consideration.

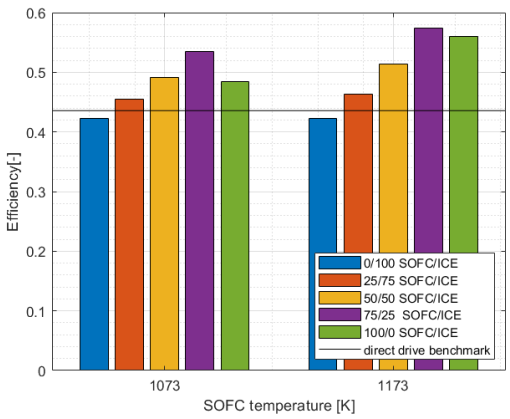

Figure 4.17: Efficiencies for different power splits per SOFC operating temperature.

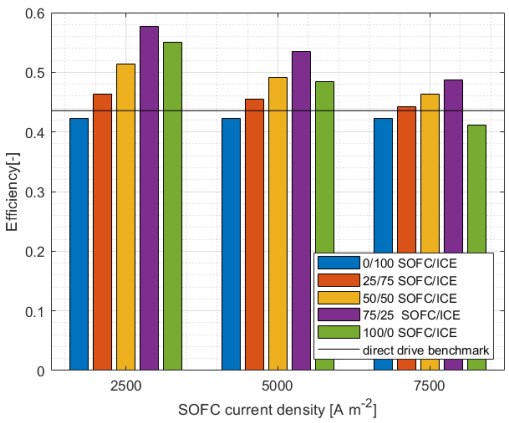

Figure 4.18: Efficiencies for different power splits per SOFC current density.

Table 4.2: Efficiencies [%] of different power configurations for different temperatures [K] and current densities [$A \cdot m^{-2}$]

temperature	current density	ice direct drive	0/100	25/75	50/50	75/25	100/0
800	2500	43.6	42.3	46.4	51.4	57.6	55.0
	5000			45.4	49.1	53.4	48.4
	7500			44.2	46.4	48.7	41.1
900	5000			46.4	51.3	57.4	56.0

4.3.2. Comparing combined cycle performance

The results will first be compared to the results from the work of Koekkoek [44]. For the ammonia-fuelled plant, the combined cycle concept has an additional advantage. As ammonia has poor combustion characteristics, a promoter fuel is required for the ICE. The idea is that the combined cycle can provide this pilot fuel in the form of hydrogen from ammonia cracking using the heat from the SOFC. However, the ammonia-fuelled cycle does not need to evaporate the water fuel mixture. This implies that the implementation of a combined cycle is advantageous for both fuel types.

The plant has almost the same standard operating parameters as in Table 4.1. However, there is no steam required for the ammonia plant and the UF is set to 0.76. As discussed in Section 2.1.1 the UF has no significant influence on the SOFC performance in the methanol-fuelled plant when it is considered in a combined configuration. Therefore, the effects due to the difference in UF are negligible. In Figure 4.19 and Table 4.3 the results regarding efficiency are shown. It can be seen that with lower powersplits, the ammonia-fuelled plant is more efficient, but at the 75/25 power split, the MeOH plant is more favourable. This is because the ammonia-fuelled ICE is more efficient and the MeOH-fuelled SOFC is more efficient. However, Koekkoek [44] provides no numerical results on the efficiency of the standalone ICE genset or the standalone SOFC with a UF of 0.8. By visual evaluation of a graphic result of Koekkoek [44] can be concluded that his ICE genset has a higher efficiency at nominal load compared to methanol fuelled ICE from this research. Regarding the SOFC standalone, Koekkoek reported efficiencies of 45.4% for a UF of 0.7 and 56.2% for a UF of 0.9, and an average of these values is taken for visualisation purposes. For both configurations, a decrease in efficiency can be observed in the standalone SOFC condition, with this decrease being more pronounced in the methanol-fuelled configuration. The cause of this is unknown, given that the amount of fuel remaining in the anode off-gas is sufficient for both the evaporation and reforming processes for both fuels. However, as the value for the ammonia-fuelled plant is an estimate, caution must be exercised when making statements regarding its accuracy. Despite these differences, the values are relatively close, suggesting a substantial degree of competitiveness between them.

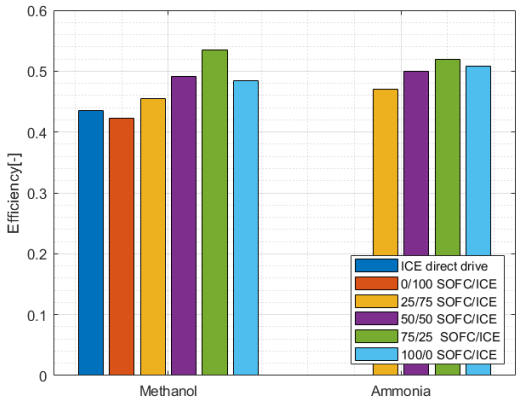

Figure 4.19: Efficiencies for different power configurations per fuel.

Table 4.3: Data on the efficiency [%] from Figure 4.19. Estimate given in *italic*.

Power configuration	NH_3	$MeOH$
ICE direct drive	-	43.6
0/100	-	42.3
25/75	47	45.4
50/50	50	49.2
75/25	52	53.4
100/0	*50.8*	48.4

Furthermore, a comparison could be drawn to the work of Cocco and Tola [21] who investigated the performance of an SOFC-GT cycle. The proposed SOFC model is a tubular cell that operates at 1173 K and a current density of 3000 $A \cdot m^{-2}$. It is modelled in ASPEN PLUS. Unfortunately, the author does not describe how the system is modelled, which makes explaining differences challenging. Also, the definition for the SOFC efficiency does not consider the fuel left in the AOG. This results in an SOFC efficiency of 50.3 %. When the same temperature and current density is set in the model from this thesis and the same definition of efficiency is used, an efficiency of 54.1% is obtained. Unfortunately, because of the undescribed method, the differences over different loss mechanisms cannot be described.

When the system is considered as a combined cycle with a powersplit of 72/28, the model from Cocco reaches an efficiency of 68.5 % compared to 57.8% from this thesis.

A third comparison is done with the work of Diskin and Tartakovsky [25]. As with this research, they evaluated a methanol-fuelled SOFC- reciprocation ICE hybrid system. Similarly to this research, the SOFC model proposed by Diskin and Tartakovsky [25] is based on the work of Aguiar et al. [1]. In his approach, his ICE model is based on the Otto cycle where he introduced a finite-speed-thermodynamics and finite-time-thermodynamics approach. It reaches a peak efficiency of 50%, which is an exceptional result for an ICE. No clear figures on the standalone SOFC efficiency were reported. Additionally, no explicit statement regarding the fuel reforming strategy was provided, making it difficult to assess the BoP power consumption. Furthermore, the exact fuel stream towards the SOFC and ICE is not specified, which makes it challenging to compare the individual components between this research and Diskin's work. Efficiencies between 50% and 60% are reported for the combined cycle, but clear statements on operational parameters are missing.

4.4. Research and modelling approach reflection

Although the level of detail is sufficient for modelling the system in question, there are points where the model may attain more fidelity without a significant increase in computational effort. Other measures could also be taken to improve the capabilities of the model. The indicated points of improvement will be discussed below.

Within the context of the SOFC model, a mean temperature value is used. However, it is important to recognise that the estimation of the operating temperature can influence the outcomes of the simulation. As depicted in Figure 4.5, it is apparent that the efficiency of the system is not linearly dependent on the temperature.

It is also assumed that the fuel instantly decomposes upon entering the cell. However, this is not correct. This could have effects on the average partial pressures of the fuel. Certain constants could be introduced to compensate for these deviations. These constants should be determined using experiments.

The existing model is limited to steady state. Therefore, the dynamic behaviour could not be evaluated.

Within the engine model, a number of physical phenomena are simplified. Among these, is the manner in which the isochoric and isobaric specific heat capacities are modelled. Rather than being dependent on temperature, these quantities are estimated to be constant. This simplification may lead to inaccuracies within the model. The same is true for the heat capacity ratio. By making these values, especially the heat capacity ratio, temperature dependent, the models accuracy would increase. However, this approach also has its limitations. Specifically, the compression and expansion phases would need to be solved in incremental steps. This would significantly increase the computational effort. However, there are indications that it may be feasible to establish a correlation between the heat capacity ratio and volume. In that case, it would be possible to immediately jump from stage 1 to 2 or from 4 to 5 and thus not significantly increase computational effort.

Another feature of the model that stands out is the fact that the bsfc at nominal load is utilised as an input parameter, rather than being calculated as a result. This is then used to determine the heat input efficiency. This approach makes it difficult to assess the potential advantages or disadvantages of using alternative fuels.

Because the model works with a predefined global peak temperature and pressure, it is challenging to predict the formation of NOx emissions. Again, the influence of changing fuel is hard to capture here. Using experimental data, an empirical method could be computed to estimate NOx emissions without a significant increase in computation effort.

Certain modifications made to the original model resulted in numerical instabilities. The underlying cause of these instabilities remains uncertain. However, these instabilities believed to be there a result of an increase in the stiffness of the system. Consequently, the PID controller is not always able to locate the initial equilibrium, which limits the range of operable parameters for the model. This makes it challenging to evaluate the impact of variations in parameters, such as the global peak temperature and pressure, on the model's performance.

The coupling between the SOFC and ICE is currently simplistic: The dehydrated AOG from steady-state operations is fed to the ICE in the form of an initial heat input during the closed-cylinder process and waste heat from the ICE is used for the evaporation of the methanol-water stream. However, this coupling does not consider the impact of back pressure following the dehydrator, nor does it account for the influence of back pressure after the turbocharger as a result of the heat exchanger in the evaporator.

As suggested in the previous section, there is room for improvement of the heat integration. A better heat integration could reduce the fuel consumption from the burner and therefore increase system efficiency. Further investigation is necessary to develop a sophisticated heat management design that incorporates an effective control strategy.

Unfortunately, there is limited literature found on methanol fuelled combined SOFC reciprocation ICE research. This makes validation or the results challenging.

If the capabilities of the model were extended so that it can simulate dynamic loading, it could be used to simulate operational profiles of ships. This would provide more detail on the efficiency gains resulting from implementing combined cycles on ships.

5

Conclusion and recommendations

5.1. Conclusion

In this thesis, a combined cycle of a methanol-fuelled solid oxide fuel cell - internal combustion engine has been modelled and evaluated. From the literature, the following performance characteristics for maritime applications were identified:

- Electrical efficiency;
- Power and energy density;
- Environmental impact;
- Load transients;
- System start-up;
- Safety and reliability;
- Economics.

To address the first, second and fourth characteristic, a trade-off has to be made depending on the ship type and its operational profile. Therefore, the power plant consists not only of an SOFC but also of an ICE and is evaluated at different power splits. The implementation of an SOFC nearly always leads to improvements in the third characteristic.

The evaluated power plant operates as follows: methanol and water are introduced into the system as liquids. The streams are preheated in an economiser prior to entering the evaporators, which utilise waste heat from the ICE. The resulting methanol vapor and steam are then blended and conveyed by the blowers. After being heated to the correct reforming temperature in a heat exchanger, it enters the methanator. Here, the methanol is cracked and, together with the steam, partially reformed to, among others, a hydrogen/methane mixture. By controlling the temperature, one can determine the reforming ratio. Before entering the anode channel, the fuel stream is further heated with additional heat exhangers. In a separate stream, the air is preheated with a heat exchanger before entering the cathode channel. Here, the fuelstream is oxydised with oxygen ions transported through the electrolyte, in the process of producing electric power. The resulting anode-of-gas (AOG) and cathode-of-gas (COG) streams are used in their respective heat exchangers. The COG is emitted into the environment. The AOG is dehydrated and led to the turbocharger intake of the ICE. After it is compressed and intercooled, together with intake air, it is led to the cylinder. Here, the AOG/air mixture, which is still out of combustible limits, is compressed. At high pressure, methanol is directly injected and ignited with a spark plug. The exhaust gases drive the charger turbine and then pass through the heat exchanger in the evaporator. Subsequently, they are discharged into the environment, unless end-of-pipe technologies, like Selective Catalytic Reduction, to clean the exhaust gases are applied.

The electrical efficiency of the combined cycle is evaluated using a first principles based model in MATLAB & Simulink. The model consists of two main components: the SOFC model and the ICE model. The SOFC model again consist of sub models and is based on the work proposed by [44] who evaluated an ammonia-fuelled SOFC-ICE combined cycle. In the newly added methanator model it

is assumed that the methanol decomposes instantly. A chemical equilibrium between the water-gas-shift and methane steam reforming reactions is set up and controlled by the steam to fuel ratio and operating temperature, while the pressure is fixed. The SOFC itself consist of three sub-models: a mass balance, an energy balance and an electrochemical model. These models are zero-dimensional and use an average temperature for the structural components and gas streams. The pressure loss over the system is overcome by a compressor with a predefined isentropic efficiency. The dehydrated AOG consist of hydrogen and CO_2. Important input parameters that should be specified are current density, operating temperature, fuel utilisation factor and number of cells.

The input for the ICE genset model is based on the Wärtsilä 12V31DF. The model core consists of a five-stage air standard Seiliger cycle. The heat that is added comes from the hydrogen in the AOG and added methanol from the fuel governor, which is controlled by a proportional controller. Key parameters that should be specified are brake specific fuel consumption at 100% load, charge pressure & temperature after the intercooler at 100% load, compression ratio, max cylinder pressure and rated power output.

The efficiency performance of the SOFC has been evaluated under various operational conditions, and it was found that the current density and operating temperature have the most significant impact on performance. The results were compared to the work of Koekkoek [44]. The electrical efficiency of both systems was found to be comparable, with values of 58.2% for the ammonia-fuelled plant and 58.6% for the methanol-fuelled plant. The standalone performance of the SOFC was also evaluated. It was found that the efficiency of the standalone SOFC system, compared to the combined cycle configuration, decreased due to the lag in waste heat generated by the ICE required for the fuel stream evaporation and the disuse of residual fuel in the exhaust. The results were also compared to experimental data by Rechberger et al. [70]. comparable figures where obtained.

The combined cycle has been evaluated for different power configurations: P_{SOFC}/P_{ICE} = 0/100, 25/75, 50/50 and 75/25 and 100/0. In addition to that, the two most influential SOFC parameters have been varied. For standard operating conditions, the results were compared to a methanol-fuelled direct drive ICE and an ammonia-fuelled combined cycle and the results are presented in Figure 5.1. The efficiency gain of the methanol-fuelled 75/25 configuration compared to the direct drive is limited. This raises the questions about whether the added complexity of introducing an SOFC is justified for the limited efficiency gain. The highest efficiency was obtained with the methanol-fuelled 75/25 power split, but due to the large proportion of SOFC power, it is less tolerant to dynamics in the load, making it questionable whether it can fully meet the dynamic power demand of a ship. Therefore, it is expected that the 50/50 power split has the most potential to be technologically feasible. Additionally, the previously discussed decline in efficiency due to using the SOFC in standalone condition, can also be observed. When considering efficiency, the values for the ammonia fuelled and methanol fuelled plant are similar.

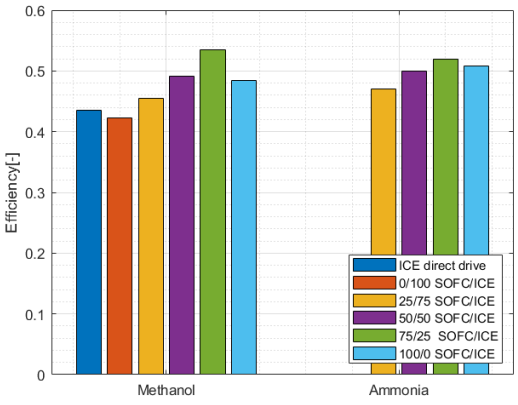

Figure 5.1: Figure 4.19From Results : Efficiencies for different power configurations per fuel with (1)=MeOH and (2) = NH3.

The 50/50 powersplit configuration is 5.6 percentpoints more efficient than the methanol-fuelled direct drive ICE and 1.2 percentpoints more efficient than the methanol-fuelled standalone SOFC. This clearly shows the synergistic benefits of combining a methanol-fuelled SOFC with an ICE. However,

when compared to the ammonia fuelled combined cycle with 50/50 power split, it is 0.9 percentpoints less efficient. Nevertheless, it is important to exercise caution when drawing further conclusions from this last figure as the model has been constructed at a system level and no thorough uncertainty analysis has been conducted. Taken in its entirety, this project demonstrates the substantial potential of the methanol-fuelled SOFC-ICE combined cycle.

5.2. Recommendations

Based on the results and conclusions presented in the preceding sections, the following recommendations for future research are proposed:

- It is recommended that case studies should be conducted, utilising different operational profiles of vessels in order to gain a deeper understanding of the capabilities and limitations of (methanol-fuelled) combined cycles in maritime applications. Such studies would provide valuable information on the feasibility of implementing combined cycles in terms of dynamic loading capabilities, power and energy density, and a more detailed understanding of the electrical efficiency.
- In order to make the before proposed study more valuable, one should implement dynamic capabilities of the SOFC as well. This would give insights in the performance during load transients and system start-up.
- additionally it is recommended to Model the SOFC in more than zero dimensions. This would provide a more detailed evaluation on the interplay between the mass balance, energy balance and the electrochemical model. It would provide more insight into the effects of the endothermic methane reforming reaction, variable temperatures and variable partial pressures on the operating voltage. In addition to that, it can provide information on thermal gradients in the cell, which causes thermal stresses and possible hot spots which can cause sintering of the electrodes.
- Adapt the ICE model so that it is no longer determined by a pre specified bsfc. In this way the change in fuel types can be better approximated. This, together with the implementation of volume dependent specific heat capacities for the five-stage Seiliger cycle, can make the engine model more versatile in evaluating different fuels in the energy transition.
- The high heat of evaporation of methanol makes it a challenging fuel for port fuel injection, while its low cetane number makes it unsuitable for compression ignition. On the other hand, its high burning velocity can be beneficial from an efficiency point of view. Therefore, a comprehensive study on the in-cylinder process, possibly with multiple zones, with regard to the injection and ignition of methanol is required. In addition, advanced ignition methods should be considered in this research. A detailed study of the in-cylinder process can also contribute to an evaluation of NOx emissions.
- A comprehensive examination of emissions would provide a deeper understanding of the benefits of implementing a methanol-fuelled SOFC-ICE combined cycle. In addition to investigating the NOx, special attention should be placed on evaluating the potential for formaldehyde emissions.
- A more detailed coupling between SOFC and ICE should be established. This coupling can be important for simulating dynamic loadings and load transients. This should incorporate the effect of back pressure as well and consider control strategies, as well as the addition of accumulators in the system lay-out. A further coupling could involve a more sophisticated heat integration with its own control strategies. This could increase efficiency due to lowering the fuel consumption regarding the methanol burner which is required for the reforming of methanol.

References

[1] P. Aguiar, C. S. Adjiman, and N. P. Brandon. “Anode-supported intermediate temperature direct internal reforming solid oxide fuel cell. I: Model-based steady-state performance”. In: *Journal of Power Sources* 138.1-2 (Nov. 2004), pp. 120–136. ISSN: 03787753. DOI: 10.1016/j.jpowsour.2004.06.040.

[2] Teresa L Alleman et al. “Biodiesel Handling and Use Guide (Fifth Edition)”. In: (2016).

[3] Afshin Barjaneh and Hoseyn Sayyaadi. “A new closed-form thermodynamic model for thermal simulation of spark ignition internal combustion engines”. In: *Energy Conversion and Management* 105 (Aug. 2015), pp. 607–616. ISSN: 01968904. DOI: 10.1016/j.enconman.2015.08.008.

[4] Ian H. Bell et al. “Pure and Pseudo-pure Fluid Thermophysical Property Evaluation and the Open-Source Thermophysical Property Library CoolProp”. In: *Industrial & Engineering Chemistry Research* 53.6 (2014), pp. 2498–2508. DOI: 10.1021/ie4033999. eprint: http://pubs.acs.org/doi/pdf/10.1021/ie4033999. URL: http://pubs.acs.org/doi/abs/10.1021/ie4033999.

[5] L. van Biert et al. “A review of fuel cell systems for maritime applications”. In: 327 (Sept. 2016), pp. 345–364. ISSN: 03787753. DOI: 10.1016/j.jpowsour.2016.07.007.

[6] L. van Biert et al. “A thermodynamic comparison of solid oxide fuel cell-combined cycles”. In: *Journal of Power Sources* 397 (Sept. 2018), pp. 382–396. ISSN: 03787753. DOI: 10.1016/j.jpowsour.2018.07.035.

[7] L. van Biert et al. “Dynamic modelling of a direct internal reforming solid oxide fuel cell stack based on single cell experiments”. In: *Applied Energy* 250 (Sept. 2019), pp. 976–990. ISSN: 03062619. DOI: 10.1016/j.apenergy.2019.05.053.

[8] Lindert van Biert. “Direct Internal Methane Steam Reforming in Operating Solid Oxide Fuel Cells”. In: (2014).

[9] Lindert van Biert. “personal discussion on dynamic behaviour of SOFCs on the 3^{th} of May”. In: (2022).

[10] Lindert van Biert. “personal discussion on fuel reforming for SOFCs on the 29^{th} of September”. In: (2022).

[11] Lindert van Biert. “Solid oxide fuel cells for ships - System integration concepts with reforming and thermal cycles”. In: (2020). DOI: 10.4233/uuid:dd1f7899-38ee-4c78-a5b0-a6fa92c90f56. URL: https://doi.org/10.4233/uuid:dd1f7899-38ee-4c78-a5b0-a6fa92c90f56.

[12] Van Biert. “Dynamic Modelling of a Solid Oxide Fuel Cell System for Maritime Applications considering Balance of Plant components”. In: (2021).

[13] Bloom. “hydrogen fuel cell Bloom Energy”. In: (2022).

[14] J.J. Bosklopper. “Experimental and simulationbased investigation of the performance of a 100 % methanol portinjected spark-ignited engine.” In: (2020).

[15] Fuelcells Bulletin. “Wärtsilä marine SOFC for Wallenius car-carrier”. In: (2010).

[16] Annamaria Buonomano et al. “Hybrid solid oxide fuel cells-gas turbine systems for combined heat and power: A review”. In: 156 (Oct. 2015), pp. 32–85. ISSN: 03062619. DOI: 10.1016/j.apenergy.2015.06.027.

[17] Cespa. “gas oil F-76”. In: (2017).

[18] Wonjae Choi et al. “Solid oxide fuel cell operation in a solid oxide fuel cell–internal combustion engine hybrid system and the design point performance of the hybrid system”. In: *Applied Energy* 254 (Nov. 2019). ISSN: 03062619. DOI: 10.1016/j.apenergy.2019.113681.

[19] G. Cinti et al. “SOFC operating with ammonia: Stack test and system analysis”. In: *International Journal of Hydrogen Energy* 41.31 (2016), pp. 13583–13590. ISSN: 03603199. DOI: 10.1016/j.ijhydene.2016.06.070.

[20] Allen W. Cline. “Engine Basics: Detonation and Pre-ignition”. In: (2000).

[21] Daniele Cocco and Vittorio Tola. “Comparative performance analysis of internal and external reforming of methanol in SOFC-MGT hybrid power plants”. In: *Journal of Engineering for Gas Turbines and Power* 129.2 (Apr. 2007), pp. 478–487. ISSN: 07424795. DOI: 10.1115/1.2364009.

[22] Livia Cohen. “Investigation into the implications of fuel cell shipboard integration into the T-AGOS 19 class”. In: (2012).

[23] Maria C. Díaz-de-Baldasano et al. “Conceptual design of offshore platform supply vessel based on hybrid diesel generator-fuel cell power plant”. In: *Applied Energy* 116 (Mar. 2014), pp. 91–100. ISSN: 03062619. DOI: 10.1016/j.apenergy.2013.11.049.

[24] Yu Ding. “Characterising combustion in diesel engines using parameterised finite stage cylinder process models”. In: (2011).

[25] David Diskin and Leonid Tartakovsky. “Finite-time energy conversion in a hybrid cycle combining electrochemical, combustion and thermochemical recuperation processes”. In: *Energy Conversion and Management* 262 (June 2022). ISSN: 01968904. DOI: 10.1016/j.enconman.2022.115673.

[26] Cüneyt Ezgi, M. Turhan Çoban, and Özgün Selvi. “Design and thermodynamic analysis of an SOFC system for naval surface ship application”. In: *Journal of Fuel Cell Science and Technology* 10.3 (2013). ISSN: 1550624X. DOI: 10.1115/1.4024254.

[27] Yongming Feng et al. “Progress and prospect of the novel integrated SOFC-ICE hybrid power system: System design, mass and heat integration, system optimization and techno-economic analysis”. In: *Energy Conversion and Management: X* (Jan. 2023), p. 100350. ISSN: 25901745. DOI: 10.1016/j.ecmx.2023.100350. URL: https://linkinghub.elsevier.com/retrieve/pii/S2590174523000065.

[28] Robert S. Gable. “Comparison of acute lethal toxicity of commonly abused psychoactive substances”. In: (2004).

[29] Zhan Gao et al. “Development of methanol-fueled low-temperature solid oxide fuel cells”. In: *International Journal of Energy Research* 35.8 (June 2011), pp. 690–696. ISSN: 0363907X. DOI: 10.1002/er.1718.

[30] J. M. Gordon and Mahmoud Huleihil. “General performance characteristics of real heat engines”. In: *Journal of Applied Physics* 72.3 (1992), pp. 829–837. ISSN: 00218979. DOI: 10.1063/1.351755.

[31] L. Gouveia et al. “Biodiesel from microalgae”. In: *Microalgae-Based Biofuels and Bioproducts: From Feedstock Cultivation to End-Products*. Elsevier Inc., June 2017, pp. 235–258. ISBN: 9780081010273. DOI: 10.1016/B978-0-08-101023-5.00010-8.

[32] Erdogan Guk et al. “Parameters and their impacts on the temperature distribution and thermal gradient of solid oxide fuel cell”. In: *Applied Energy* 241 (2019), pp. 164–173. DOI: 10.1016/j.apenergy.2019.03.034.

[33] Elbert Hendricks and Spencer C Sorenson. “Mean Value Modelling of Spark Ignition Engines”. In: 99 (1990), pp. 1359–1373.

[34] Jun Hou, Jing Sun, and Heath Hofmann. “Mitigating power fluctuations in electrical ship propulsion using model predictive control with hybrid energy storage system”. In: (2014), pp. 4366–4371. ISSN: 07431619. DOI: 10.1109/ACC.2014.6858803.

[35] Chung Yao Hsuan et al. “Water-In-Oil emulsion as boiler fuel for Reduced NOx emissions and improved energy saving”. In: *Energies* 12.6 (2019). ISSN: 19961073. DOI: 10.3390/en12061002.

[36] IMO. *Fourth IMO Greenhouse Gas Study*. 2020. URL: https://wwwcdn.imo.org/localresources/en/OurWork/Environment/Documents/Fourth%5C%20IMO%5C%20GHG%5C%20Study%5C%202020%5C%20Executive-Summary.pdf.

[37] IMO. "METHANOL AS MARINE FUEL: ENVIRONMENTAL BENEFITS, TECHNOLOGY READINESS, AND ECONOMIC FEASIBLITY". In: (2016).

[38] IPCC. "Climate change 2021, The physical science basis, summary for policymakers". In: (2021).

[39] IPCC. "Climate Change 2022: Impacts, Adaptation and Vulnerability, Summary for Policymakers". In: (2021).

[40] Maarten de Jong. "An investigation into the possibilities concerning Solid Oxide Fuel Cells in naval vessels". In: (2020).

[41] Ying Wei Kang et al. "Dynamic temperature modeling of an SOFC using least squares support vector machines". In: *Journal of Power Sources* 179.2 (May 2008), pp. 683–692. ISSN: 03787753. DOI: 10.1016/j.jpowsour.2008.01.022.

[42] Daniel Ketzer et al. *Land Use Conflicts between Agriculture and Energy Production Systems Approaches to Allocate Potentials for Bioenergy and Agrophotovoltaics.* ISBN: 9789179110147.

[43] Jaehyun Kim et al. "Analysis on the operating performance of 5-kW class solid oxide fuel cell-internal combustion engine hybrid system using spark-assisted ignition". In: *Applied Energy* 260 (Feb. 2020). ISSN: 03062619. DOI: 10.1016/j.apenergy.2019.114231.

[44] A. Koekkoek. "An ammonia fuelled SOFC - ICE Hybrid system for ships". In: (2021).

[45] A. Koekoek. "Ammonia fuelled solid oxide fuel cell – internal combustion engine hybrid system for marine applications Literature study". In: (2021).

[46] H.J. Kruize. "Improving Methanol Powered Solid Oxide Fuel Cell – Gas Turbine Power Units for Naval Support Vessels through Fuel and Heat Recovery". In: (2021).

[47] N. Laosiripojana and S. Assabumrungrat. "Catalytic steam reforming of methane, methanol, and ethanol over Ni/YSZ: The possible use of these fuels in internal reforming SOFC". In: *Journal of Power Sources* 163.2 (Jan. 2007), pp. 943–951. ISSN: 03787753. DOI: 10.1016/j.jpowsour.2006.10.006.

[48] James. Larminie and Andrew. Dicks. *Fuel cell systems explained*. J. Wiley, 2003, p. 406. ISBN: 047084857X.

[49] Young Duk Lee et al. "Exergetic and exergoeconomic evaluation of an SOFC-Engine hybrid power generation system". In: *Energy* 145 (Feb. 2018), pp. 810–822. ISSN: 03605442. DOI: 10.1016/j.energy.2017.12.102.

[50] Keno Leites et al. "SchIBZ - Design Of Different Diesel Based Fuel Cell Systems for Seagoing Vessels and Their Evaluation". In: *ECS Transactions* 42.1 (Apr. 2012), pp. 49–58. ISSN: 1938-5862. DOI: 10.1149/1.4705479.

[51] Reed & Lerner. "Methanol: Aversatile fuel for immedaia use". In: (1973).

[52] Elizabeth Lindstad et al. "Reduction of maritime GHG emissions and the potential role of E-fuels". In: *Transportation Research Part D: Transport and Environment* 101 (Dec. 2021). ISSN: 13619209. DOI: 10.1016/j.trd.2021.103075.

[53] Mingfei Liu et al. "Direct liquid methanol-fueled solid oxide fuel cell". In: *Journal of Power Sources* 185.1 (Oct. 2008), pp. 188–192. ISSN: 03787753. DOI: 10.1016/j.jpowsour.2008.06.076.

[54] DIVISION ON TECHNOLOGY AND. UNITED NATIONS CONFERENCE ON TRADE LOGISTICS and DEVELOPMENT. *REVIEW OF MARITIME TRANSPORT 2021.* UNITED NATIONS, 2022. ISBN: 9789211130263. URL: https://unctad.org/system/files/official-document/rmt2021_en_0.pdf.

[55] Ilaria Lucentini et al. "Review of the Decomposition of Ammonia to Generate Hydrogen". In: *Industrial and Engineering Chemistry Research* 60.51 (Dec. 2021), pp. 18560–18611. ISSN: 15205045. DOI: 10.1021/acs.iecr.1c00843.

[56] Machiele. "Summary of the fire safety impacts of methanol as a transportation fuel." In: (1990).

[57] MAHLE. "Mahle Powertrain Jet Ignition". In: (2022).

[58] MAN. “Methanol in Shipping”. In: (2021).

[59] Sara McAllister, Jyh-Yuan Chen, and A. Carlos Fernandez-Pello. “Fundamentals of Combustion Processes”. In: Mechanical Engineering Series (2011). DOI: 10.1007/978-1-4419-7943-8. URL: https://link.springer.com/10.1007/978-1-4419-7943-8.

[60] Methanex. “Physical Properties of Pure Methanol”. In: (2020).

[61] R Metkemeijer and P Achard. “COMPARISON OF AMMONIA AND METHANOL APPLIED INDIRECTLY IN A HYDROGEN FUEL CELL”. In: 19.6 (1994), pp. 535–542.

[62] molland. “The Maritime Engineering Reference Book - chapter 6”. In: (2008).

[63] Shraddha Dilip More. “INVESTIGATION ON THE DEGRADATION OF ALUMINUM IN METHANOL-GASOLINE BLENDS”. In: (2018).

[64] Kai Morganti. “Improving the Efficiency of Conventional Spark-Ignition Engines using Octane-on-Demand Combustion.” In: (2016).

[65] United Nations. “UN climatechange prevention”. In: (20).

[66] NIST. “NIST chemistry webbook”. In: (). URL: https://webbook.nist.gov/.

[67] Sung Ho Park, Young Duk Lee, and Kook Young Ahn. “Performance analysis of an SOFC/HCCI engine hybrid system: System simulation and thermo-economic comparison”. In: *International Journal of Hydrogen Energy* 39.4 (Jan. 2014), pp. 1799–1810. ISSN: 03603199. DOI: 10.1016/j.ijhydene.2013.10.171.

[68] Brant A. Peppley. “Methanol-steam reforming on Cu/ZnO/Al2O3. Part 1: the reaction network”. In: (1999).

[69] Afton D. Puckett. “KNOCK RATINGS OF GASOLINE SUBSTITUTES”. In: (1945).

[70] Juergen Rechberger et al. “Development of a Methanol SOFC APU Demonstration System”. In: *ECS Transactions* 25.2 (Sept. 2009), pp. 1085–1092. ISSN: 1938-5862. DOI: 10.1149/1.3205635.

[71] J W Reurings. *A modeling study to investigate performance of SOFC-ICE hybrid systems for marine applications*. Tech. rep. 2019. URL: http://repository.tudelft.nl/..

[72] H D Sapra. “Combined gas engine-solid oxide fuel cell systems for marine power generation”. In: (). DOI: 10.4233/uuid:12393b11-a4c3-4697-8757-2b2dbc1291ec. URL: https://doi.org/10.4233/uuid:12393b11-a4c3-4697-8757-2b2dbc1291ec.

[73] Harsh Sapra et al. “Hydrogen-natural gas combustion in a marine lean-burn SI engine: A comparitive analysis of Seiliger and double Wiebe function-based zero–dimensional modelling”. In: *Energy Conversion and Management* 207 (Mar. 2020). ISSN: 01968904. DOI: 10.1016/j.enconman.2020.112494.

[74] Harsh Sapra et al. “Integration of solid oxide fuel cell and internal combustion engine for maritime applications”. In: *Applied Energy* 281 (Jan. 2021). ISSN: 03062619. DOI: 10.1016/j.apenergy.2020.115854.

[75] Cenk Sayin. “Engine performance and exhaust gas emissions of methanol and ethanol-diesel blends”. In: *Fuel* 89.11 (Nov. 2010), pp. 3410–3415. ISSN: 00162361. DOI: 10.1016/j.fuel.2010.02.017.

[76] Martin Seemann and Henrik Thunman. “Methane synthesis”. In: (Jan. 2019), pp. 221–243. DOI: 10.1016/B978-0-12-815554-7.00009-X.

[77] Sang Hern Seo and Chang Sik Lee. “A study on the overall efficiency of direct methanol fuel cell by methanol crossover current”. In: *Applied Energy* 87.8 (2010), pp. 2597–2604. ISSN: 03062619. DOI: 10.1016/j.apenergy.2010.01.018.

[78] O. Siddiqui and I. Dincer. “Development and Assessment of a Novel Integrated System Using an Ammonia Internal Combustion Engine and Fuel Cells for Cogeneration Purposes”. In: *Energy and Fuels* 33.3 (Mar. 2019), pp. 2413–2425. ISSN: 15205029. DOI: 10.1021/acs.energyfuels.8b04323.

[79] D Stapersma. *Diesel Engines Volume 1 Performance Analysis*. 2009.

[80] D Stapersma. *Diesel Engines Volume 3 emissions and heat transfer*. 2009.

[81] Klein Woud; Stapersma. “design of propulsion and elctric power generation systems”. In: (2019).

[82] Eric Stauffer. “Flammable and Combustible Liquids”. In: (2008).

[83] C. Strazza. “Conceptual design of offshore platform supply vessel based on hybrid diesel generator-fuel cell power plant”. In: (2009).

[84] Congbiao Sui et al. “Mean value first principle engine model for predicting dynamic behaviour of two-stroke marine diesel engine in various ship propulsion operations”. In: *International Journal of Naval Architecture and Ocean Engineering* 14 (Jan. 2022). ISSN: 20926790. DOI: 10.1016/j.ijnaoe.2021.100432.

[85] “Sustainability-Methanol-as-Marine-Fuel”. In: ().

[86] Martin Svanberg et al. “Renewable methanol as a fuel for the shipping industry”. In: *Renewable and Sustainable Energy Reviews* 94 (Oct. 2018), pp. 1217–1228. ISSN: 18790690. DOI: 10.1016/j.rser.2018.06.058.

[87] Global Combustion Systems. “Oil Fuel Properties”. In: (2022).

[88] R S Tol and Ir Y Linden. “Effect of Gas-To-Liquid (GTL) fuels on marine diesel engines compared to F-76”. In: 14 (Oct. 2018). DOI: 10.24868/issn.2515-818x.2018.010.

[89] R.S. Tol. “Combustion of methanol/diesel blends in a compression ignited engine”. In: (2020).

[90] United-Nations. “The six-sector solution to the climate crisis”. In: (2020). URL: https://www.unep.org/interactive/six-sector-solution-climate-change/.

[91] Karin Van Kranenburg et al. “E-FUELS: TOWARDS A MORE SUSTAINABLE FUTURE FOR TRUCK TRANSPORT, SHIPPING AND AVIATION”. In: (2020).

[92] Sebastian Verhelst et al. “Methanol as a fuel for internal combustion engines”. In: 70 (Jan. 2019), pp. 43–88. ISSN: 03601285. DOI: 10.1016/j.pecs.2018.10.001.

[93] De Vos. “AmmoniaDrive: a solution for zero-emission shipping?!” In: (). DOI: 10.1016/j.enconman.2020. URL: https://doi.org/10.1016/j.enconman.2020..

[94] K. Wang et al. “A Review on solid oxide fuel cell models”. In: 36.12 (June 2011), pp. 7212–7228. ISSN: 03603199. DOI: 10.1016/j.ijhydene.2011.03.051.

[95] Zhibin Wang et al. “The Development Trend of Internal Combustion Engine”. In: 1626.1 (Nov. 2020). ISSN: 17426596. DOI: 10.1088/1742-6596/1626/1/012139.

[96] Wärtsilä. “Wärtsilä 31 Product Guide”. In: (2021).

[97] Wärtsilä. “Wärtsilä 32 Methanol”. In: (2021).

[98] Wärtsilä. “Wärtsilä 32 Product Guide”. In: (2021).

[99] wärtsilä. “Wärtsilä generating sets - tailored to optimize performance”. In: (). URL: https://www.wartsila.com/marine/products/engines-and-generating-sets/generating-sets/wartsila-gensets.

[100] Wartsila. “Combustion engines and gas turbines”. In: (2022).

[101] K O Xavier et al. “Doping effects of cerium oxide on Ni/Al 2 O 3 catalysts for methanation”. In: (1999).

[102] Hui Xing et al. “Fuel cell power systems for maritime applications: Progress and perspectives”. In: *Sustainability (Switzerland)* 13.3 (Feb. 2021), pp. 1–34. ISSN: 20711050. DOI: 10.3390/su13031213.

[103] Jie Yang et al. “Improving the load-following capability of a solid oxide fuel cell system through the use of time delay control”. In: *International Journal of Hydrogen Energy* 42.2 (Jan. 2017), pp. 1221–1236. ISSN: 03603199. DOI: 10.1016/j.ijhydene.2016.10.107.

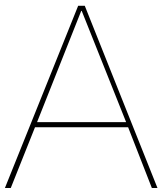

Appendix: Diesel model description

3 Simulation model for control verification

3.1 Introduction

The simulation model accurately represents all characteristics of a real vessel that are relevant for this research. The ship model consists of two sub-models. (1) A sub-model to analyse and validate the control actions of the energy management strategy. This simulation model has a flexible interface for connection of the energy management system and matches the behaviour of hybrid vessel as close as possible. (2) A model that matches the behaviour of the conventional vessel as closely as possible. This model serves as a benchmark for analysing the fuel consumption of the vessel equipped with the hybrid drive train in combination with the ECMS relative to the fuel consumption of a vessel that is equipped with a conventional drive train.

The two sub-models are based on the general ship modelling approach as applied by the Marine Engineering department at Delft University of Technology. But some adjustments were required for modelling the hybrid vessel because of the presence of the electric machine and battery. The general ship model is shown in Figure 45 and the model shown in Figure 46 represents the hybrid system. The harbour tug is equipped with two drive trains. The overview in Figure 46 shows only one of the two drive trains (port or starboard).

The ship model is a forward facing -or integrating model, i.e. a dynamic model. The inputs for the ship model are the speed settings for the diesel engine and electric machine and the pitch setting of the thruster. The output amongst others is the resulting ship speed and propeller torque and thrust.

First the dynamic model of the conventional ship is explained. The conventional ship consist the following sub-models: (1) diesel engine, (2) shaft rotational dynamics, (3) propeller, (4) ship dynamics, and (5) ship resistance. The latter two are explained in the section: “manoeuvring model”

Secondly the dynamic model of hybrid ship will be explained. This model is extended with an electric machine, battery and a flexible interface for connection to the controller model.

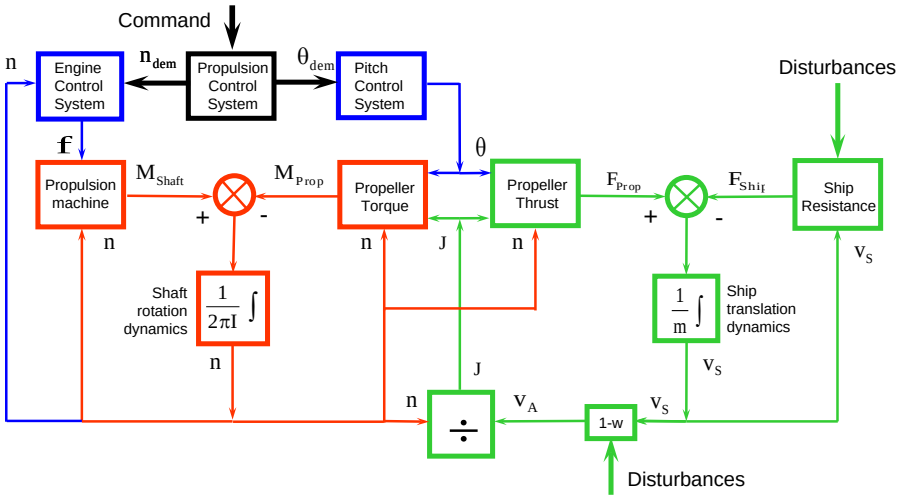

Figure 45: General ship propulsion model as presented in [Grimmelius et al., 2007].

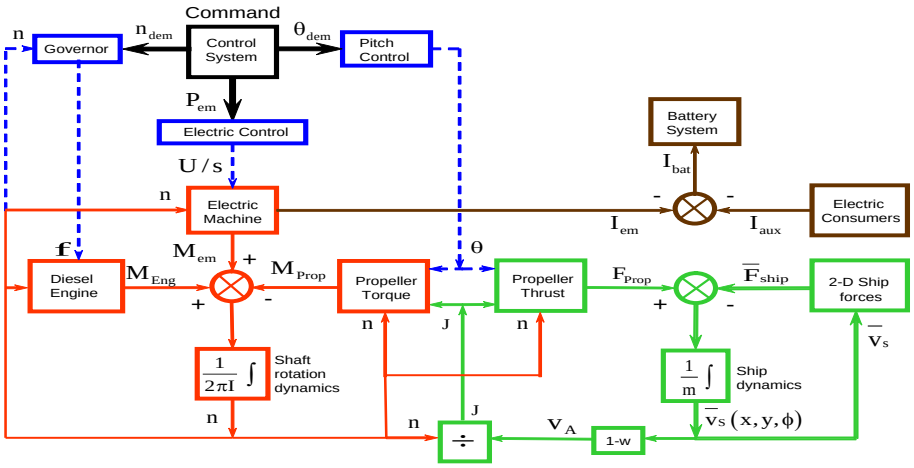

Figure 46: Schematic overview hybrid ship model as presented in [Grimmelius, et al., 2011]

3.2 Conventional ship model

As described in the introduction of this section the model used for this conventional ship model is based on the general ship model developed by the Marine Engineering department at Delft University of Technology. The sub-models used for this conventional ship model are briefly explained in this section.

3.2.1 Diesel engine

The diesel engine described in this section is a relatively simple model of a diesel engine. This diesel engine model is developed with the intention of developing an accurate model using easily accessible data from the project guide. The diesel engine model is based on the five points Seiliger process. The five point Seiliger process is shown in Figure 47. The diesel engine model calculates the torque from a difference between the engine speed and the set point of the engine speed. The model consists of three sub models: (1) fuel pump and governor, (2) the heat release per cylinder, and (3) exhaust system.

Fuel pump and governor

The inputs of the diesel engine model are the engine speed set point and the engine. Both inputs will first enter the fuel pump and governor sub-model and controlling the diesel engine speed. The amount of fuel injected per cycle is controlled by means of a PID-controller in combination with a torque, air –and fuel rack limiter. The latter resemble the physical limitation of the diesel engine and governor.

The heat release per cylinder

The heat release sub-model contains sub-blocks representing the five different stages during the Seiliger cycle. The Seiler cycle can be divided in 5 different stages. (1) 1-2 adiabatic compression. (2) 2-3 Addition of heat at constant volume. (3) 3-4 Addition of heat at constant pressure. (4) 4-5 adiabatic expansion. (5) 5-1 Rejection of heat at constant volume.

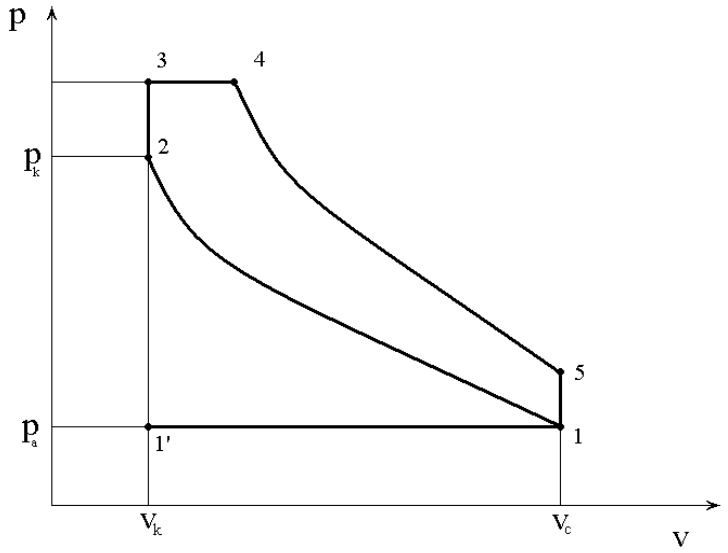

Figure 47: Five point Seiliger process

The input variables are: (1) the fuel per cycle, (2) rotational speed of the diesel engine, and (3) charge air pressure. The output variables are: (1) the heat rejection flow per cylinder, (2) the Mean Effective Pressure (MEP), and (3) the torque output of the diesel engine. The main output, the diesel engine torque, is used as input for the ship propulsion model. The torque of the diesel engine is an input variable for calculating the mean effective pressure per cylinder.

The MEP is calculated as follow:

$$MEP = \frac{M_{eng} \cdot k \cdot 2 \cdot \pi}{(V_1 - V_2) \cdot i} \tag{3.1}$$

Where:

$$V_1 - V_2 = V_s \tag{3.2}$$

Function 3.2 can be rewritten:

$$V_1 = x \cdot V_s + V_2 \tag{3.3}$$

Because ε=R_c is assumed, it follows x=1

The engine torque is a function of the indicated torque and torque losses. The engine torque is calculated as follows:

$$M_{eng} = M_i - M_{loss} \tag{3.4}$$

The torque losses are a function of the engine speed and nominal torque losses. The function for the torque losses is as follows:

$$\mathrm{M_{loss\,nom}} = \frac{\mathrm{P_{eng\,nom}} \cdot (1 - \eta_{\mathrm{m\,nom}})}{2 \cdot \pi \cdot n_{\mathrm{eng\,nom}} \cdot \eta_{\mathrm{m\,nom}}}$$

$$\mathrm{M_{loss}} = \mathrm{M_{loss\,nom}} \cdot 0.5 + \mathrm{M_{loss\,nom}} \cdot 0.5 \cdot \frac{\mathrm{n_{eng}}}{\mathrm{n_{eng\,nom}}} \tag{3.5}$$

The indicated torque is as follows:

$$\mathrm{M_i} = \frac{m_a \cdot w_i \cdot i}{k \cdot 2 \cdot \pi} \tag{3.6}$$

Where m_a = air mass flow, w_i = indicated work per cylinder during one cycle, i = amount of cylinders and k = two or four stroke engine.

The indicated work is calculated as follows:

$$w_i = w_{out} - w_{in} \tag{3.7}$$

The delivered work and the work needed during compression are defined as follows:

$$w_{out} = w_{3-4} + w_{4-5}$$

$$w_{in} = w_{1-2} \tag{3.8}$$

The indicated work during the different stages of the Seiliger cycle will be determined as follows, except stage 2-3 where the indicated work is 0 J/kg:

$$w_{1\text{-}2} = \frac{\text{-}R}{\kappa \text{ - } 1} \cdot (T_2 \text{ - } T_1)$$

$$w_{3\text{-}4} = R \cdot (T_4 \text{ - } T_3) \tag{3.9}$$

$$w_{4\text{-}5} = \frac{\text{-}R}{n_e \text{ - } 1} \cdot (T_5 \text{ - } T_4)$$

The pressure, volumes and temperatures during the Seiliger cycle are calculated according to the formulas in Table 3.

Table 3: Formulas Seiliger cycle

Stage	Volume ratio	Pressure ratio	Temperature ratio
1-2	$\frac{V_1}{V_2} = r_c$	$\frac{p_1}{p_2} = r_c^{\kappa}$	$\frac{T_1}{T_2} = r_c^{\kappa-1}$
2-3	$\frac{V_3}{V_2} = 1$	$\frac{p_3}{p_2} = a$	$\frac{T_3}{T_2} = a$
3-4	$\frac{V_4}{V_3} = b$	$\frac{p_4}{p_3} = 1$	$\frac{T_4}{T_3} = b$
4-5	$\frac{V_5}{V_4} = \frac{r_c}{b}$	$\frac{p_4}{p_5} = \left(\frac{r_c}{b}\right)^{n_e}$	$\frac{T_4}{T_5} = \left(\frac{r_c}{b}\right)^{n_e-1}$

The sub-blocks 1-2, 2-3, 3-4, and 4-5 represent the 4 stages during the Seiliger cycle and are shown in Appendix B Figure 98 within the Simulink environment.

The entire Seiliger cycle can be calculated using the formulas mentioned in table 3, when parameters a and b are known. Parameters a and b are respectively functions of the specific heat release at constant-volume and the specific heat release at constant pressure. Parameters a and b are calculated as follows:

$$a = \frac{q_{cv}}{c_v \cdot T_2} + 1$$
$$b = \frac{q_{cp}}{c_p \cdot T_3} + 1 \qquad (3.10)$$

The specific heat release at constant volume and the specific heat release at constant pressure are calculated in the heat release block shown in Figure 98. The specific heat release at constant volume –and pressure depends on the effective heat release and engine speed, represented by parameter X_a.

$$q_{cv} = q_{eff} \cdot X_a$$
$$q_{cp} = q_{eff} \cdot (1 - X_a) \qquad (3.11)$$

The parameter X_a is a function of the ratio q_{cv} and q_{eff}, i.e. $X_{a\,\text{nom}}$ and the ratio of the engine speed and nominal engine speed. The function X_a is as follows:

$$X_a = 2 \cdot X_{a\,\text{nom}} - X_{a\,\text{nom}} \cdot \frac{n_{eng}}{n_{eng\,\text{nom}}} \qquad (3.12)$$

The effective heat release per cycle, per cylinder and per kilo is a function of the air mass and heat release per cycle and per cylinder.

$$q_{eff} = \frac{Q_{eff}}{m_a \cdot \eta_{comb}} \tag{3.13}$$

The mass of air into the diesel engine is a function of the charge air pressure, the volume of the cylinder and temperature of the charge air, which can be found in the project guide:

$$m_a = \frac{p_1 \cdot V_1}{R_a \cdot T_1} \tag{3.14}$$

The effective heat release is a function of the combustion efficiency, the mass of injected fuel and chemical content of the fuel. The combustion efficiency is calculated according to Betz et al. (Betz et al, 1986).

$$Q_{eff} = \eta_q \cdot m_f \cdot H_0 \tag{3.15}$$

Exhaust system

The exhaust system together with the turbocharger system is modelled with a so-called heat to pressure estimator. The input for the exhaust system model is the heat release flow per cylinder during stage 5-1 from the Seiliger cycle and is calculated as follows:

$$\dot{Q}_{5-1} = \frac{\eta_{eng} \cdot m_a \cdot c_v}{k} \cdot (T_5 - T_1) \tag{3.16}$$

The charge pressure is estimated in the following way:

$$p_1 = p_{amb} \cdot \left(\frac{\eta_{tc} \cdot \dot{Q}_{5-1}}{c_p \cdot T_{amb}} + 1 \right)^{\frac{\kappa}{\kappa - 1}} \tag{3.17}$$

3.2.2 Shaft rotational dynamic

The shaft rotation dynamics sub-model has two inputs. (1) The torque delivered by the diesel engine and (2) the torque required by the propeller. The required propeller torque will be reduced by the gearbox and is compared with the combined torque of the diesel engine. The difference between the combined torque and the required torque of the propeller results in the rotational speed of the propeller shaft according to Newton's second law of rotational motion:

$$\sum_{t\ \mathrm{end}}^{t=0} M = \frac{d(I \cdot \omega)}{dt} \Rightarrow I \cdot \frac{d\omega}{dt} = \sum_{t\ \mathrm{end}}^{t=0} M - \omega \cdot \frac{d(I)}{dt} \tag{3.18}$$

When the rotational inertia is assumed to be constant, the differential equation for the rotational speed will be as follows:

$$\frac{dn}{dt} = \frac{1}{2\pi} \cdot \frac{d\omega}{dt} = \frac{1}{2\pi} \cdot \frac{M_{eng} - M_{load}}{I}$$

$$n = \int \frac{1}{2\pi} \cdot \frac{M_{eng} - M_{load}}{I} \cdot dt + n_0 \qquad (3.19)$$

The gearbox will be incorporated in the rotational dynamics. The gearbox will transform the torque as required by the propeller into a load torque and the engine speed into the shaft speed by reducing it with the gearbox reduction ratio. The rotational speed will be the output of the rotational dynamics sub-model and serve as input of the propeller –and diesel engine sub-model.

3.2.3 Propeller

The propeller sub-model calculates the torque and thrust of the propeller at a certain rotational shaft speed and thrust angle. The torque and thrust needs to be balanced by the diesel engine and the ship's resistance.

The real vessel is equipped with a KA 5-75 Fixed Pitch Propeller (FPP) mounted in NO.19A nozzle. MARIN executed extensive measurements with this combination of propeller and nozzle. There are two common ways to represent the measurement data of the propeller. (1) Using a four-quadrant representation normally presented using the β, C_T and C_Q nomenclature. (2) The open water curve representation normally presented using the J, K_T, and K_Q nomenclature.

The results for the above mentioned propeller/nozzle combination is presented in the open water curve representation. The open water curves for different pitch angles are shown in Figure 48.

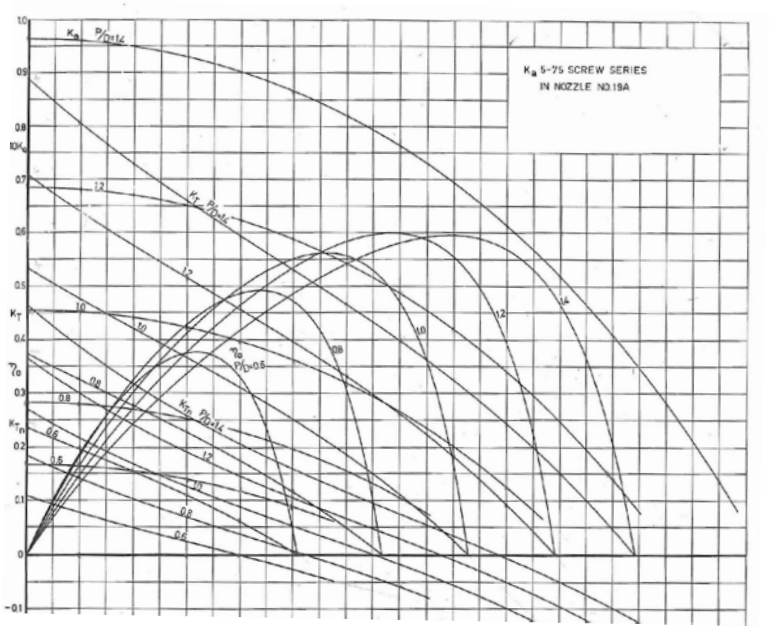

Figure 48: Open water curve at different pitch angles (KA 5-75 screw in NO.19A nozzle)

The correlation between the β, C_T and C_Q nomenclature and the traditional J,K_T and K_Q definitions used with open water data is shown in the equations below. The transformation is done so it can be

B

Appendix: MATLAB code for pressure ratio calculation

```
clear all
close all

%created by Luca Sopar (luca.sopar@gmail.com)


%This file determines the minimum pressure ratio required for fully evaporated
%fuel(methanol) for PFI for a given air excess ratio and ambient
%temperature


lamda = 1.81;                                % air exces ratio, according to verhelst there is no soot formation at 3.0
T_a = 300;                                   % [K] ambient temp
eta_comp = 0.8;                              % estimated efficiency of compressor

%other variables
stoich = 6.5;                                % [g/g] stoichiometric ratio methanol https://www.enginelabs.com/engine-tech/by-the-numbers-tuning-with-air-fuel-ratio-and-lambda/
p_a = 101325;                                % [pa] ambient pressure
Tmeoh = 50+273;                              % temperature of injected methanol (estimate)
mass_air = 1;                                % [kg] evaluated mass of air achter charger
mass_meoh = mass_air/(stoich*lamda);         % [kg] evaluated mass of meoh
kappa_a = 1.4;                               % [-], kappa (=c_p/c_v) of air

%% evaluating minimum pressure ratio for complete evaporation assuming isentropic compression in turbocharger

prloop = linspace(1,7);                                                                 %[-] pressureratios of turbocharger that are being evaluated
 for i = 1:length(prloop);
 S_a  = py.CoolProp.CoolProp.PropsSI('S','P',p_a,'T',T_a,'air');                        %[J/kg/K] entropy before charger
 T_b(i) = py.CoolProp.CoolProp.PropsSI('T','S',S_a,'P',prloop(i)*p_a,'air');            %[K] temp after charger
 T_evap(i) = py.CoolProp.CoolProp.PropsSI('T','P',prloop(i)*p_a,'Q',0.5,'methanol');    %[K] evaporation T of methanol at P after charger
 cp(i) = py.CoolProp.CoolProp.PropsSI('CPMASS','S',S_a,'T',T_b(i),'air');               %[J/kg/K] specific heat of air after charger
 cp_meoh(i) = py.CoolProp.CoolProp.PropsSI('CPMASS','P',prloop(i)*p_a,'T',Tmeoh,'methanol');  %[J/kg/K] specific heat of methanol right after injection
 H_v(i) = py.CoolProp.CoolProp.PropsSI('H','P',prloop(i)*p_a,'Q',1,'methanol');         %[J/kg] saturated vapor enthalpy of methanol after charger
 H_l(i) = py.CoolProp.CoolProp.PropsSI('H','P',prloop(i)*p_a,'Q',0,'methanol');         %[J/kg] saturated liquid enthalpy of methanol after charger
```

```
 q1(i) = mass_air*cp(i)*(T_b(i)-T_evap(i));                                    %[J] total heat loss from air to methanol
 q2(i) = mass_meoh*(cp_meoh(i)*(T_evap(i)-Tmeoh)+ H_v(i)-H_l(i));              %[J] total heat gain from air to methanol
%
 end
d_q = abs(q1-q2);                                                                                    %[J] absolute difference between heat loss/gain
[r,position]=find(d_q==min(d_q(:)));                                          %finding the coordinate of minimum required pr (heat required for evaporation is same as heat available for evaporation)
pr_is = prloop(position)                                                                          %[-] minimum pr for isentropic compressor in turbocharger
T_b_is = T_b(position);                                                                           %[K] corresponding T after charger
T1_is = T_evap(position);                                                                        %[K] T after evaporated methanol
```

```
%% evaluating minimum pressure ratio for complete evaporation assuming isentropic efficiency of compressor in turbocharger


pr_estimate = 3.6;                                          %estimated pressure ratio of the turbo charger in non isentropic process
%converting to isentropic efficiency
syms eta
eqn = 1+1/eta_comp*((pr_estimate)^((kappa_a-1)/kappa_a)-1) == pr_estimate^((kappa_a-1)/(kappa_a*eta));
var = eta;
eta = double(vpasolve(eqn,var));
%used in eta = (h2s - h1)/(h2 - h1)

for i = 1:length(prloop);

 S_a  = py.CoolProp.CoolProp.PropsSI('S','P',p_a,'T',T_a,'air');                 %[J/kg/K] entropy before charger
 h_a  = py.CoolProp.CoolProp.PropsSI('H','P',p_a,'T',T_a,'air');                 %[J/kg] enthalpy before charger
 h_b(i) = py.CoolProp.CoolProp.PropsSI('H','S',S_a,'P',prloop(i)*p_a,'air');     %[J/kg] ideal H after charger
 h_b_r(i) = (h_b(i)-h_a*(1-eta))./eta;                                           %[J/kg] real H after charger
 T_b(i) = py.CoolProp.CoolProp.PropsSI('T','H',h_b_r(i),'P',prloop(i)*p_a,'air');     %[K] temp after charger
 T_evap(i) = py.CoolProp.CoolProp.PropsSI('T','P',prloop(i)*p_a,'Q',0.5,'methanol');  %[K] evaration T of methanol at P after charger
 cp(i) = py.CoolProp.CoolProp.PropsSI('CPMASS','S',S_a,'H',h_b_r(i),'air');      %[J/kg/K] specific heat of air after charger
 cp_meoh(i) = py.CoolProp.CoolProp.PropsSI('CPMASS','P',prloop(i)*p_a,'T',Tmeoh,'methanol');  %[J/kg/K] specific heat of methanol right after injection
 H_v(i) = py.CoolProp.CoolProp.PropsSI('H','P',prloop(i)*p_a,'Q',1,'methanol');  %[J/kg] saturated vapor enthalpy of methanol after charger
 H_l(i) = py.CoolProp.CoolProp.PropsSI('H','P',prloop(i)*p_a,'Q',0,'methanol');  %[J/kg] saturated liquid enthalpy of methanol after charger
 q1(i) = mass_air*cp(i)*(T_b(i)-T_evap(i));                                    %[J] total heat loss from air to methanol
 q2(i) = mass_meoh*(cp_meoh(i)*(T_evap(i)-Tmeoh)+ H_v(i)-H_l(i));              %[J] total heat gain fraom air to methanol
end
```

```
76
77 d_q = abs(q1-q2);
                                                                    %[J]
       absolute difference between heat loss/gain
78 [r,position]=find(d_q==min(d_q(:)));
                                                  %finding the coordinate of
       minimum required pr (heat required for evaporation is same as heat available for
       evaporation)
79 pr = prloop(position)
                                                                %[-] minimum pr
80 T_b = T_b(position);
                                                                 %[K]
       corresponding T after charger
81 T1 = T_evap(position);
                                                               %[K] T after
       evaporated methanol
```

C

Appendix: MATLAB code for AOG flammability

```
%% stays the AOG with air outside the combustible mixture?
clear all
close all

LHV = 19.9;                          % [MJ/kg]lower heating value of methanol
stoich = 6.5;                        % [kg/kg] stoichiometric air to fuel ratio methanol
fuelflow = 0.16;                     % [kg/s] methanol fuel flow SOFC
fuf = 0.8;                           % fuel utilisation factor same as Koekkoek
eta_sofc = 0.55;                     % estimate efficiency of the fuelcell
eta_ice = 0.45;                      % estimate efficiency of ice
P_sofc = eta_sofc*fuelflow*LHV;      % [MW] power of the fuelcell
powersplit = 0.5;                    % P_sofc/P_ice
LHV_H2 = 120;                        % [MJ/kg]lower heating value of hydrogen
stoich_H2 = 34;                      % [kg/kg] stoichiometric air to fuel ratio methanol
lamda_H2 = 1;                        % air excess for the H2 combustion
lambda_meoh = 1;                     % air excess for the H2 combustion

%the methanol that is not used in the SOFC is transformed into hydrogen.
%The AOG is dehydrated resulting in:

H2_flow = fuelflow*(1-fuf)*2/32;                        % [kg/s] H2 massflow
P_ice = P_sofc*(1/powersplit-1);                        % [MW] power of the ice
ice_meohflow = (P_ice/eta_ice-H2_flow*LHV_H2)/LHV;      % [kg/s] massflow of methanol
meoh_airflow = ice_meohflow*stoich*lambda_meoh;         % [kg/s] air mass flow for meoh
    combustion
H2_airflow = H2_flow*stoich_H2;                         % [kg/s] air mass flow for H2
    combustion

air_mass = H2_airflow+meoh_airflow;                     % [kg/s] total air mass flow
r_equiv = air_mass/H2_flow*1/stoich_H2;                 % [kg/s] equivalence ratio
exceed = r_equiv/flamlim;                               % excedence over flammability limit
```

D

Appendix: Tables with data from result section

Table D.1: molar fractions [-] data used for Figure 4.1 and 4.2.

$r_{s/f}$	Temperature [K]	H_2	CH_4	CO_2	H_2O	CH_3OH	CO
$1:1$	843	0.4264	0.1033	0.1331	0.2719	0	0.0653
$1.5:1$	813	0.3760	0.0955	0.1332	0.3593	0	0.0360
$2:1$	793	0.3392	0.0851	0.1264	0.4268	0	0.0226
$2.5:1$	778	0.3102	0.0756	0.1183	0.4805	0	0.0154
$3:1$	763	0.2818	0.0692	0.1099	0.5285	0	0.0106
$1:1$	723	0.2136	0.2110	0.1357	0.4308	0	0.0088
$1:1$	773	0.3015	0.1702	0.1420	0.3633	0	0.0229
$1:1$	823	0.3920	0.1230	0.1381	0.2964	0	0.0503
$1:1$	873	0.4735	0.0744	0.1223	0.2393	0	0.0904
$1:1$	923	0.5324	0.0345	0.1013	0.2004	0	0.1314

Table D.2: Losses data used in Figures 4.3 to 4.6.

T [K]	973	1073	1173		
System efficiency	0.347	0.586	0.6522		
Ohmic loss	0.0974	0.0364	0.0171		
Annode activation loss	0.1251	0.0393	0.0119		
Cathode activation loss	0.1688	0.0709	0.0240		
Annode concentration loss	0.0052	0.0063	0.0075		
Cathode concentration loss	0.0003	0.0004	0.0005		
ACDC converter loss	0.0205	0.0313	0.0346		
Loss due to blowers	0.0420	0.0084	0.0045		
Loss due to MeOH burner	0.0950	0.0950	0.0950		
Reversible loss	0.0987	0.126	0.1527		
steam ratio [-]	01 : 01	1.5 : 1	02 : 01	2.5 : 1	03 : 01
System efficiency	0.5860	0.5838	0.5781	0.5714	0.5668
Ohmic loss	0.0364	0.0370	0.0372	0.0374	0.0375
Annode activation loss	0.0393	0.0399	0.0402	0.0403	0.0405
Cathode activation loss	0.0709	0.0721	0.0726	0.0728	0.0732
Annode concentration loss	0.0063	0.0063	0.0064	0.0066	0.0069
Cathode concentration loss	0.0004	0.0004	0.0004	0.0004	0.0004
ACDC converter loss	0.0313	0.0312	0.0309	0.0307	0.0305
Loss due to blowers	0.0084	0.0085	0.0097	0.0113	0.0125
Loss due to MeOH burner	0.0950	0.0818	0.0778	0.0771	0.0742
Reversible loss	0.1260	0.1390	0.1467	0.1520	0.1575
i [$A \cdot m^{-2}$]	2500	5000	7500	10000	
System efficiency	0.6555	0.5860	0.5131	0.4380	
Ohmic loss	0.0189	0.0364	0.0545	0.0727	
Annode activation loss	0.0216	0.0393	0.0563	0.0712	
Cathode activation loss	0.0413	0.0709	0.0954	0.1146	
Annode concentration loss	0.0032	0.0063	0.0095	0.0127	
Cathode concentration loss	0.0002	0.0004	0.0005	0.0007	
ACDC converter loss	0.0346	0.0313	0.0282	0.0254	
Loss due to blowers	0.0023	0.0084	0.0222	0.0447	
Loss due to MeOH burner	0.0950	0.0950	0.0950	0.0950	
Reversible loss	0.1274	0.1260	0.1253	0.1250	
UF [-]	0.7	0.8	0.9	1	
System efficiency	0.5862	0.5860	0.5831	0.5784	
Ohmic loss	0.0359	0.0364	0.0367	0.0370	
Annode activation loss	0.0387	0.0393	0.0397	0.0400	
Cathode activation loss	0.0699	0.0709	0.0716	0.0722	
Annode concentration loss	0.0064	0.0063	0.0064	0.0066	
Cathode concentration loss	0.0004	0.0004	0.0003	0.0003	
ACDC converter loss	0.0312	0.0313	0.0312	0.0311	
Loss due to blowers	0.0066	0.0084	0.0106	0.0131	
Loss due to MeOH burner	0.1071	0.0950	0.0853	0.0774	
Reversible loss	0.1176	0.1260	0.1351	0.1439	

Table D.3: Losses data used in Figure 4.10.

T [K]	*973*	*1073*	*1173*
Operating voltage [V]	*0.421618*	*0.712012*	*0.792448*
Ohmic loss [V]	*0.118345*	*0.044227*	*0.020777*
Annode activation loss [V]	*0.152001*	*0.047751*	*0.014459*
Cathode activation loss [V]	*0.205098*	*0.086146*	*0.029161*
Annode concentration loss [V]	*0.006318*	*0.007655*	*0.009113*
Cathode concentration loss [V]	*0.000365*	*0.000486*	*0.000608*

Table D.4: Losses data used in Figure 4.11.

T[K]	NH_3	$MeOH$
System efficiency	0.5815	0.5860
Ohmic loss	0.0369	0.0364
Annode activation loss	0.0399	0.0393
Cathode activation loss	0.0720	0.0709
Annode concentration loss	0.0066	0.0063
Cathode concentration loss	0.0003	0.0004
ACDC converter loss	0.0323	0.0313
Loss due to blowers	0.0321	0.0084
Loss due to MeOH burner	0.1155	0.0950
Reversible loss	0.0829	0.1260

Table D.5: Efficiency data used in Figure 4.17.

T	ICE direct drive	$0/100$	$25/75$	$50/50$	$75/25$	$0/100$
1073	0.4357	0.4226	0.4543	0.4912	0.5344	0.4840
1173	0.4357	0.4226	0.4636	0.5131	0.5744	0.5600

Table D.6: Efficiency data used in Figure 4.18.

i	ICE direct drive	$0/100$	$25/75$	$50/50$	$75/25$	$100/0$
7500	0.4357	0.4226	0.4639	0.5140	0.5762	0.4114
5000	0.4357	0.4226	0.4543	0.4912	0.5344	0.4840
2500	0.4357	0.4226	0.4422	0.4636	0.4871	0.5499

E

Concept paper: A methanol-fuelled SOFC-ICE combined cycle for maritime applications

Concept paper: A methanol-fuelled SOFC-ICE combined cycle for maritime applications.

Abstract

The current body of research on combining SOFCs and ICEs has primarily focused on assessing natural gas-fuelled plants. This study presents a new drive system that utilises a methanol-fuelled SOFC-ICE combined cycle for maritime applications, in order to investigate the potential of these novel drive systems and high-potential alternative fuels. In this work a separate zero-dimensional NG-fuelled SOFC and conventional-fuelled ICE model were adopted, adapted for methanol use and then combined. The combined cycle was evaluated for various power configurations, and the current density and operating temperature of the SOFC were altered from the nominal condition. The nominal SOFC condition was operating at 1073K, with a steam-to-fuel ratio of 1:1, a fuel utilisation factor of 0.8 and a current density of 5000 $A \cdot m^{-2}$. The lower power splits have limited efficiency gain, which raises the questions about whether the added complexity of introducing an SOFC is justified. for the nominal condition, the highest efficiency was obtained with the 75/25 power split configuration (53.4%), but its large proportion of SOFC power raises concerns about its ability to meet dynamic power demands. It is expected that the 50/50 power split (49.2%) has the most potential to improve efficiency while remaining technologically feasible in maritime applications.

Keywords: Combined cycle, Modelling, Maritime, Methanol, SOFC-ICE

Nomenclature

AOG	Anode of gas	LT-HEX	Low temperature heat exchanger
atm	Atmospheric condition	MDO	Marine diesel oil
DI	Direct injected	MDR	Methane decomposition rate
GHG	Greenhouse gas	MeOH	Methanol
GT	Gas turbine	MeOHDR	Methanol decomposition reaction
HCCI	Homogeneous charge compression ignition	MSR	Methane steam reforming
HEX	Heat exchanger	NG	Natural gas
HFO	Heavy fuel oil	PEN	Positive-electrolyte-negative
HOR	Hydrogen oxidation rate	Powersplit	P_{SOFC}/P_{ICE}
HT-HEX	High temperature heat exchanger	SI	Spark ignition
ICE	Internal combustion engine	SOFC	Solid oxide fuel cell
IMO	International maritime organisation	TPB	three-phase boundary
LHV	Lower heating value	UF	Utilisation factor
LNG	Liquefied natural gas	WGS	Water gas shift

E.1. Introduction

In June 2021, only 6.7% of the global fleet used a modern eco-engine. Modern eco-engines refer to engines with electronic injection and contracted in 2012 or later [54]. This indicates that a large portion of the current world fleet still uses underdeveloped drive systems. These systems often use highly polluting fuels. By 2018, Heavy Fuel Oil (HFO) was the dominant type of fuel: 79% of the maritime energy consumption consists of HFO.

However, the International Maritime Organisation (IMO) does see development trends in the shipping industry. The IMO estimates that, even though total GHG emissions have increased in relative and absolute value, the relative and absolute use of HFO have decreased by 3% and 7% respectively [36]. Besides the transition in fuel type usage, also advanced drive systems are under development.

One such advanced drive system that is under development is the combination of a fuel cell and an internal combustion engine (ICE) in a combined cycle. This system combines the high efficiency and low emissions of a fuel cell with the reliability and flexibility of an ICE. The hybrid system can use a variety of fuels, such as diesel, natural gas (NG), hydrogen, ammonia or methanol, to generate electricity and power the ship's propulsion system. Research has shown that these hybrid systems have the potential to significantly improve the efficiency and reduce the emissions of ships [6] [74] [21] [67] [44]. However, the development of these systems is still in the early stages and further research and development is needed to optimise their performance and make them ready for deployment in the maritime industry.

E.1.1. Hybrid cycle research

Park et al. [67] compared the performance of a stand-alone solid oxide fuel cell (SOFC), an SOFC-GT and an SOFC-HCCI cycle on NG. The authors modelled the stack as lumbed body (0D) for the thermal analysis and used SOFC specifications that were in line with the technology state during the time of writing. The gas turbine (GT) was modelled as an isentropic model with corresponding efficiencies. The HCCI ICE was modelled as an Otto cycle. with an SOFC fuel utilisation factor of 0.75, the combined SOFC-ICE cycle reached a net efficiency of 59.5%, the SOFC-GT 58.6% and the standalone SOFC an efficiency of 51.7%. However, in this research, the ICE replaced the catalytic combustor, i.e. it was a bottoming cycle and not a combined cycle. This is reflected in the ICE/SOFC power split of 13/87.

Sapra et al. [74] evaluated an NG hybrid plant as well. He modelled an SOFC by extrapolating a single-cell model. The 0-dimensional model is based on the work of Aguiar et al. [1]. The lean-burning SI engine model was based on the Seiliger-cycle and experimental data. The engine operated on AOG and additional introduced NG, making it a combined cycle. The optimal

performance from an efficiency perspective was obtained with a power split of 67/33 and a fuel utilisation factor of 0.85 resulting in a total efficiency close to 45%. This is low compared to the work of Park et al.[67], which can be explained by the fact that Sapra et al.[74] modelled an ICE with limited efficiency,as well as the fact that they modeled a combined cycle, combined cycle and Park et al. [67] a bottoming cycle.

Koekkoek [44] conducted a similar research for his graduation thesis, however, he employed ammonia instead of NG as fuel. Ammonia itself is not a suitable fuel for an ICE as a pilot fuel is required. This pilot fuel is provided from an excess of reformed ammonia from either internal reforming in the SOFC or from an external reformer. In order to provide enough hydrogen in all evaluated power splits and prevent heat management problems, an external reformer was added to the plant. The SOFC model was again based on the work of Aguiar et al. [1]. As with the research of Sapra et al.[74], the ICE was modeled with a Seiliger-cycle and obtained an efficiency of 43%. With a $P_{SOFC}P_{ICE}$ 75/25 power split, an efficiency of 58% was obtained.

One research was found that modelled an SOFC combined cycle on methanol and compared a plant with internal and external reforming to an internally reforming NG combined cycle. However, in this research by Cocco and Tola [21], the SOFC was combined with a GT. For the internal reforming methanol plant using a fuel utilisation factor (UF) of 0.85, a power split of 72/28 was obtained, resulting in a total efficiency of 63.6%. The external reforming methanol plant operated at a power split of 73/27 and a total efficiency of 68.5%. Limited literature is found on methanol-fuelled SOFC-(reciprocating)ICE combined cycles.

The motivation of this paper is to develop and implement a novel type of power plant, fuelled with an alternative clean fuel in maritime applications. This research focusses on an SOFC combined with a reciprocating ICE fuelled with green methanol.

E.1.2. Maritime scope

Suitability characteristics of maritime power plant have to be defined, in order to evaluate the implementation of a methanol fuelled SOFC-ICE in maritime applications. Van Biert [11] indicated the following characteristics in his PhD thesis:

- Electrical efficiency;
- Power and energy density;
- Environmental impact;
- Load transients;
- System start-up;
- Safety and reliability;
- Economics.

The aim of this research is to address the first four characteristics. To address the first, second and fourth characteristic, a trade-off has to be made depending on the ship type and its operational profile. Therefore, the power plant consists not only of an SOFC but also of an ICE and is evaluated at different power splits. The implementation of an SOFC nearly always leads to improvements in the third characteristic.

E.2. Modelling approach

The evaluated power plant operates as follows: methanol and water, which is added to prevent carbon depositting [47], are introduced into the system as liquids. The streams are preheated in an economiser prior to entering the evaporators, which utilise waste heat from the ICE. The resulting methanol vapor and steam are then blended and conveyed by the blowers. After being heated to the correct reforming temperature in a heat exchanger, it enters the methanator. Here, the methanol is cracked and, together with the steam, partially reformed to, among others, a hydrogen/methane mixture. By controlling the temperature, one can determine the reforming ratio. Before entering the anode channel, the fuel stream is further heated with additional heat exhangers. In a separate stream, the air is preheated with a heat exchanger before entering the cathode channel. Here, the fuelstream is oxydised with oxygen ions transported through the electrolyte, in the process of producing electric power. The resulting anode-of-gas (AOG) and cathode-of-gas (COG) streams are used in their respective heat exchangers. The COG is emitted into the environment. The AOG is dehydrated and led to the turbocharger intake of the SI-ICE. After it is compressed and intercooled, together with intake air, it is led to the cylinder. Here, the AOG/air mixture, which is still out of combustible limits, is compressed. At high pressure, methanol is directly injected. The exhaust gases drive the charger turbine and then pass through the heat exchanger in the evaporator. Subsequently, they are discharged into the environment, unless end-of-pipe technologies, like Selective Catalytic Reduction, to clean the exhaust gases are applied. In Figure E.1 the system layout can be seen. This work presents an in MATLAB & Simulink constructed model consisting of an SOFC and an ICE submodel.

The ICE model core consists of a turbocharged five-state Seiliger cycle. It simulates Wärtsilä 12V31DF [96] fuelled with methanol and dehydrated hydrogen-rich anode of gas (AOG). The SOFC efficiency and its separate losses are evaluated for different temperatures, current densities, fuel utilisation factors UF and steam-to-fuel ratio's in combined cycle operations. Additionally, the standalone SOFC performance, without the use of waste heat from the ICE and disuse of residual fuel in the AOG, is evaluated, but only for the nominal condition. The ICE efficiency and losses are evaluated for a power range between 1% and 100%. By varying the ammount of cells, the following power splits P_{SOFC}/P_{ICE} have been evaluated: 0/100 25/75; 50/50; 75/25 and 100/0. The combined cycle performance is evaluated for different temperatures and current densities.

E.2.1. SOFC model

The zero-dimensional SOFC submodel, which is based on the work of Aguiar et al. [1], consists of a temperature controlled methanator which maintains an external reforming ratio of 0.5; a cell mass balance; a cell energy balance, and an electrochemical model.

Methanator

The proposed SOFC model runs on hydrogen. Therefore, the fuel has to be reformed to hydrogen. Internal steam reforming is an efficient way of cooling the system, but it can also cause instabilities. However, methanol is relatively unstable compared to methane [10]. This instability causes methanol to rapidly decompose within the SOFC, inducing a strong cooling effect on the cell entrance. The consumption of hydrogen, however, is a less spontaneous process. Due to this misalignment in heat

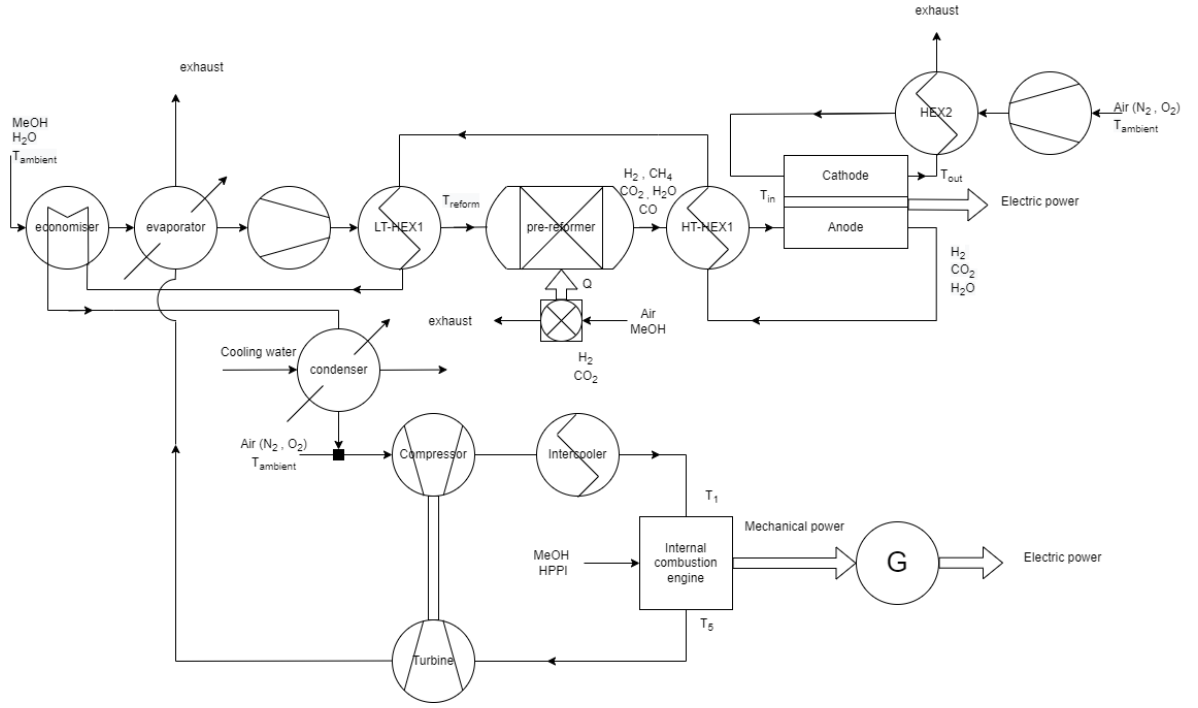

Figure E.1: Schematic representation of the combined SOFC-ICE cycle.

consumption and heat production, large thermal gradients can occur, which in term cause stresses, possibly damaging the PEN structure.

In the reformer multiple processes take place. In this research, it is assumed that the following reactions are dominant such that others can be neglected:

$$CH_3OH \longrightarrow 2H_2 + CO \tag{E.1}$$

$$CH_4 + H_2O \rightleftarrows 3H_2 + CO \tag{E.2}$$

$$CO + H_2O \rightleftarrows CO2 + H_2. \tag{E.3}$$

As a result of the instability of methanol, the methanol decomposition reaction (MeOHDR) is assumed to be, and therefore modelled as, a one-way going reaction. The methane steam reforming (MSR) and water gas shift (WGS) however, are equilibrium reactions. It is anticipated that the rate of these reactions is sufficient to allow for the assumption of reaction until equilibrium. Because MeOHDR is modelled to occur spontaneously, the process can be split into two processes.

The following three stages are defined: stage 1, before entering the methanator; stage 2, after the MeOHDR; stage 3, after the methanisation and thus after the methanator. For process two, the resulting five unknown molar flowrates have to be determined. This is done by solving three stoichiometric equations, using Reactions E.3 and E.2, and two equilibrium equations for a given temperature, pressure and $\dot{N}^0$:

$$\dot{N}^2_{H_2} = \dot{N}^1_{H_2} + \dot{N}^2_{CO_2} - 3 \cdot \dot{N}^2_{CH_4} \tag{E.4}$$

$$\dot{N}^2_{CO} = \dot{N}^1_{CO} - \dot{N}^2_{CO_2} - \dot{N}^2_{CH_4} \tag{E.5}$$

$$\dot{N}^2_{H_2O} = \dot{N}^1_{H_2O} - \dot{N}^2_{CO_2} + \dot{N}^2_{CH_4} \tag{E.6}$$

$$K_{WGS} = \frac{p^2_{CO_2} \cdot p^2_{H_2}}{p^2_{CO} \cdot p^2_{H_2O}} = \frac{\dot{N}^2_{CO_2} \cdot \dot{N}^2_{H_2}}{\dot{N}^2_{CO} \cdot \dot{N}^2_{H_2O}} \tag{E.7}$$

$$K_{MSR} = \frac{p^2_{CO} \cdot (p^2_{H_2})^3}{p^2_{CH_4} \cdot p^2_{H_2O}} = \frac{\dot{N}^2_{CO} \cdot (\dot{N}^2_{H_2})^3}{\dot{N}^2_{CH_4} \cdot \dot{N}^2_{H_2O}} \cdot f_p \tag{E.8}$$

$$f_p = \left(\frac{p_{eq}}{p_{ref}}\right)^2 \frac{1}{(\sum_{i=1}^{5} \dot{N}^2_i)^2} \tag{E.9}$$

$$i \epsilon \{H_2O, CH_4, H_2, CO, CO_2\} \tag{E.10}$$

With $\dot{N}_i^{\#}$ the molar flow rate at stage $\#$ of substance i; K representing the reaction constants; p_i partial pressures of substance i; p_{eq} the reaction pressure at equilibrium; p_{ref} a reference pressure set to p_{atm}; and f_p the pressure correction factor. The constants are determined per reaction using:

$$K = e^{\frac{-\Delta(G}{RT}} \tag{E.11}$$

where temperature-dependent G is determined using the Shomate polynomials using data from NIST [66].

To provide heat to the net endothermic reaction a burner is installed. The amount of heat required is determined by solving for Q:

$$0 = \dot{\bar{N}}^{in}\bar{h}^{in} - \dot{\bar{N}}^{out}\bar{h}^{out} + Q \tag{E.12}$$

According to Van Biert [10], a common figure for the external cracking ratio is 0.5. This provides stable operation of the SOFC as well as the advantage of cooling due to internal ferforming.

Mass balance of the cell

For solving the mass balance, the same method as Kang et al.[41] is used. This method is based on the assumption that only a hydrogen oxidation reaction (HOR) and a fuel decomposition reaction (methane decomposition reaction, MDR) occur at the anode of the SOFC. Additionally it assumed that all carbon monoxide is consumed in the WGS on entering the cell. The reactions that occur are:

$$CH_4 + H_2O \longrightarrow 3H_2 + CO \tag{E.13}$$

$$CO + H_2O \longrightarrow CO2 + H_2 \tag{E.14}$$

$$H_2 + O^{2-} \longrightarrow H_2O + 2e^- \tag{E.15}$$

The rates at which these reactions occur are the input to the mass balance. The HOR rate per surface area is determined by the current density:

$$r_{HOR} = \frac{i}{n_e F} \tag{E.16}$$

Here i is the current density $[A/m^2]$. It is assumed that all methane is decomposed. This means that the MDR rate is determined by the molar flow of methane. The mass balance for a substance is then defined as:

$$\begin{aligned}\frac{PV}{RT}\frac{\mathrm{d}x^{out}}{\mathrm{d}t} = \dot{N}^{in} - \dot{N}^{out} \\ + WL \cdot (v_{HOR}r_{HOR} + v_{MDR}r_{MDR})\end{aligned} \tag{E.17}$$

Here $\dot{N}$ is the molar flow in the channel; W the width of the channel; L the length of the channel; v the stoichiometric coefficient of the substance in the corresponding reaction; and $\frac{dx}{dt}$ denotes the dynamic component of the total molar change of the substance. This can be done for both the anode and the cathode.

Cell energy balance

The proposed model neglects the heat capacity of gaseous substances, instead focussing exclusively on the solid components of the cell, specifically the PEN structure and interconnects, in the calculation of the $m \cdot c_p$ component. $\dot{\bar{N}}$ is the molar flow vector containing all substances. Using the corresponding enthalpy vector $\bar{h}$, the inflow and outflow enthalpies are determined. The heat loss $\dot{Q}_{loss}$ is assumed to be 5% of sensible heat gain of the cell structure. This results in Equation E.18.

$$m \cdot c_p \frac{\mathrm{d}T^{out}}{\mathrm{d}t} = \dot{\bar{N}}^{in}\bar{h}^{in} - \dot{\bar{N}}^{out}\bar{h}^{out} - iV_{cell}WL - \dot{Q}_{loss} \tag{E.18}$$

Cell electrochemical model

The assumption is made that all CH_4 and CO immediately decompose upon entering the cell, leading to the operation of the cell as a pure hydrogen fuel cell. Since the SOFC is modelled with zero dimensions, an average temperature and partial pressure is estimated.

The open circuit voltage is determined using the Nernst equation:

$$E = -\frac{\Delta g^0}{n_e F} + \frac{\bar{R}T}{2F} ln\left(\frac{\frac{P_{H_2}}{p^0} \cdot \left(\frac{p_{O_2}}{p^0}\right)^{\frac{1}{2}}}{\frac{p_{H_2O}}{p^0}}\right) \tag{E.19}$$

With Δg^0 as the standard Gibbs free energy for the HOR. The obtained voltage is corrected with the activation loss, ohmic loss and concentration loss, which are defined respectively:

$$\Delta V_{act} = \frac{2\bar{R}T^{stack}}{n_e F}\left(sinh^{-1}\left(\frac{i}{2 \cdot i_{0,cat}}\right) + sinh^{-1}\left(\frac{i}{2 \cdot i_{0,an}}\right)\right) \tag{E.20}$$

Where i_0 is the temperature dependent exchange current density.

$$\Delta V_{con} = \frac{\bar{R}T^{stack}}{2F} ln\left(\frac{p_{H_2O,TPB} \cdot p_{H_2}}{p_{H_2O} \cdot p_{H_2,TPB}}\right) + \frac{\bar{R}T^{stack}}{4F} ln\left(\frac{p_{O_2}}{p_{O_2,TPB}}\right) \tag{E.21}$$

With $p_{,TPB}$ as the partial pressure at the three-phase boundary.

$$\Delta V_{ohm} = i\left(\frac{\tau_{an}}{\sigma_{an}} + \frac{\tau_{el}}{\sigma_{el}} + \frac{\tau_{ca}}{\sigma_{ca}}\right) \tag{E.22}$$

With thickness τ and conductivity σ. Where the electrode condictivities are assumed constant and the electrolyte conductivity is temperature dependant as follows:

$$\sigma_{el} = 33.4 \cdot 10^3 \cdot e^{\frac{-10300}{T}} \tag{E.23}$$

This results in the following:

$$V_{cell} = E - \Delta V_{act} - \Delta V_{con} - \Delta V_{ohm} \tag{E.24}$$

E.2.2. ICE model

An existing zero-dimensional model of a zero-dimensional turbocharged cylinder process, is utilised and modified to suit the fuel requirements of methanol in the ICE, similar to the SOFC model. The generated mechanical power drives a generator. The fuel supply is managed by the fuel governor using a PID controller. For the cylinder process, the five-stage Seiliger cycle is used.

The key engine parameters regarding the thermodynamic model are:

- Charge pressure & temperature after intercooler; determine the initial condition before compression;
- Compression ratio; determines stage two;
- Max cylinder pressure; provides pressure ratio and thus temperature ratio for stage three. Also determines the division of heat input over the combustion phases and therefore condition four;
- Brake specific fuel consumption (bsfc);
- Rated power output;

Combined cycle

The SOFC and ICE are related in two ways: via the AOG which is fed to the cylinder; and the the use of heat from the exhaust to provide for the evaporator.

After the heat exchangers, the AOG is dehydrated. This results in a mixture of H_2 and CO_2. This hydrogen-rich gas is added to the ICE intake air. The amount of H_2 and CO_2 added per thermodynamic cycle is obtained via:

$$m_{H_2,cyc} = \frac{\dot{N}_{H_2} \cdot M_{H_2} \cdot k}{n_{eng} \cdot i} \tag{E.25}$$

$$m_{CO_2,cyc} = \frac{\dot{N}_{CO_2} \cdot M_{CO_2} \cdot k}{n_{eng} \cdot i} \tag{E.26}$$

In which M is the molar mass, k the indicator for two- or four-stroke (1 or 2), n the engine speed and i the amount of cylinders. The additional mass of H_2 and CO_2 is accounted for in the specific heat input [J/kg] which is used in determining the efficiency:

$$q_{spec} = \frac{m_{H_2,cyc} \cdot LHV_{H_2} + m_{MeOH,cyc} \cdot LHV_{MeOH}}{m_{a,cyc} + m_{CO_2,cyc} + m_{H_2,cyc}} \tag{E.27}$$

The properties of the SOFC and ICE model are defined in Appendix E.5

E.3. Results

E.3.1. SOFC performance

Since the SOFC will be incorporated in a combined cycle, its performance will be analysed in that specific configuration. This means that any residual fuel in the anode off-gas will not be considered as a loss, as it can be utilised in the ICE. Furthermore, there is an abundance of heat available in the ICE exhaust, which can be utilised to heat the evaporator, thus eliminating the need for consumption of fuel in the evaporator.

The parameters that will be varied in this evaluation of the SOFC are $r_{s/f}$, UF, operating temperature and current density. The standard operating conditions are defined as in table E.1.

The influence of $r_{s/f}$ can be seen in Figure E.2. To change $r_{s/f}$ and maintain the power output (assuming constant efficiency), the amount of steam fed to the system should be increased, resulting in lower fuel concentrations and therefore lowering the open circuit voltage. The largest loss increase is the consumption by the methanator burner. When the amount of steam is increased, the operating temperature of the methanator has to change in order to maintain the err. This temperature change influences the enthalpy of formation of the different substances. These effects combined result in a small difference with the highest efficiency for $r_{s/f}$ = 1:1 and the lowest for 1:3, resulting in 58.6 % and 56.7 % respectively.

By varying UF the system efficiency barely changes, see Figure E.3. To change the UF and maintain power output (assuming constant efficiency), the amount of fuel fed to the system should be increased. The same concentration effect occurs as with the variation of $r_{s/f}$. This effect is counteracted by the increase of burner power as a result of a larger amount of methanol that should be cracked. This results in an efficiency of 58.6 % to 58.31 % for a UF of 0.7 to 0.9 respectively.

When the operating temperature is varied, larger differences occur, see Figure E.4. First, the open circuit voltage decreases with increasing T. However, the loss mechanisms are more affected by increasing T and, therefore, the system efficiency increases. The ohmic loss is dominated by the temperature dependent electrolyte. Temperature also has a significant influence on the activation losses. Finally, for decreasing temperature, an increase in blower loss can be seen. To maintain a lower operating temperature and to compensate for the additional heat production due to a lower efficiency, more cooling air in the cathode channel is required. The resulting efficiencies are between 34.7% and 65.2% for temperatures between 973 and 1173 K respectively.

In Figure E.5 the dependency on the current density can be observed. The current density does not have a significant influence on the open circuit voltage. However, a decrease in system efficiency can be observed. When the current density increases, the fuel consumption increases. As more fuel is consumed, the partial pressure at the triple phase boundary (TPB) of the fuel is reduced and that of the reaction product increases. The same blower behaviour can be observed as with varying the temperature. The efficiencies decrease from 65.6% to 43.8% for current densities from 2500 to 10.000 $A \cdot m^{-2}$.

The standalone configuration has a different performance compared to the combined configuration„ see Figure E.6. The residual fuel in the AOG will not be used in the ICE but, it can be used for evaporating the fuel and fuelling the methanator. As a result, the efficiency is reduced to 45.4% compared to 58.6% in the combined configuration. This clearly shows the synergistic benefits of combining a methanol-fuelled SOFC with an ICE.

Table E.1: Standard operating of the SOFC

Parameter	Value	Unit
UF	0.8	-
$r_{s/f}$	1:1	-
T_{op}	1073	K
i	5000	$A \cdot m^{-2}$

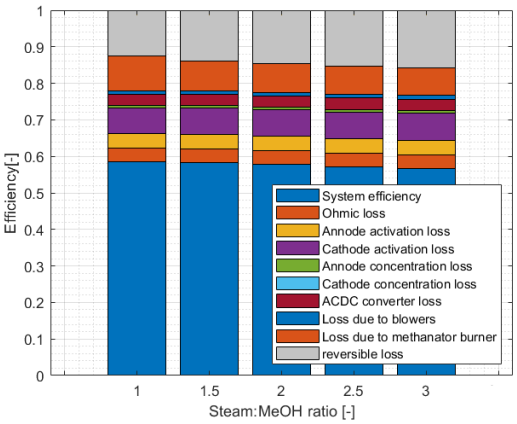

Figure E.2: Different losses per steam:methanol ratio.

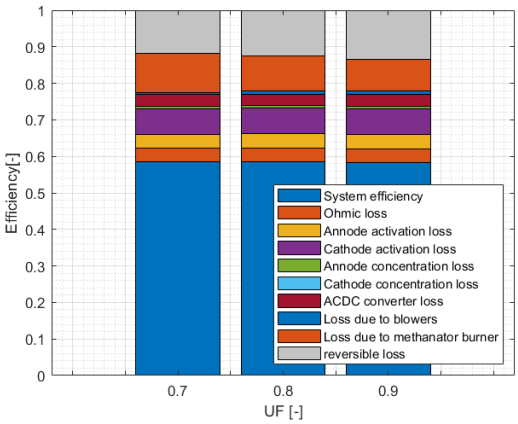

Figure E.3: Different losses per UF.

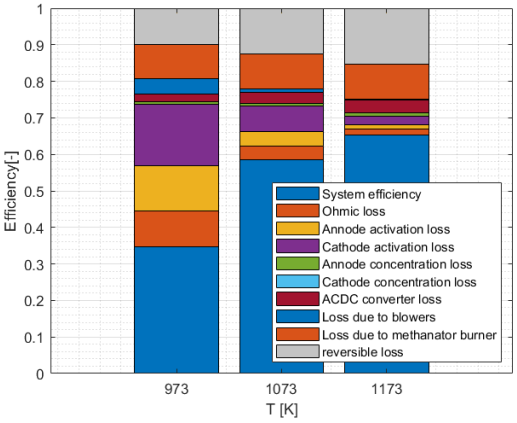

Figure E.4: Different losses per T.

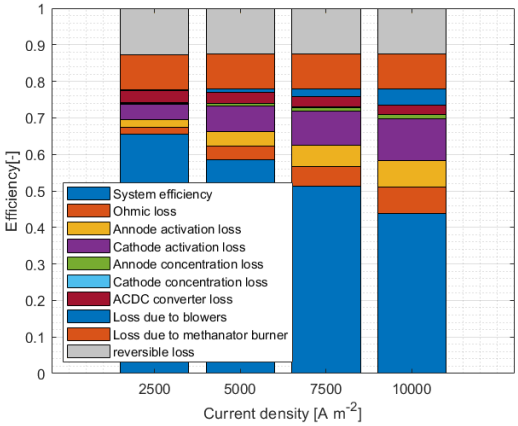

Figure E.5: Different losses per current density.

E.3.2. ICE results performance

In Figure E.7 the different losses and efficiencies of the ICE can be seen. As stated previously, the BSFC at the nominal point is one of the input parameters, thus the effective efficiency at the nominal point is given. The mechanical efficiency is given as a percentage of the nominal power. Therefore, at low power, it makes up a larger portion of the total loss. The efficiency of the generator is dependent on the power output. However, it ranges from 95% to 97% so its dependency is limited. The thermodynamic efficiency is the result of the reversible cycle. The heat input efficiency captures the hard to determine factors as unburned fuel in the exhaust and heat loss to the cylinder wall. This factor is iteratively fitted to the nominal point and assumed constant through the simulation.

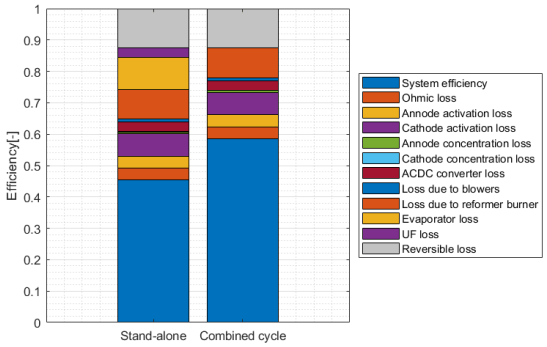

Figure E.6: Methanol-fuelled SOFC efficiency performance in standalone and combined cycle condition.

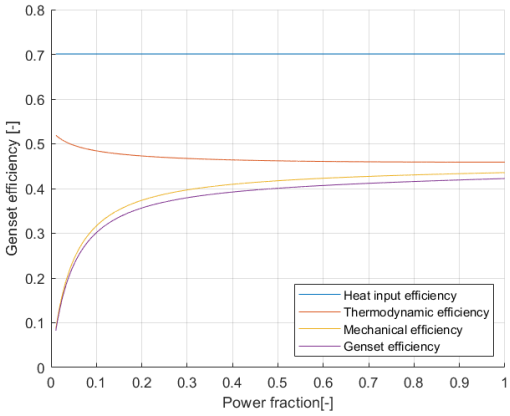

Figure E.7: Different efficiencies between 1% and 100% nominal power.

E.3.3. Combined SOFC-ICE performance

In the combined configuration, several power splits (P_{SOFC}/P_{ICE}) will be evaluated. Also, the ICE direct drive efficiency will be shown. Evaluation will be carried out for several conditions from Table E.1, however only efficiency improving results will be discussed.

In figure E.8 the efficiency of the system can be seen for different operational temperatures. The impact of the lack of waste heat from the engine is evident in the 100/0 condition, which is presented here solely for the sake of completeness and is deemed less practical given its lack of load-following capabilities from the ICE. Please note that these simulations are conducted an nominal load. If the SOFC maintains its power output while the ICE operates in part-load, the heat management system may encounter challenges. In the 25/75 configuration, the ICE provides adequate heat across a significant portion of its power range. Conversely, the 75/25 configuration experiences heat management issues at relatively high part-loads. These observation also holds true for configurations with varying current densities in Figure E.9.

When comparing the 1173 K and 2500 $A \cdot m^{-2}$ case, there are only very small differences (0.06 to 0.5%). In maritime applications, where power density is a limiting factor, this would advocate for increasing the operational temperature compared to decreasing the current density. However, the increase in cost and durability due to the need for other materials is not evaluated in this research.

All values can be found in Table E.2. The choice for a certain power split depends on the availability of space onboard the ship and the fluctuations in power demand.

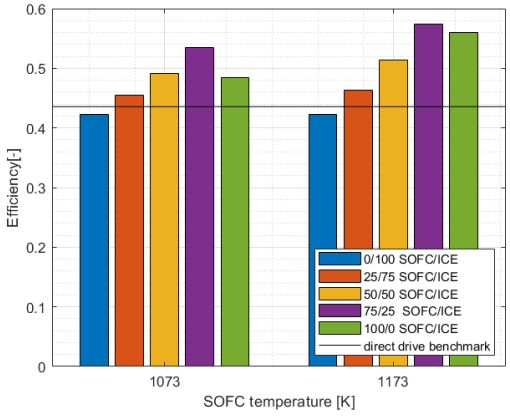

Figure E.8: Efficiencies for different power splits per SOFC operating temperature.

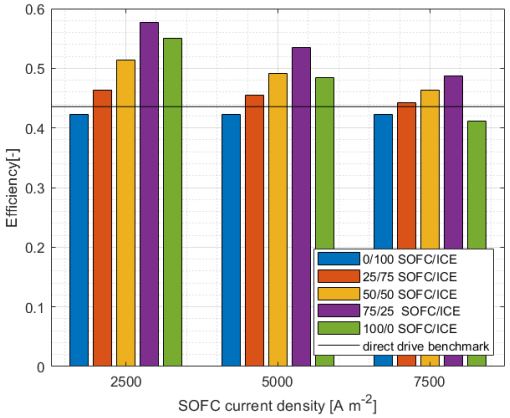

Figure E.9: Efficiencies for different power splits per SOFC current density.

MeOH-NH3 comparison

The results will be compared to the results from the work of Koekkoek [44] in order to assess the difference in performance between two high-potential fuels. For the ammonia-fuelled plant, the idea is that the combined cycle can provide the pilot fuel in the form of hydrogen from ammonia cracking using the heat from the SOFC. However, the ammonia-fuelled cycle does not need to evaporate the water fuel mixture. This implies that the implementation of a combined cycle is advantageous for both fuel types.

The plant has almost the same standard operating parameters as in Table E.1. However, there is no steam required for the ammonia plant and the UF is set to 0.76. As previously discussed, the UF has no significant influence on the SOFC performance

Table E.2: Efficiencies [%] of different power configurations for different temperatures [K] and current densities [$A \cdot m^{-2}$]

temperature	current density	ice direct drive	0/100	25/75	50/50	75/25	100/0
800	2500	43.6	42.3	46.4	51.4	57.6	55.0
	5000			45.4	49.1	53.4	48.4
	7500			44.2	46.4	48.7	41.1
900	5000			46.4	51.3	57.4	56.0

when it is considered in a combined configuration. Therefore, the effects due to the difference in UF are negligible. In Figure E.10 and Table E.3 the results regarding efficiency are shown. It can be seen that with lower powersplits, the ammonia-fuelled plant is more efficient, but at the 75/25 power split, the MeOH plant is more favourable. This is because the ammonia-fuelled ICE is more efficient and the MeOH-fuelled SOFC is more efficient. However, Koekkoek [44] provides no numerical results on the efficiency of the standalone ICE genset or the standalone SOFC with a UF of 0.8. By visual evaluation of a graphic result of Koekkoek [44] can be concluded that his ICE genset has a higher efficiency at nominal load compared to methanol fuelled ICE from this research. Regarding the SOFC standalone, Koekkoek reported efficiencies of 45.4% for a UF of 0.7 and 56.2% for a UF of 0.9, and an average of these values is taken for visualisation purposes. For both configurations, a decrease in efficiency can be observed in the standalone SOFC condition, with this decrease being more pronounced in the methanol-fuelled configuration. The cause of this is unknown, given that the amount of fuel remaining in the anode off-gas is sufficient for both the evaporation and reforming processes for both fuels. However, as the value for the ammonia-fuelled plant is an estimate, caution must be exercised when making statements regarding its accuracy. Despite these differences, the values are relatively close, suggesting a substantial degree of competitiveness between them.

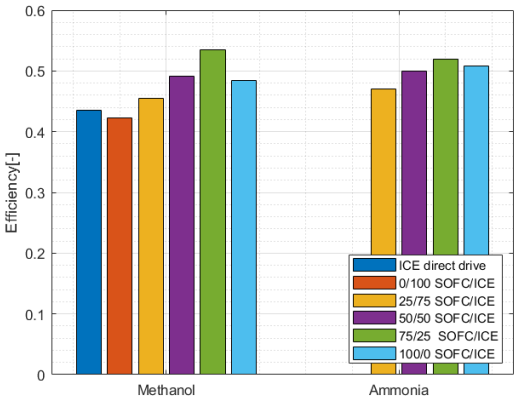

Figure E.10: Efficiencies for different power configurations per fuel.

Table E.3: Data on the efficiency [%] from Figure E.10. Estimate given in *italic*.

Power configuration	NH_3	$MeOH$
ICE direct drive	-	43.6
0/100	-	42.3
25/75	47	45.4
50/50	50	49.2
75/25	52	53.4
100/0	*50.8*	48.4

E.3.4. Research and modelling approach reflection

Within the context of the SOFC model, a mean temperature value is used. However, it is important to recognise that the estimation of the operating temperature can influence the outcomes of the simulation. As depicted in Figure E.4, it is apparent that the efficiency of the system is not linearly dependent on the temperature. It is also assumed that the fuel instantly decomposes upon entering the cell. This could have effects on the effective partial pressures of the fuel.

The ICE model lacks spatial dimensions as well, which can pose challenges in accurately capturing various combustion behaviours relative to conventional fuels. This includes the accurate determination of fuel-related losses and the prediction of harmful emissions.

The coupling between the SOFC and ICE is currently simplistic: The dehydrated AOG from steady-state operations is fed to the ICE in the form of an initial heat input during the closed-cylinder process and waste heat from the ICE is used for the evaporation of the methanol-water stream. However, this coupling does not consider the impact of back pressure. Also a more advanced heat integration can be obtained with a further developed coupling. A more detailed coupling would also facilitate the modelling of dynamic behaviour to further explore the potential and constraints of the proposed plant.

E.4. Conclusion

In this work a novel drive system consisting of a methanol-fuelled SOFC-ICE combined cycle for maritime applications is presented. The combined cycle has been evaluated for different power configurations: P_{SOFC}/P_{ICE} = 0/100, 25/75, 50/50 and 75/25 and 100/0. In addition to that, the two most influential SOFC parameters have been varied. For standard operating conditions, the results were compared to a methanol-fuelled direct drive ICE and an ammonia-fuelled combined cycle. The efficiency gain of the methanol-fuelled 75/25 (45.4%) configuration compared to the direct drive(43.6%) is limited. This raises the questions about whether the added complexity of introducing an SOFC is justified for the limited efficiency gain. The highest efficiency was obtained with the methanol-fuelled 75/25 power split (53.4%), but due to the large proportion of SOFC power, it is less tolerant to dynamics in the load, making it questionable whether it can fully meet the dynamic power demand of a ship. Therefore, it is expected that the 50/50 power split (49.2%) has the most potential to be technologically feasible.

The 50/50 powersplit configuration is 5.6 percentpoints more efficient than the methanol-fuelled direct drive ICE and 1.2 percentpoints more efficient than the methanol-fuelled standalone SOFC. This clearly shows the synergistic benefits of combining a methanol-fuelled SOFC with an ICE. However, when compared to the ammonia fuelled combined cycle with 50/50 power split, it is 0.9 percentpoints less efficient. Nevertheless, it is important to exercise caution when drawing further conclusions from this last figure as the model has been constructed at a system level and no thorough uncertainty analysis has been conducted.

E.5. Appendix: modelling parameters

Table E.4: Properties of the SOFC system

parameter	value	unit	description
W	0.1	m	Cell width
L	0.1	m	Cell length
h	$1 \cdot 10^{-3}$	m	Channel height
τ_{an}	$500 \cdot 10^{-6}$	m	Thickness of anode
τ_{ca}	$50 \cdot 10^{-6}$	m	Thickness of cathode
τ_{el}	$20 \cdot 10^{-6}$	m	Thickness of electrolyte
τ_I	$500 \cdot 10^{-6}$	m	Thickness of interconnect
σ_{an}	$80 \cdot 10^3$	$\Omega^{-1}m^{-1}$	Electric conductivity of anode
σ_{ca}	$8.4 \cdot 10^3$	$\Omega^{-1}m^{-1}$	Electric conductivity of cathode
σ_{el}	$33.4 \cdot 10^3 exp(\frac{-10300}{T})$	$\Omega^{-1}m^{-1}$	Ioninc conductivity of electrolyte
$D_{eff,an}$	$3.66 \cdot 10^{-5}$	$m^2 \cdot s^{-1}$	Effective diffusion coefficient of anode
$D_{eff,ca}$	$1.37 \cdot 10^{-5}$	$m^2 \cdot s^{-1}$	Effective diffusion coefficient of cathode
$c_{p,PEN}$	500	$J \cdot kg^{-1} \cdot K^{-1}$	Specifi heat capacity of PEN structure
$c_{p,I}$	500	$J \cdot kg^{-1} \cdot K^{-1}$	Specific heat capacity of interconnect
ρ_{PEN}	5000	$kg \cdot m^{-3}$	Mass density of PEN structure
ρ_I	8900	$kg \cdot m^{-3}$	Mass density of interconnect
k_{an}	$2.35 \cdot 10^3$	$A \cdot m^{-2}$	Pre-exponential factor of i_0 at anode
k_{ca}	$6.54 \cdot 10^3$	$A \cdot m^{-2}$	Pre-exponential factor of i_0 at cathode
E_{an}	$140 \cdot 10^3$	$J \cdot mol^{-1}$	Activation energy of i_0 at anode
E_{ca}	$137 \cdot 10^3$	$J \cdot mol^{-1}$	Activation energy of i_0 at cathode
η_{is}	0.6	$-$	Isentropic efficiency of the fuel and air blowers
η_{mech}	0.9	$-$	Mechanical efficiency of the fuel and air blowers
η_{DCAC}	0.95	$-$	DC-AC converter efficiency
$heatloss$	0.05	$-$	Heat loss of the SOFC to the environment
T_{op}	1073	K	Operating temperature of the SOFC
p_{op}	101325	pa	Operating pressure of the SOFC
T_{meth}	843	K	Operating temperature of the methanator
p_{meth}	101325	pa	operating pressure of the methanator
i	5000	$A \cdot m^{-2}$	Current density
$r_{s,f}$	$1:1$	$-$	Steam to fuel ratio

Table E.5: Properties of the ICE

Parameter	Value	Unit	Description
P_{nom}	7200	kW	Nominal power output
n	750	rpm	Engine speed
ϵ	16	$-$	Geometric compression ratio
D	0.32	m	Bore
S	0.4	m	Stroke
i	12	$-$	Number of cylinders
k	2	$-$	revolutions per cycle
p_{charge}	$3.6 \cdot 10^5$	pa	Nominal charge pressure
T_1	328	K	Starting T of the closed cylinder process
p_{max}	$186 \cdot 10^5$	pa	Max cylinder pressure
η_{mech}	0.95	$-$	Mechanical efficiency at nominal speed
η_{gen}	$0.95 - 0.97$	$-$	Speed dependant generator efficiency
$bsfc$	380	g/kWh	Brake specific fuel consumption